國立臺灣大學高分子科學與工程學研究所

碩士論文

Institute of Polymer Science and Engineering

College of Engineering

National Taiwan University

Master Thesis

新型含三苯胺結構之高性能高分子合成與記憶體元件應用之研究

Synthesis and Memory Device Applications of Novel Triphenylamine Moiety Based High-Performance Polymers

胡益誠

Yi-Cheng Hu

指導教授：劉貴生 博士

Advisor: Guey-Sheng Liou, Ph. D.

中華民國 101 年 8 月

Aug., 2012

國立臺灣大學碩士學位論文
口試委員會審定書

新型含三苯胺結構之高性能高分子合成與記憶體元件應用之研究

Synthesis and Memory Device Applications of Novel Triphenylamine Moiety Based High-Performance Polymers

本論文係胡益誠君（R99549031）在國立臺灣大學高分子科學與工程學研究所完成之碩士學位論文，於民國 101 年 8 月 14 日承下列考試委員審查通過及口試及格，特此證明

口試委員：劉文生（簽名）

（指導教授）賴朝松

簡勝雄

系主任、所長 林江珍（簽名）

ACKNOWLEDGEMENTS

I feel an immense gratitude to my advisor, Prof. Guey-Sheng Liou, for everything in this two year. In addition, I appreciate Prof. Sheng-Huei Hsiao, Assistant Prof. Shih-Huang Tung, and Prof. Chao-Sung Lai for their perceptive criticisms and useful comments on this dissertation and all teachers at Institute of Polymer Science and Engineering in the National Taiwan University. A financial supports from the National Science Council of the Republic of China and a congenial environment for my graduate studies provided by the Institute of Polymer Science and Engineering at the National Taiwan University are also greatly appreciated.

I appreciate Associate Prof. Sheng-Shu Hou and all the teachers in Dept. of Chemical Engineering, National Cheng Kung University for the tuitions and the partners of studying group for graduate school entrance exams in the K-House; all of you gave me the opportunity of taking my master degree here.

I also appreciate Hung-Ju Yen for his advice and suggestion at key times, princess Chen for her humor and aid, Wan-Jiun Wu for being together with me and her thoughtfulness, Feng-Jeng Lin for the assistance in photographing TEM images, and the fellows in G. S. Liou's Lab. : Chia-Liang Tsai, Jia-Hao Wu, Pei-Hsuan Wang, Kun-Ying Lin, Shiue-Ming Kuo, Zheng-Wei Liu, Chih-Lung Heish, Lin-En Chi, Wen-Chang Wang, Wei-Yao Tung, Ya-Wen Chuang, Shih-Han Chen, Jhe-Huang Lin. I can not finish this thesis without their supports and encouragement.

I would like to show my appreciation to the members in baseball teams of KSHS, NCKUCHE, NCKU, NTU, and YS confidence baseball club, for all of you delight my life.

Finally, I am grateful to my family for their endless love and supports, especially to my mother who makes me never blind even facing adversities or prosperities. I would like to dedicate all my achievements to them.

ABSTRACT

This study has been separated into five chapters. Chapter 1 is general introduction. Chapter 2 includes two distinct approaches to synthesize the active layer in the application of memory devices. The first one is introducing PCBM as the acceptor via blending into the donor-containing poly-4-methoxytriphenylamine (**P-TPA**) leading the donor-acceptor hybrid films **P-TPA:PCBM**, another one is incorporating the acceptor anthraquinone via covalent bond to the electron-donating moiety then resulting donor-acceptor containing polymers poly-**2-**diphenylaminoanthracene-9,10-dione (**P-TPAAQ**) and poly-**2-**(4-diphenylaminophenoxy)anthracene-9,10-dione (**P-TPAOAQ**). Chapter 3 describes the memory devices based on dual competitive electron acceptors system with novel electron-donating triphenylamine (TPA) based electroactive functional polyimides **AQ-PIs** and **OAQ-PIs** derived from two diamines, 2-(bis(4-aminophenyl)amino)anthracene-9,10-dione and 2-(4-(bis(4-aminophenyl)amino)phenoxy)anthracene-9,10-dione, respectively, having electron-withdrawing pendent anthraquinone moiety. Chapter 4 describes the structurally related TPA-based polyimide**s (PIs)**, polyamides **(PAs)**, and polyethers **(PEs)** with different donor-linkage-acceptor (D-L-A) units for the systematical study and comparison of both linkage and acceptor effects on the memory behaviors. The synthesis and basic characterization of the obtained aromatic TPA-based polymers were described. Chapter 5 contains conclusions. Besides, the memory characteristics were investigated by I-V measurements and compared. The corresponding morphology study, optical characteristic, electrochemical and spectroelectrochemical properties, and theoretical analysis results were used to demonstrate that the resulting memory behaviors could be elucidated by the charge-transfer mechanism.

Keyword: triphenylamine, memory, highperformance polymers, donor, acceptor,

charge transfer mechanism.

中文摘要

本論文分成五個章節，第一章為總體序論。第二章描述了兩種合成作為記憶體主動層材料的方法。第一種為將電子受體藉由混摻的方式導入含電子施體的高分子 poly-4-methoxytriphenylamine (**P-TPA**) 而得具電子施體與受體的複合材料:**P-TPA:PCBM**。 另一種為將可作為電子受體的蒽醌基團藉由化學共價鍵的方式導入含電子施體的結構再進而聚合而得具電子施體與受體的高分子 poly-**2-**diphenylaminoanthracene-9,10-dione (**P-TPAAQ**) 與 poly-**2-**(4-diphenylaminophenoxy)anthracene-9,10-dione (**P-TPAOAQ**)。第三章係探討分別以具電活性的二胺化合物 2-(bis(4-aminophenyl)amino)anthracene-9,10-dione 與 2-(4-(bis(4-aminophenyl)amino)phenoxy)anthracene-9,10-dione 所合成之含電子施體三苯胺與側鏈上具拉電子能力的蒽醌取代基而得具兩個相互競爭的電子受體基團的新穎性聚醯亞胺 **AQ-PIs** 與 **OAQ-PIs** 所製得之記憶體元件。第四章係以三苯胺作為電子施體的聚醯亞胺(**PIs**)與類似結構但含不同連接基團與電子受體的聚醯胺(**PAs**)與聚醚 (**PEs**)於連接基團與電子受體對於記憶體性質的影響做一有系統的研究與比較。第五章節為結論。上述含三苯胺之芳香族高分子的合成、基本特性皆被研究。此外，所有的記憶體性質皆由其 I-V 的特性來進行探討。並由相關的表面型態分析、光學性質、電化學及光譜電化學分析及理論計算可推論本研究中所得的記憶體性質可由電荷轉移(charge-transfer)機制解釋。

關鍵字： 三苯胺、記憶體、高性能高分子、電子施體、電子受體、電荷轉移機制

TABLE OF CONTENTS

CHAPTER 1

General Introduction

CHAPTER 2

Electrically Bistable Memory devices Derived from Poly(triphenylamine)s Derivatives and its PCBM Hybrid Films

CHAPTER 3

Memory Behaviors Resulted From Functional Polyimide Systems Containing Triphenylamine With Dual Competitive Electron Acceptors

CHAPTER 4

High Performance Polymers
With Different D-L-A Containing
for Memory Application

CHAPTER 5

CONCLUSIONS

LIST OF TABLES

CHAPTER 1

CHAPTER 2

CHAPTER 3

CHAPTER 4

LIST OF FIGURES

CHAPTER 1

CHAPTER 2

CHAPTER 3

CHAPTER 4

CHAPTER 1

General Introduction

1.1 HIGH PERFORMANCE POLYMERS

In nowadays world, polymers are indispensable to our life. Polymers have been widely researched in the 21st century. In particular, high-performance polymers attract lots of attention due to its high thermal stability and good chemical resistance and well mechanical strength which could be modified by introducing different functional groups into the molecular structure. The quest for high-performance polymers began in the late 1950s to meet the demands for military, aerospace, machine-building, electronics, and many industrial applications. Since then, a lot of novel high-performance polymers have been prepared for certain applications. Hill and Walker first found that the incorporation of aromatic segments into a polymer generally results in a tremendous increase in its thermal stability.[1] From this viewpoint, much of the research work has been directed toward aromatic compositions. As the result, high-performance polymers usually tend to contain more aromatic units within structure. Several of these aromatic high-performance polymers have reached commercialization such as aromatic polyamides, polyimides, polyesters, polysulfones, and heterocyclic polymers (Table 1.1). Aromatic polyamides (aramids) and polyimides, such as DuPont's Kevlar fiber and Kapton film, have been well known for a long time and constantly draw much interest more than other high-performance polymers for their several practical properties such as excellent thermal and oxidative stability, high mechanical strength, low flammability, good chemical and radiation resistance, and low dielectric constant (for polyimide).[2-9]

Table 1.1. Some Typical Aromatic High Performance Polymers

Polymer		T_g (℃)	T_m (℃)
Aromatic polyamide			
Kevlar	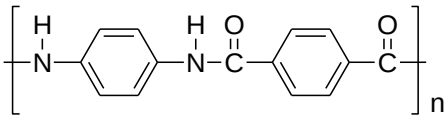	—[a]	—
Nomex	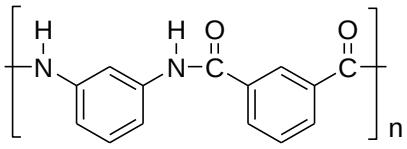	272	435
Aromatic polyimide			
Kapton	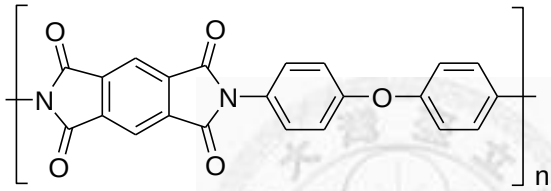	399	—
Upilex R	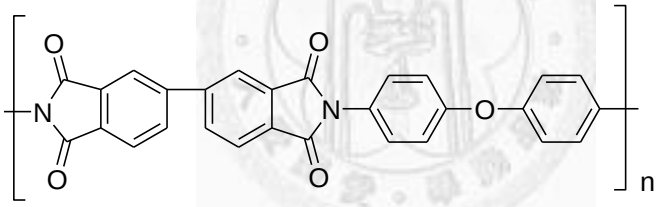	303	—
Aromatic polyester			
U-polymer	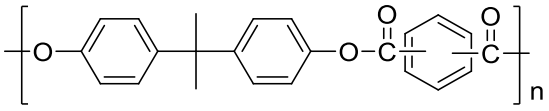	188	—
Aromatic polysulfone			
PST	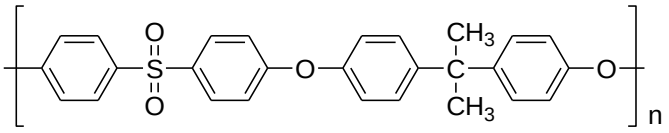	189	—
Aromatic heterocyclic polymer			
PBT	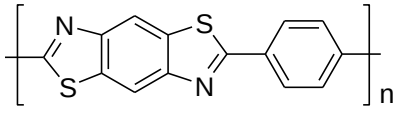	—	—

[a] Not detected

1.1.1 Preparation of Aromatic Polyamides[10]

The properties of aromatic polyamides (aramids) are quite different from those of the aliphatic polyamides (nylons), for instance, thermal resistance and low flammability. In general, they have high melting points above 300 ^{o}C and in many cases higher than 350 ^{o}C. Some of the commercial available aromatic polyamides are collected in Table 1.2. Nomex and Kevlar aramid fibers which were synthesized and commercialized by DuPont are the most well-known. It is renowned for its high thermal stability and typically used to fabricate fire protective textile in early time. In nowadays, it is used as the high modulus and high strength fiber for bulletproof vests, radial tires, ropes, thermal insulating clothing, and advanced composites. Nomex aramid was prepared by DuPont in 1961 as first commercial high-temperature synthetic fiber. It is based on poly(*m*-phenyleneisophthalamide), which contains *meta*-oriented chain segments of the AA-BB configuration. Subsequently, Kevlar aramid was synthesized and commercialized by DuPont in 1972. It is based on poly(*p*-phenyleneterephthalamide), one of the *para*-oriented aromatic polyamides synthesized by S.L. Kwolek (a researcher of DuPont). Kevlar aramid can be prepared in some synthesis routes. The classical procedure contains the low temperature polycondensation of *p*-phenylene diamine and terephthaloyl chloride in an amide solvent such as *N*-methyl-2-pyrrolidone (NMP) with the presence of metal salts like lithium chloride. Kevlar aramid, just like other *para*-oriented aromatic polyamides, is insoluble in conventional solvents except for strong acids such as concentrated sulfuric acid. The most efficient processes for the preparation of aromatic polyamides illustrated in the following pages are concluding the reaction of diacid dichlorides with diamines at low temperature and direct condensation reactions in solution of aromatic diacids with diamines at high temperatures.

1.1.2 High-temperature Solution Methods

In 1971, Ogata[11] reported a superior synthesis route for aromatic polyamides by the direct polycondensation of aromatic diamines with aromatic dicarboxylic acids in the presence of an aryl phosphite and an organic base. In the original publication of this novel synthesis for the preparation of polyamides first reported by Ogata was referred to as a phosphorylation reaction,[12] resulted the low-molecular-weight polymer . Two significant modifications, presented by Yamazaki, were developed by using triphenyl phosphite (TPP) and pyridine as condensing agents[13] and addition of LiCl to the solvent[14] for the reaction and led to a considerable increase in the molecular weight of the produced polymers by promoting the solubility (as shown in scheme 1.1). In order to make further progress from that time, many approaches have been developed to optimize the reaction conditions for increasing the molecular weight of polyamides. For example, Preston and Hofferbert[15] reported that the polymerization temperature was raised from 80 to 100 ^{o}C, and the higher temperature was subsequently suitable for the synthesis of various polyamides. In 1982, Higashi et al.[16] demonstrated that poly(*p*-phenylene terephthalamide) (Kevlar) with inherent viscosity of 4.5 dL/g could be received by using a solvent medium with presence of both LiCl and $CaCl_2$. Krigbaum and coworkers[17-19] have referred to these as Higashi conditions in a series of studies, and they claimed that[20,21] the inherent viscosity of Kevlar using Higashi conditions could be enhanced to of 6.2 dL/g via increasing the reaction temperature from 100 to 115 ^{o}C. In general, the direct polycondensation could be carried out by high-temperature heating method, adding TPP as the condensation promoter, thus diminishing the reaction times from hours to minutes. It is the most famous and facile procedure for preparing high-molecular-weight aromatic polyamides.

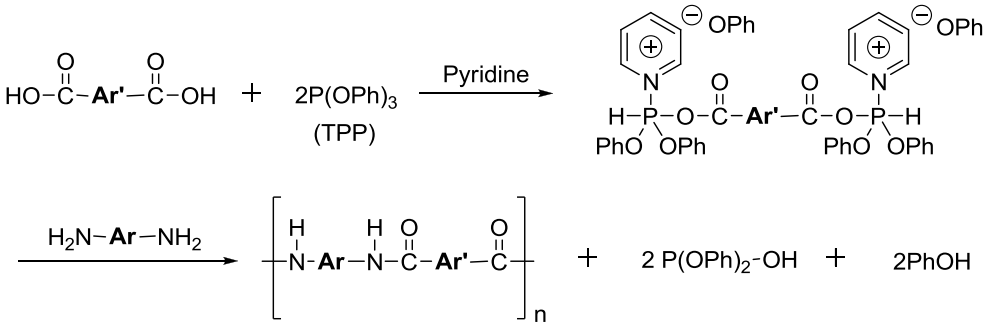

Scheme 1.1 Direct polycondensation.

Table 1.2. Commercially Available Aromatic Polyamides

Polymer		T_g (°C)	T_m (°C)
Kevlar	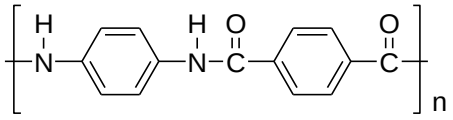	—	—[a]
PBA	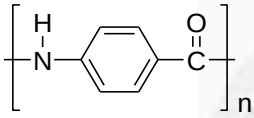	—	—
KM-21	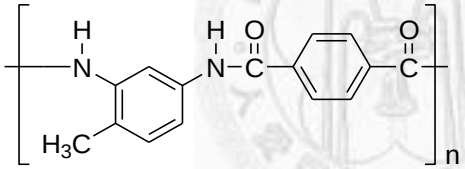	—	—
Nomex	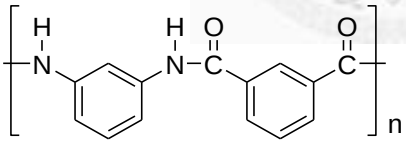	272	435
MeMPD-I	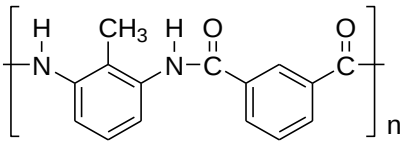	260	405

[a] Not detected.

1.1.3 Low-temperature Solution Methods[22]

The low temperature solution method has priority when the diacid chloride can be easily obtained from the corresponding aromatic diacid. For example, Kavlar was prepared in NMP by *p*-phenylenediamine (PPD) and terephthaloyl dichloride (TPC) with some solubility prompters ($CaCl_2$) (as shown in scheme 1.2). The major

disadvantage of this way is the monomer with high purity is necessary for getting high molecular weight of polyamide.[23]

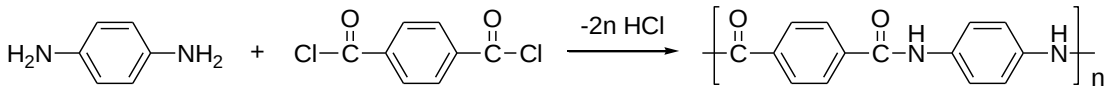

Scheme 1.2

1.1.4 Preparation of Aromatic Polyimides

Aromatic polyimides can be regarded as an indispensable materials because of their many excellent characteristics and often replace glass and metals in many industrial usages, especially in the semiconductor and electric packaging industry. The outstanding properties of aromatic polyimides result from their rigid backbones and strong intramolecular and intermolecular interactions between the polymer chains due to the charge transfer complex formation between electron-abounding (diamine moiety) and electron-lacking (dianhydride moiety) segments. Some of the commercial available aromatic polyimides are summarized in Table 1.3. In 1956, Endrey, a researcher of DuPont, received the assignment for seeking an aromatic polyimide film prepared via a soluble intermediate polymeric precursor. He successfully evaluated several solvents that dimethyl formamide (DMF) was an excellent solvent and synthesized the first poly(amic acid) film and demonstrated thermal conversion to polyimide film based on oxydianiline-pyromellitic dianhydride (ODA-PMDA). In 1965, the first commercial aromatic polyimide film was synthesized and named as Kapton, widely used in a lot of applications such as substrate for flexible printed circuit and insulation for transformer and capacitor. In addition, other significant aromatic polyimides have been prepared such as the Upilex series derived from biphenyl dianhydride (BPDA) invented by Ube industries. LARC-TPI is a thermoplastic polyimide developed by NASA Langley Research Center, primarily as a high temperature adhesive. Occidental Chemical Co. pioneered the synthesis of

oxydiphthalic dianhydride (ODPA) and defined the properties of ODPA-based polyimides. Aromatic polyimides can be prepared from a variety of starting materials, by a variety of synthetic routes. The typical synthetic methods are shown as the following. Polymerization of diamines and dianhydrides in the classic two-stage method of polyimides synthesis, an aromatic tetracarboxylic dianhydride is added to a solution of aromatic diamine in a polar aprotic solvent. The generated soluble poly(amic acid) can be fabricated into shaped products, and then cyclodehydrated to the corresponding polyimide by extended heating at elevated temperatures (thermal imidization) or by treatment with chemical dehydrating agents (chemical imidization) (as shown in scheme 1.3).[24-27] In addition, a simple one-step preparation method of soluble polyimides with high molecular weight was accomplished by heating to 200 ^{o}C in *m*-cresol.[28]

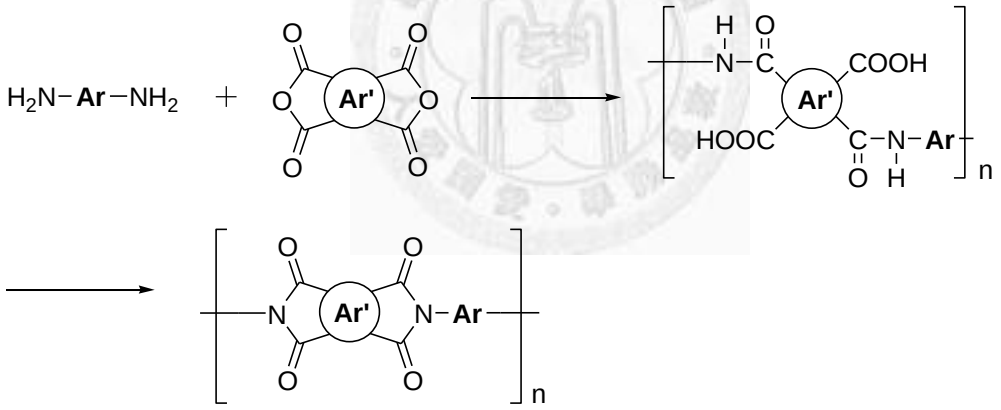

Scheme 1.3 Two-step method of polyimides synthesis.

Table 1.3. Commercially Available Aromatic Polyimides

Polymer		T_g (°C)	T_m (°C)
Kapton	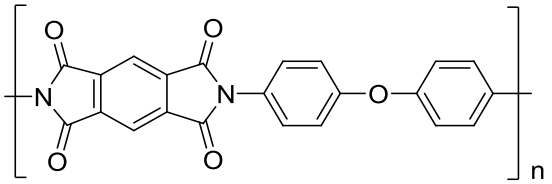	399	—[a]
LARC-TPI	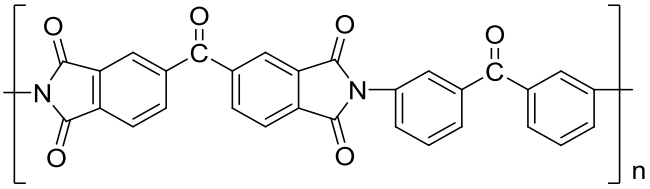	264	—
PIS	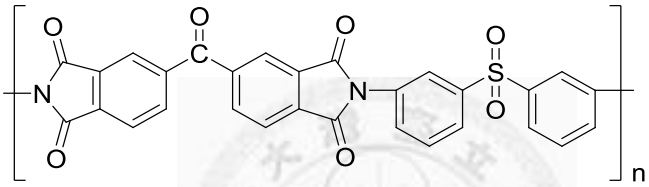	273	—
Ultem	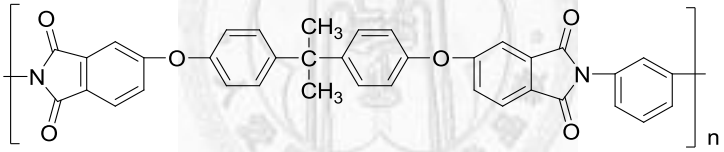	217	—

[a] Not detected.

1.2 Introduction to Polymer Memory

1.2.1 General Concepts

In the field of Information of Technology (IT), the memory is usually defined as a storage device or recording medium that retains retrievable digital data over a time interval. An electronic memory is fast in response and compact in size, and can be read and written when connected to a central processing unit. This feature distinguishes the electronic memory from other forms of storage, such as CD, DVD, ZIP disk, floppy disk, hard disk and video/audio tape. Differ from conventional memory, which were depended on semiconductor-based integrated circuits, new polymeric materials contains electrical bistability resulting from certain intrinsic properties, such as polarity, magnetism, conformation or especially conductivity, in response to the applied electric field.[29]

Electronic memories can be divided into two primary classifications by its volatility: volatile and non-volatile memories. Volatile type loses the stored data as soon as the system is turned off. It needs a constant power supply to keep the stored information. However, non-volatile type can retain the stored information even when the electrical power supply has been removed. They can be further divided into sub-categories, as shown in Figure 1.1, with the write-once read-many times (WORM) memory, the non-volatile and rewritable (flash) memory. The different between them is that WORM type can remain data permanently and not allow to erase data once it has written, and it works as CD-R, DVD±R. Another flash type memory stored state can be electrically reprogrammed and it has the ability to write, read, erase and retain the stored data, and it have been used in many portable electronic systems, such as mobile computer, PDA, cell-phone and digital camera etc. On the contrary, volatile type includes the dynamic random access memory (DRAM) and the static random access

memory (SRAM). DRAM exhibits ability to write, read, erase and refresh the electric states. The SRAM possess longer storage time after removing the electrical field.[30-32] Nowadays, DRAM is used as main memory of most computers.

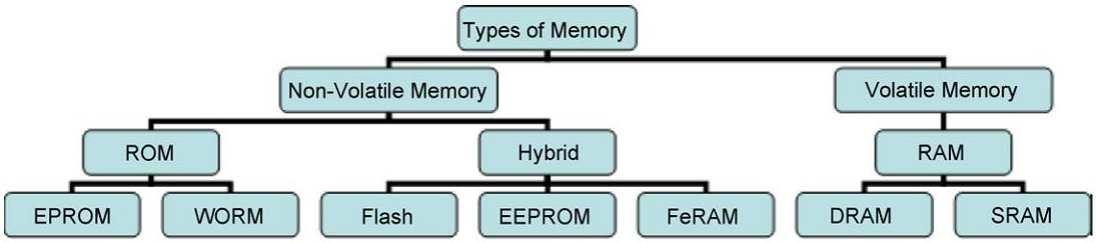

Figure 1.1. Classification of electronic memories.

1.2.2 Fundamentals and Device Architecture of Resistor-type Polymeric Memory

Polymer is regarded as promising candidate for memory application for the advantages of the low cost solution process ability and the capability for fabricating three-dimensional device. Instead of the more elaborated process of vacuum evaporation and deposition of inorganic and organic molecule component, solution processes such as spin-coating, dip-coating, roller-coating and ink-jet printing can be used to deposit polymer on kinds of substrates in facile.[33] In the typical device, polymer thin film is used as the storage medium and sandwiched between two electrode as metal-insulator-metal (MIM) structure, as shown in Figure 1.2.

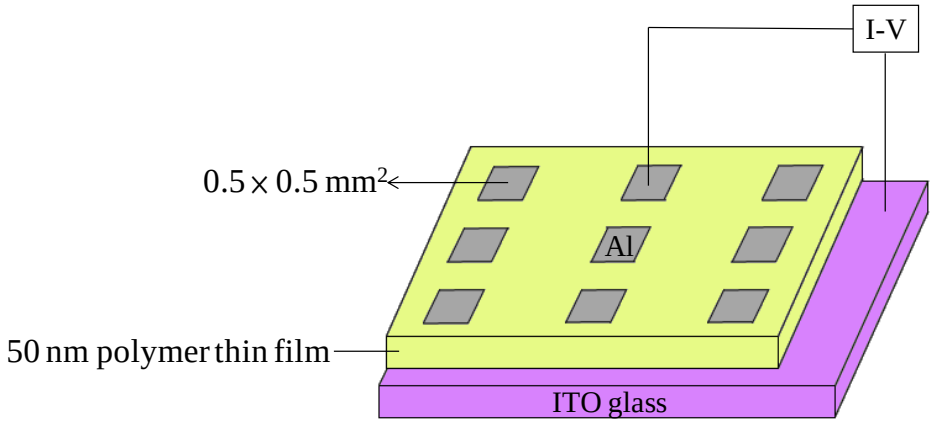

Figure 1.2. Architecture of MIM sandwich polymer memory device.

Devices including switchable resistive materials are generically classified as resistor-type memory, or resistive random access memory (RRAM). It's different from the conventional memory technologies with the memory effects associated with a especial cell structure (e.g. FET), resistance change memory stores data in an entirely different form. For example, data is stored based on the electrical bistability (ON and OFF states) of materials resulting from changes in certain intrinsic properties, such as charge transfer, phase change, conformation change and reduction–oxidation (redox), in response to the applied electric field as low conductive state and high conductive state and then can be defined as "0" or "1" for digital memory application.[29]

When discussing about polymeric memory devices, some basic parameters of importance to the performance of polymer RRAM device include: (i) ON/OFF current ratio (a higher value is essential for the device to function with minimal misreading error), (ii) switching (write and erase) time, (iii) read time, (iv) retention ability for non-volatile RRAM, (v) programming (or WRER) cycles and long-term stability, (vi) stability under electrical field stress and under read pulses. Examples of evaluation results for some of these parameters are shown in Figure 1.3. Unlike those capacitor-type and transistor-type polymer memories, which still need to be integrated to basic CMOS logic circuits,[34] the RRAMs are not based on silicon CMOS technology.

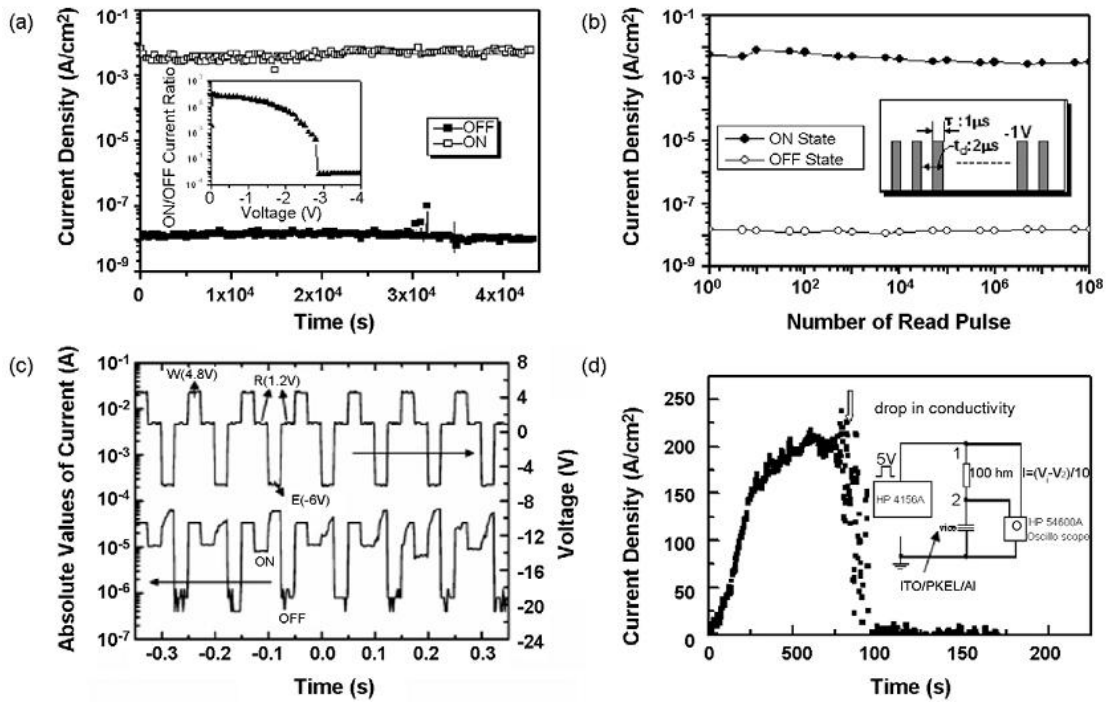

Figure 1.3. Some evaluation parameters for molecular/polymer memories. (a) Stability under voltage stress and ON/OFF ratio (inset); (b) Number of read pulses; (c) Write–read–erase–read (WRER) cycles; (d) Switching time measurement.[34-36]

1.3 Mechanisms of Polymer Memory

RRAMs are based on conductivity of the active layer change in response to the applied electric field. The electrical conduction mechanism in polymers is much more complex than in ordered inorganic materials. It cannot be appropriately explained by the basis of band theory, due to most polymers are amorphous in nature.[37] As the result, the conduction in polymers is normally explained by (i) intrinsic charge carrier generation and (ii) charge carrier injection from contacts at high fields. The density of intrinsic carriers in polymers except for doped conducting polymers is usually low and the carriers are usually trapped by localized states at room temperature. The local field may promote the detrapping process thus abruptly enhance the conductivity of the polymer thin film.[37]

1.3.1 Filamentary Mechanism

In general, the ON state current is highly localized to a small fraction of the device area, the result is defined as filamentary conduction.[38,39] There are two extensive reported types of filamentary conduction in polymeric RRAM systems as shown in Figure 1.4. In some cases, the resulting filaments could be observed by an optical or scanning electron microscope. One type is carbon-rich filaments which is related to the formation of local degradation of polymer films;[40] the other one is related to metallic filaments resulting from local fusing, migrating or sputtering of the electrode into the thin film due to the applied electrical field.[38] Once the filament present in the thin film, (i) the ON state current shows metallic I-V characteristics,[39] and (ii) the injected current will be almost independent to the device area which can be contributed to the dimension of the filament is much smaller than the device area.[40] The parameters to the occurrence of filament are controlled by electrode thickness, film thickness and the nature of the ambient atmosphere.

Bistable switching and memory behavior from devices based on a thermoplastic resin derived from vinylidene chloride, were prepared in 1970.[40] Since then, kinds of insulating polymers with threshold and memory switchable characteristic have been widely reported, such as polystyrene (PS),[40] polyethylene (PE),[41] polymethylmethacrylate (PMMA),[42] polyaniline (PANI),[43] polyvinylfluoride (PVF)[44] and polyacrylonitrile (PAN) etc.[45] Most of the devices with switching ability from filamentary conduction are difficult to control and reproduce. However, some tunable filamentary conduction have been demonstrated in polymers for non-volatile memory application.[46]

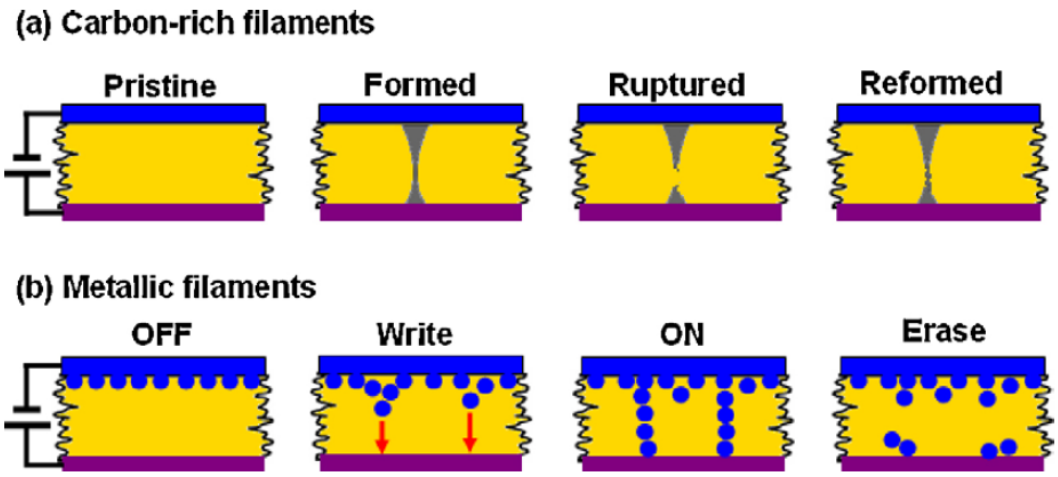

Figure 1.4. Schematic illustration of the formation of (a) carbon-rich filaments and (b) metallic filaments, and the relevant switching effects.[29]

1.3.2 Trapping-Detrapping Mechanism

As the contact between electrode and polymer is Ohmic contact and the polymer is trap-free, the accumulation of charge carriers around the electrode constructs a space charge region. Intrinsic repulsion between charges confine the amount of charges injected into the thin film layer, and the resulting current is so-called space charge limited current (SCLC). On the other hand, once there are traps in the polymer, the value of SCLC will reduce for several orders. Generally, space charges in polymer

thin films are generated from three ways, such as (i) electron or/and hole injection from electrode, (ii) ionized dopants in interfacial depletion region and (iii) accumulation of free ions at the surface of electrode. Traps may be occurred both in the bulk of the polymer and at the interface which will reduce the mobility of the carrier or furthermore affect charge injection into the film.[47]

The mechanism is illustrated in Figure 1.5. As soon as the applied voltage overcomes the Schottky barrier, carriers are generated nearby the anode increasing the accumulation of space charges and then build up an electrical field. Therefore, the SCLC model dominates in this region. At around the threshold voltage, some of the traps will be filled by the generated carriers and the Al cathode also becomes an electron-injecting contact to the charged "HOMOs" or radical cations, forming double injections and subsequently increasing the concentration and mobility of the carriers. The resulting current enhances rapidly then the device can be switched to ON state. According to recent studies, the traps are always related to the HOMO and LUMO energy level of the donor-acceptor copolymers and work function of the electrodes. Another influential factor for determining the type of memory is the trap depth of acceptor or donor group. For example, the PFOxPy has been designed and exhibit DRAM property.[32]

Moreover, the conduction mechanism in polymer-particle nano-trap RRAM has been investigated in details experimentally and theoretically. In the Al/AuNP:PS/Al memory device, AuNP exhibits a work function of around 5.1 eV, which is lower than the LUMO of PS. Therefore, AuNP can be treated as a trap in PS. As a consequence, the current in the memory, as shown in Figure 1.6, can be summarized to regions I (Ohmic conduction with high resistance), II (SCLC model), III (almost fill up traps, and the current is proportional to exponential of voltage), and IV (Ohmic conduction with low resistance) which is indicated the switching mechanism be explained by the

Trapping-Detrapping mechanism.[48]

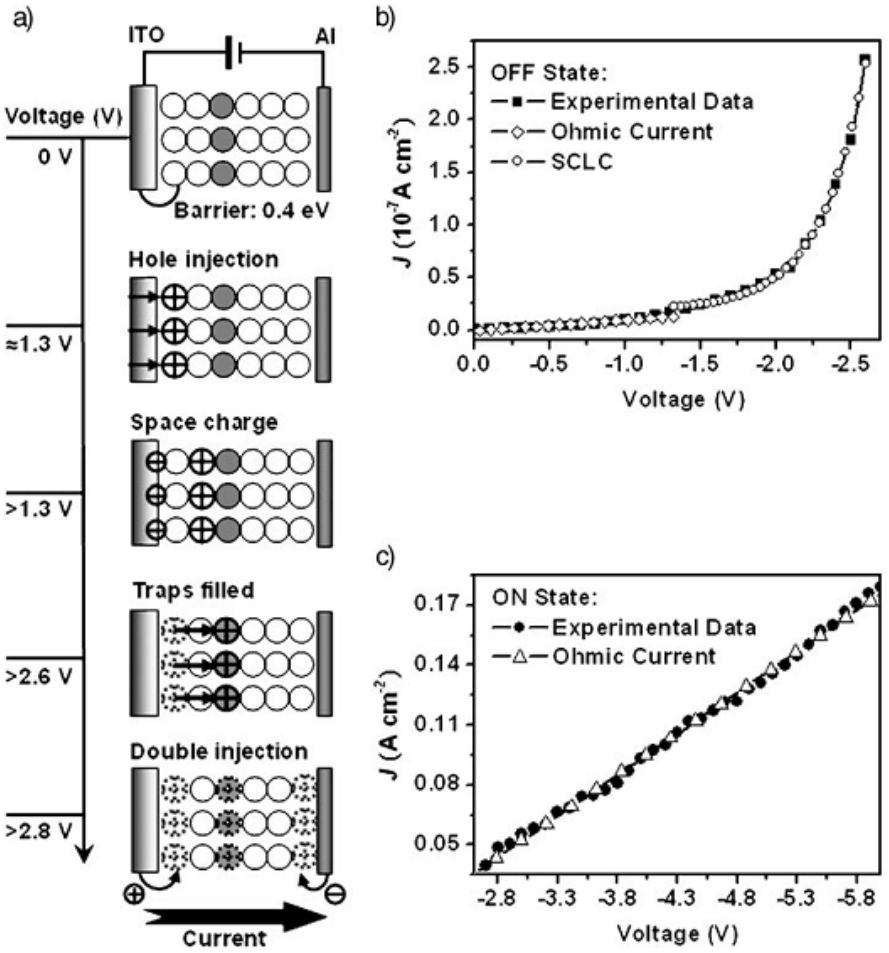

Figure 1.5. (a) Operational mechanism of the memory. Experimental and fitted J–V curves of the ITO/PFOxPy/Al device (b) OFF state with the Ohmic current (<1.3 V) and SCLC (1.3–2.6 V) models, (c) ON state with the Ohmic current model (>2.8 V).

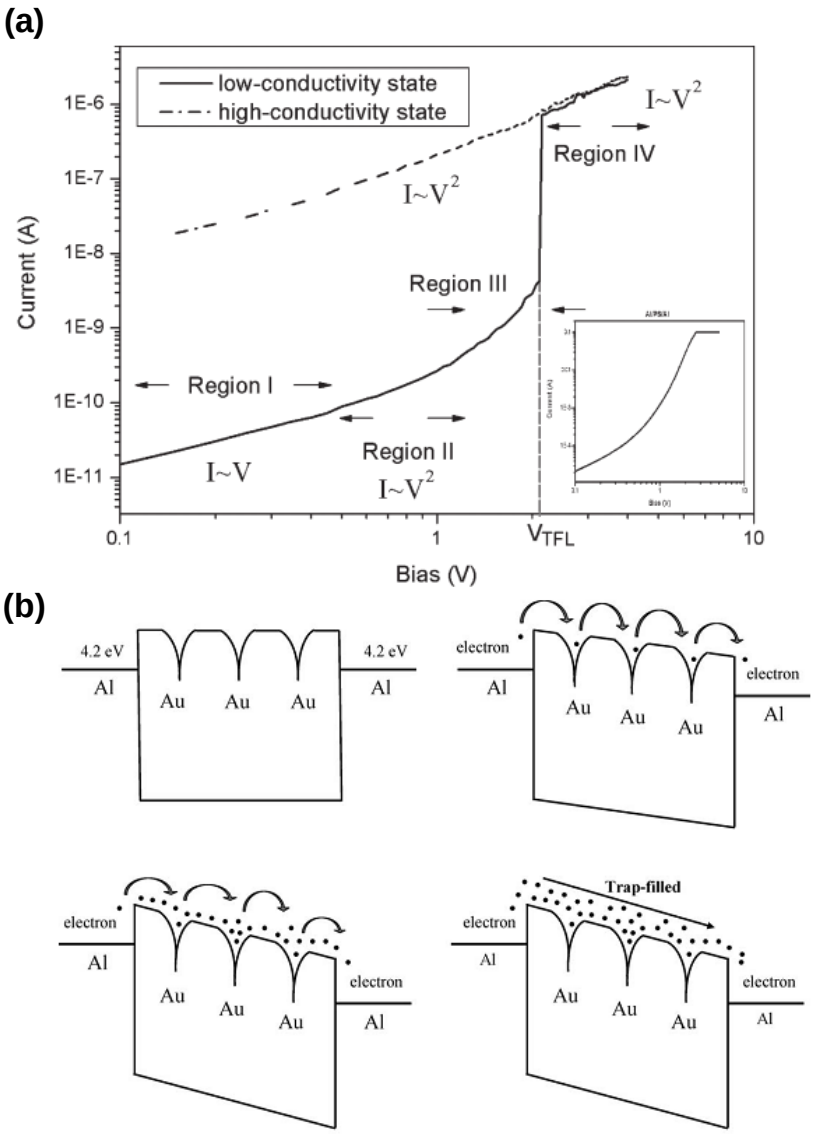

Figure 1.6. (a) I–V (in log scale) curves of the Al/Au:NP/Al bistable memory device. (b) Schematic band diagrams for the transport mechanism of trap-filled SCLC: (i) Region I: thermally generated carrier conduction, (ii) Region II: with traps, (iii) Region III: nearly filled, and (iv) Region IV: traps filled.

1.3.3 Charge Transfer Mechanism

The charge transfer (CT) complex is defined as an electron donor (D)–electron acceptor (A) complex, characterized by electronic transition(s) to an excited state in which there is a partial transfer of electronic charge from the donor to the acceptor moiety.[49] The switching and electrical memory phenomena of CT complexes was

observed in Cu-TCNQ system in the first instance.[50] Subsequently, a wide variety of organometallic and all-organic CT complexes have been synthesized for applying in non-volatile organic memories.[51] The formation of an organic conductor from a donor, acceptor, and mixed donor–acceptor molecules is depicted schematically in Figure 1.7.[52]

For a stable CT material, a relationship between ionic binding and conductivity exists. For instance, in the 1:l TCNQ charge transfer salts, donors, which are characterized by small size and low ionization potential, form strongly ionic salts with TCNQ. Under this situation, there is complete charge transfer (or with the CT degree value, $\delta > 0.7$) from the donor to TCNQ and, therefore, these ionic salts are insulators (due to Coulomb interactions). On the opposite, donors which are too large and/or with too high ionization potential will result neutral molecular solids ($\delta < 0.4$). In particular, the situation between above two extreme situations, donors with intermediate size and ionization potential tend to form weakly ionic salts with TCNQ. These partially ionic, mixed-valence salts tend to have incomplete charge transfer ($0.4<\delta<0.7$) and are likely to exhibit high conductivity.[52-54]

Functional polyimide containing donor and acceptor moieties has been firstly applied to polymeric memory device by Kang *et al*. They investigated the charge transfer route induced by the electrical field, which is demonstrated in Figure 1.8, then reported a DRAM fabricated by **TP6F-PI**.[55-56] Triphenylamine (TPA) plays the role of electron donor, and the phthalimide ring acts as electron acceptor. According to the result of molecular simulation performed by Gaussian package program by means of the density functional theory (DFT) method at the B3LYP level of theory (Beckesstyle three-parameter density functional theory using the Lee-Yang-Parr correlation functional) with the 6-31G(d) basic set, the HOMO is located on donor moiety meanwhile the first and second LUMOs are located on acceptor moiety. Charge

transfer can occur indirectly, some electrons at the HOMO will transfer to the empty LUMO3 within the donor moiety to form excited state then to LUMO for becoming charge transfer state at the threshold voltage. However, charge transfer can also occur directly from HOMO to LUMO2 and LUMO then become conductive CT complex. As the result, the device will be switched from OFF state to ON state.

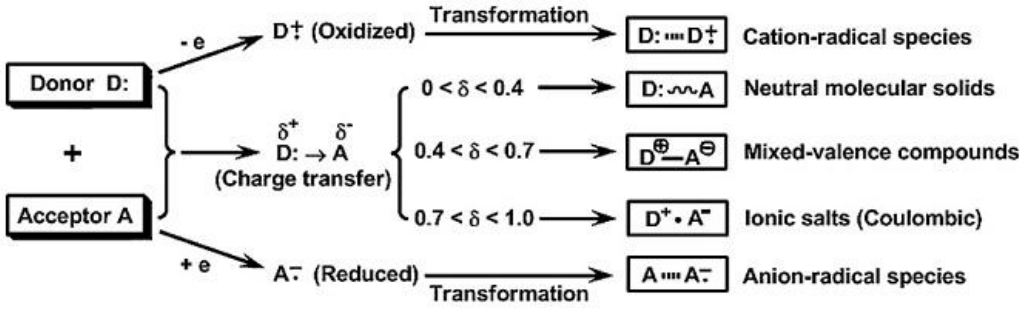

Figure 1.7. Schematic representation of the formation of ion-radical species and charge transfer complexes.[52]

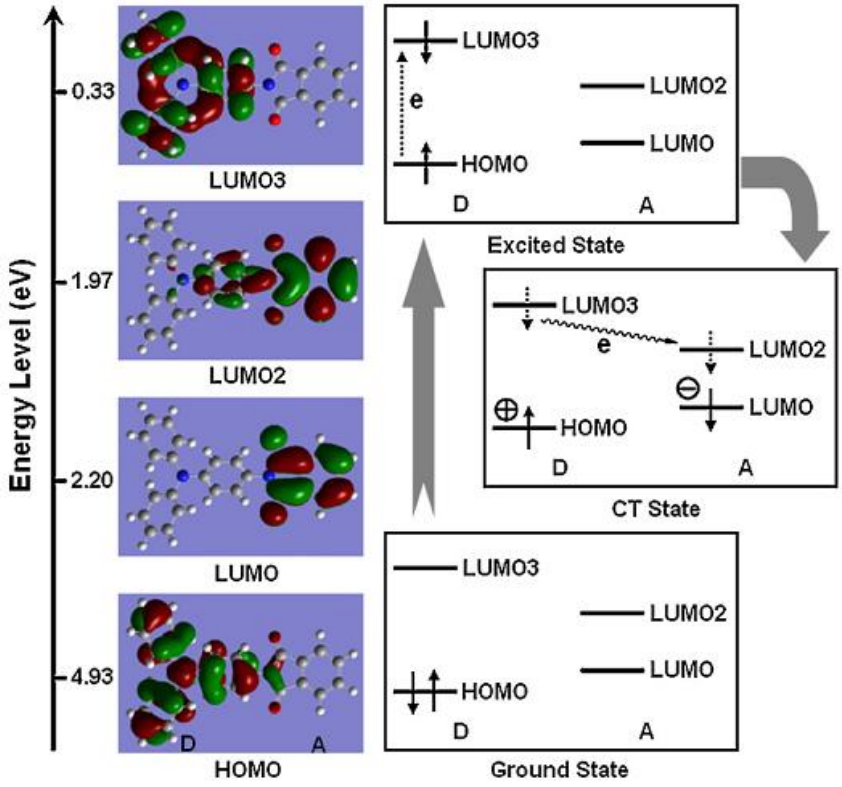

Figure 1.8. Molecular orbitals (left) of the basic unit of TP6F–PI and the transitions (right) from the ground state to the charge transfer state induced by the electric field.[56]

1.4 Evolution of Polymer Memory

The donor–acceptor containing polymers are widely researched recently for resistive switching memory applications including polymer composites conjugated polymers, non-conjugated pendent polymers, and functional polyimides, as shown in Figure 1.9.[57]

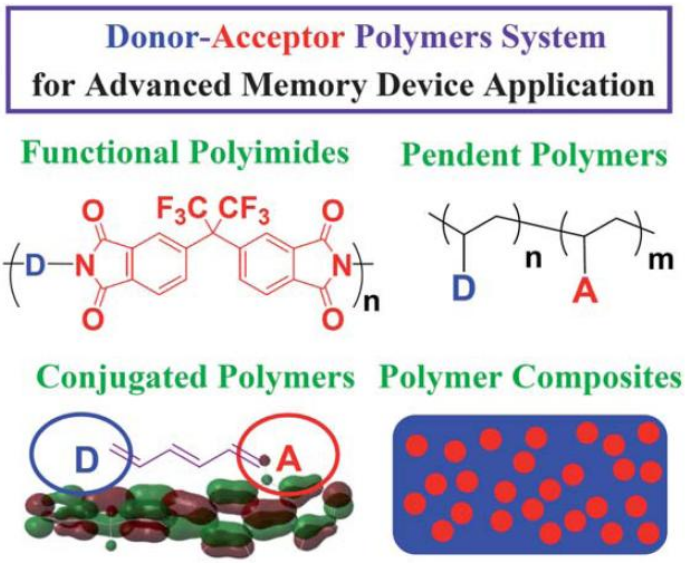

Figure 1.9. Molecular structures of donor–acceptor polymer systems for advanced memory device applications.[57]

1.4.1 Polymer Composites

The hybrid composites were extensively prepared for memory device applications. The supplementary component such as organic molecule or nano materials could be viewed as the data storage media or have the electronic activated domain which is dispersed in the polymer matrix. The operating mechanism of polymer hybrid composite can be attributed to charge transfer or trapping-detrapping for memory application. The domain size of the electronic activated material in the polymer matrix is the key issue for the nano-scale memory device.

Yang and co-workers proposed the memory device based on blending well-dispersed capped-gold (Au) nano-particles and aromatic 8-hydroxy quinoline (8-HQ) compound within a polystyrene (PS) matrix.[31] Furthermore, small organic molecule can be also regarded as the charge transfer medium, for example, they subsequently reported another organic electrically bistable nonvolatile WORM device based on PCBM:TTF:PS composited film. The operating mechanism is attributed to field induced charge transfer from the donor TTF to acceptor PCBM.[58]

Afterward, Kang's group proposed the **PVK-CNT** composite based memory devices. The devices exhibit insulator, WORM, and conductor controlled by the amount of CNT in the hybrid film. The switching mechanism of the WORM device can be considered as electronic trapping in the carbon nanotubes within the both electronic donating and hole transporting PVK matrix.[59] Moreover, functional block copolymers were a candidate for hybrid composite memory devices due to the ability to control the domain size of the fullerene through certain physical interaction.[60]

1.4.2 Conjugated Polymers

It has long be known, kinds of π-conjugated polymeric materials have been developed for memory devices applications. The sandwich device ITO/**PFOxPy**/Al, containing electron donor (fluorine moiety) and electron acceptor (oxadiazole and bipyridine moieties), could be switched from the low conductivity state to the high conductivity state. The device exhibit low reading, writing, erasing voltages and a short retention time of the ON state. Therefore, this conjugated copolymer fulfilled the requirement for DRAM. The switching behavior was explained by trapping-detrapping mechanism.[61]

Moreover, the fluorene and pendent TPA donors and pyridine acceptors containing conjugated polymer **F12TPN** was applied for WORM memory device. The injected hole could pass through the positive continuous channel along the polymer chain then

be trapped by the pyridine acceptors. The detrapping process of the filled traps could not be easily proceed via any process, leading to the WORM property.[62]

Besides, the device based on conjugated poly[9,9-bis (4-diphenylaminophenyl)-2,7-fluorene] donors covalently bonded with Disperse Red 1 acceptors (**DR1-PDPAF-DR1**) possessed the fresh type memory characteristic. The electron at HOMO could be excited then transfer to LUMO1 or LUMO2 and raised the conductivity resulted from the charge separation state.[63] Furthermore, TPA-based conjugated polyazomethine covalently grafted with graphene oxide (**TPAPAM-GO**) was designed for non-volatile rewritable memory application. Electrons migrated from the HOMO of the hole transporting polymer **TPAPAM** into LUMO of graphene layer by intramolecular CT interaction then provided the charge transport pathways and switched the device from the OFF to ON state. The excited electron can be separated and delocalized in graphene nanosheets then stabilize the CT state of **TPAPAM-GO**, resulting the non-volatile characteristic.[64]

Meanwhile, a typical WORM memory device could be derived from polyfluorene based copolymers containing the pendent electron-donating TPA and electron-withdrawing cyano groups. The operating mechanism was resulting from the positive charges on the TPA or fluorene moieties were rapidly consumed by the cyano groups then caused the increase in conductivity.[65]

On the other hand, Ree's group reported all π-conjugated polymer based on poly(diethyl dipropargylmalonate) (**PDEDPM**), or polyaniline (**PAN)** derivatives applying in RRAM devices. These devices include DRAM and WORM type depending on the film thickness.[66]

In general, the introduction of variety electron acceptors into conjugated polymeric donors significantly influences the memory behaviors, which can either furnish a extra trapping site or provide the CT conducting channel in the electrical switching.

The stability of charge trapping or CT complex process governs the volatility of memory device.

1.4.3 Non-conjugated Polymers With Specific Pendent Groups

A wide range of vinyl polymers consisted of side-chain donor–acceptor have been intensively investigated and used for memory applications. As the non-conjugated polymers generally exhibit greater solubility than conjugated polymers, which is facilitating their application to solution-processed memory devices. According to this view point, vinyl polymers containing charge transported pendant groups have been explored for memory application.

The carbazole groups were widely used in the molecular design as the role for electron-donating and hole-transporting and the corresponding memory effect was obtained by incorporating suitable acceptors in the structures. Kang and coworkers designed the non-conjugated copolymers containing pendent carbazole donor and europium complex acceptor (**PKEu**) that could reach the requirement of non-volatile electrically bistable memory devices.[67] Furthermore, the additional incorporation of the pendent 1,3,4-oxdiazole (Ox) group into methacrylate copolymer consisting of a carbazole and Eu complex, named **PCzOxEu**, exhibited a significant improvement in performance under ambient conditions, leading to a longer retention time and higher ON/OFF current ratio.[68] At the threshold voltage, the resultant CT complex create numbers of conducting channels which is mainly caused by holes hopping between the neighboring carbazole units) switched the device to the ON state.[34,69] The large dipole moment of the Ox moiety acted as a mediator to decrease the internal energy barrier and facilitate carrier transport, which gave assistance to keep of the separated charges for the longer retention time with improved device stability.[68] The same group also incorporated C_{60} into PVK with covalent bond as the electron acceptor. The

device of Al/**PVK-C_{60}**/ITO performed as nonvolatile flash memory. The CT occurs when then voltage bias is applied then forms the conducting channels by charged HOMO of Cz and charged LUMO of C_{60}.[34]

Meanwhile, Chen's group reported the nonconjugated polymers containing pedent electron-donating carbozole units (VPK) and electron-withdrawing oxadiazole derivatives units (OXD or BOXD) with different donor/acceptor ratios for memory device applications.[69] The low HOMO energy level of OXD or BOXD units as compared to VPK units created the extra trapping environment. Therefore, distinct electrical characteristics changed between the diode, volatile memory, and insulator tuning by the ratios of donor/acceptor. The unstable ON state of volatile nature SRAM in the **P(VPK_8OXD_2)** or **P(VPK_8BOXD_2)** device was due to the shallow trapped holes with spontaneous back transferring of charge carriers when removing the electric field.[38] Besides, the tunable switching behaviors were explored through the distinct ratio of pendant TPA donors and BOXD acceptors.[70] The relative extent of charge trapping/spontaneously back-transferring of trapped carriers controlled the switching behavior. The additional pendent cyano substituted TPA donors groups exhibited NDR behavior probably due to the interaction of the Al atoms with the cyano group.[70]

Moreover, other pendant group containing nonconjugated polymers such as grafted PVK (**PVDR**) substituted by CN or NO_2 as acceptor,[71] pendent azobenzene chromophores for D-A structures,[72,73] demonstrated the nonvolatile characteristic, the donor and acceptor moieties played the roles in elucidating the mechanism of charge transfer or space charges and traps effect for the switchable polymers.

1.4.4 Functional High Performance Polymers

Functional high performance polymers such as polyimides (PI), polyamide (PA) are favorable materials for microelectronic device applications due to their high performance properties. Therefore, various investigations among the development of all types of PI switching behaviors have been reported widely.

The idea of using functional PI as active layer for memory application was first emerged in 2006 reported by Kang's group. **TP6F-PI** with TPA moieties as electron donor and phthalicimide ring as electron acceptor exhibited DRAM behavior.[56] Moreover, they found that the conformational change between donor and acceptor moieties induced by charge transfer could provide an energy barrier for back electron transfer from CT state to ground state then extend the retention time of the ON state.[74] Both **OXTA-PI** and **AZTA-PI** containing pendent TPA donor exhibit WORM memory characteristic in Al/polymer/ITO sandwich devices due to the orthogonal overlap in orbitals between acceptor and pendant donor which could provide a higher energy barrier for back transfer further maintain the device in the ON state after removing the applied electrical field.[75.76] Furthermore, Chen and Ueda reported the polymer memory devices based on **PI(AAPT-6FDA)** derived from 4-amino-4'-(p-aminophenoxy)triphenylamine **(**AAPT) and 4,4'-(hexafluoroisopropylidene)diphthalic anhydride (6FDA) and **PI(APT-6FDA)** from 4,4'-bis(*p*-amino-phenoxy)triphenylamine (APT) and 6FDA. The main difference between two polymer is there are two phenoxyl linkages (L) between TPA (D) and phthalimide (A) moieties in **PI(APT-6FDA)** but only one in **PI(AAPT-6FDA)**. According to their results, the **PI(APT-6FDA)** containing $(L\text{-}D\text{-}L\text{-}A)_n$ structure showed a SRAM property and **PI(AAPT-6FDA)** containing $(D\text{-}L\text{-}A)_n$ structure revealed a DRAM property. The dual-mediated phenoxyl linkage of **PI(APT-6FDA)** led to the more twist conformation compared to the

monosubstituted **PI(AAPT-6FDA)**. It thus produced a higher energy barrier then delaying back CT and the elucidated the SRAM behavior.[77]

Moreover, Ree and our lab fabricated polymer memory device based on TPA containing polyimide system, the results showed that the memory device exhibited nonvolatile write-once-read-many-times (WORM) and volatile DRAM (dynamic random access memory) characteristics depending on the thickness of polymer films.[78] Recently, our lab reported that the functional polyimide **(**$(OMe)_2$TPPA-6FPI (**6FPI**) and the polyamide $(OMe)_2$TPPA-6FPA (**6FPA**) consisting of electron-donating *N*,*N'*-bis(4-aminophenyl)-*N*,*N'*-di(4-methoxylphenyl) and 1,4-phenylenediamine [$(OMe)_2$TPPA-diamine] for memory application. **6FPI** exhibited dynamic random access memory (DRAM) performance, whereas **6FPA** showed static random access memory (SRAM) behavior. The probable reasons are that the **6FPA** structure exhibits higher dipole moment and nonplanar linkage resulted in specific SRAM property, which was different from $(OMe)_2$TPPA-6FPI system.[79] Moreover, for comparison study in acceptor effect, the corresponding $(OMe)_2$TPPA-ODPI (**ODPI**), $(OMe)_2$TPPA-DSPI (**DSPI**), $(OMe)_2$TPPA-PMPI (**PMPI**), and $(OMe)_2$TPPA-NPPI (**NPPI**) with different dianhydride moiety were synthesized for memory device application. With the electron-withdrawing moiety intensity of polyimides increasing, the retention time of corresponding memory device increases. **ODPI** didn't have memory properties, and **PMPI** with stronger electron-withdrawing linkage revealed SRAM behavior. **NPPI** with the strongest electron-withdrawing linkage showed WORM type non-volatile memory behavior. Interestingly, **DSPI** have the LUMO energy levels between **6FPI** and **PMPI** but revealed non-volatile WORM behavior resulting from the highest dipole moment 5.45D.[80]

1.5 Research Motivations

Donor-acceptor containing polymers have shown great potential for digital memory devices applications. However, the relations between effect of donor-acceptor in the molecular structure and their memory properties have not been fully investigated systematic. Therefore, the primary goal of this thesis is to design and synthesize series of high performance aromatic polymers containing different donor and acceptor moiety or different linkage group between donor and acceptor for discussing the donor-acceptor and linkage group effect to the memory property.

In the first part, we would to explore two distinct approaches, as shown in Figure 1.10, to fabricate the memory devices by blending the PCBM as the acceptor with the donor-containing **P-TPA**, or incorporating the electron acceptor anthrquinone covalently resulting **P-TPAAQ** and **P-TPAOAQ**, respectively. The goal of this part of research is developing the tunable memory characteristics due by the structural design of the electrical functionality and linkage group effect of the TPA-based polymer and morphological control over the embedded PCBM.

The TPA-containing with dual electron acceptor polyimides **AQ-PIs** and **OAQ-PIs** as shown in Figure 1.11, were used to fabricate the memory devices. In addition to the carbonyl or phthalimide acceptor moiety in main chain, the anthraquinone as pendent acceptor group was also introduced to TPA via ether linkage or directly attached into the backbone. The electron charge withdrawing capability of these two acceptors could be studied by molecular simulation, electrochemical, and spectroelectrochemical behaviors. Linkage effect and the electron-withdrawing effect would be investigated in second part of this thesis.

In the final topic of this thesis, three series of polymers with same TPA donor but containing different acceptor or different linkage group between donor and acceptor

unit, as shown in Figure 1.12, will be prepared for high-performance polymeric memory devices and the following measurements. Then, the effect of different electro-withdrawing ability or different chain conformation caused distinct linkage group to their memory properties would be investigated systematically.

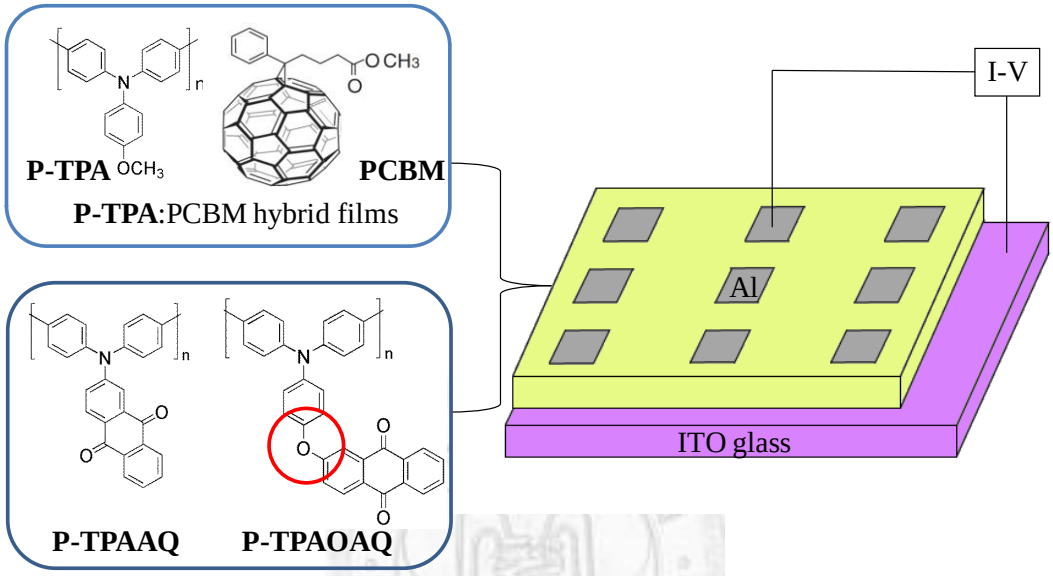

Figure 1.10. Memory devices based on poly(triphenylamine)s derivatives and its PCBM hybrid film.

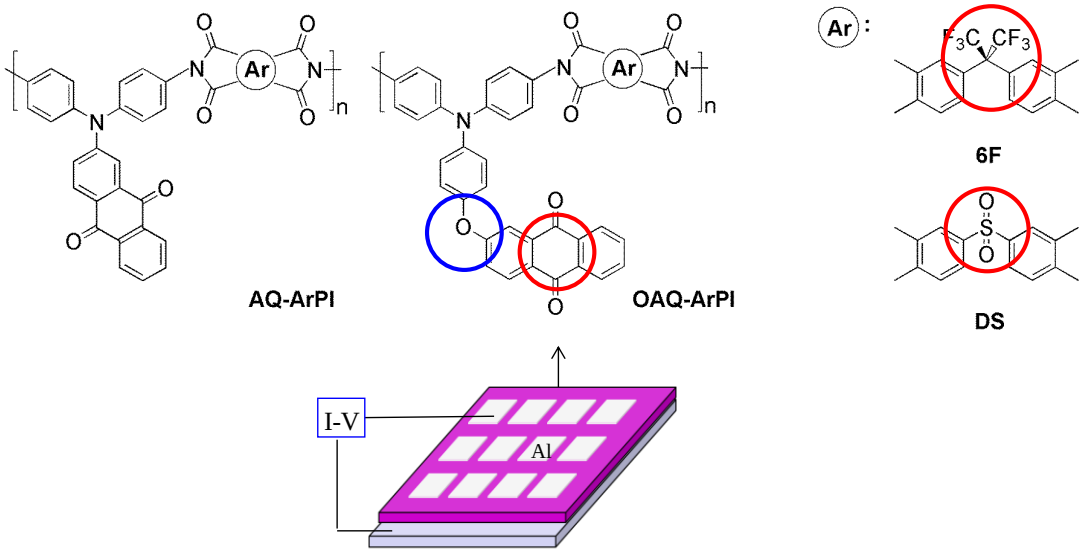

Figure 1.11. Memory devices fabricated by functional polyimide containing TPA with dual competitive electron acceptors.

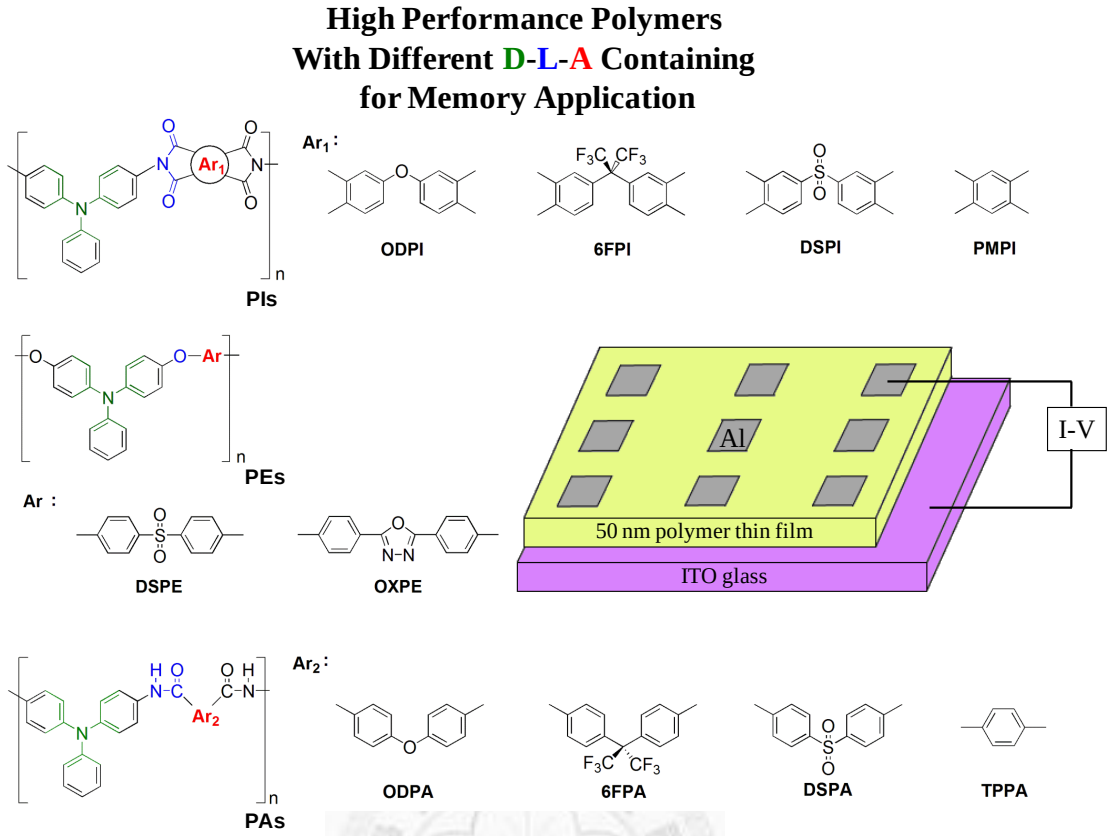

Figure 1.12. The approaching way for discussing the linkage group effect on their memory characteristic in corresponding D-L-A containing polymers of **PIs**, **PAs**, and **PEs**, and the schematic diagram of the memory device consisting of a polymer thin film sandwiched between an ITO bottom electrode and an Al top electrode.

REFERENCES AND NOTES

1. R. Hill, E. E. Walker, *J. Polym. Sci.*, 1948, **3**, 609.
2. P. W. Morgan, *Chemtech.*, 1979, **9**, 316.
3. P. E. Cassidy, *Thermally Stable Polymers*, New York: Marcel Dekker 1980.
4. P. M. Hergenrother, *Die Angew. Markromol. Chem.*, 1986, **145**, 323.
5. H. H. Yang, *Aromatic High-Strength Fibers*, New York: John Wiley & Sons 1989.
6. H. H. Yang, *Kevlar Aramid Fiber*, New York: John Wiley & Sons 1993.
7. D. Wilson, H. D. Stenzenberger, P. M. Hergenrother, *Polyimides*, New York: Blackie 1990.
8. M. J. M. Abadie, B. Mittal, *Polyimides and Other High-Temperature Polymers*, Amsterdam: Elsevier 1991.
9. M. K. Ghosh, K. L. Mittal., *Polyimides: Fundamentals and Applications*, New York: Marcel Dekker 1996.
10. W. T. Leu, *Thesis for Doctor of Philosophy Department of Chemical Engineering Tatung University*. **2006**.
11. N. Ogata, H. Tanaka, *Polym. J.*, 1971, **2**, 672.
12. N. Ogata, G. Suzuki, *Macromolecular Syntheses*, New York: JohnWiley & Sons **1974**.
13. N. Yamazaki, F. Higashi, J. Kawabata, *J. Polym. Sci. Polym. Chem. Ed.* 1974, **12**, 2149.
14. N. Yamazaki, M. Matsumoto, F. Higashi, *J. Polym. Sci. Polym. Chem. Ed.* 1975, **13**, 1373.
15. J. Preston, W. L. Hofferbert, *J. Polym. Sci. Polym. Symp.*, 1978, **65**, 13.
16. F. Higashi, S. Ogata, Y. Aoki, *J. Polym. Sci. Polym. Chem. Ed.*, 1982, **20**, 2081.
17. J. Preston, W. R. Krigbaum, R. Kotek, *J. Polym. Sci. Polym. Chem. Ed.*, 1982, **20**,

3241.

18. R. Kotek, W. R. Krigbaum, J. Preston, *J. Polym. Sci. Polym. Chem. Ed.*, 1983, **21**, 2387.
19. W. R. Krigbaum, R. Kotek, J. Preston, *J. Polym. Sci. Polym. Chem. Ed.*, 1984, **22**, 873.
20. W. R. Krigbaum, R. Kotek, Y. Mihara, J. Preston, *J. Polym. Sci. Polym. Chem. Ed.*, 1984, **22**, 4045.
21. W. R. Krigbaum, R. Kotek, Y. Mihara, J. Preston, *J. Polym. Sci. Polym. Chem. Ed.*, 1985, **23**, 1907.
22. P. W. Morgan, *Condensation Polymers by Interfacial and Solution Methods*, New York: Interscience, 1965.
23. J. M. Garcia, F. C. Garcia, F. Serna, J. L. de la Pena, *Prog. Polym. Sci.*, 2009, **35**, 623.
24. A. L. Endrey, U. S. Patent No.3179631, 1965.
25. W. M. Edwards, U. S. Patent No.3179614, 1965.
26. C. E. Sroog, A. L. Endrey, S. V. Abramo, C. E. Berr, W. M. Edwards, K. L. Olivier, *J. Polym. Sci. Part A.*, 1965, **3**, 1373.
27. C. E. Sroog, *J. Polym. Sci. Macromol. Rev.*, 1976, **11**, 161.
28. S. Z. D. Cheng, F. E. Jr. Arnold, A. Zhang, S. L. C. Hsu, F. W. Harris, *Macromolecules*, 1991, **24**, 5856.
29. Q. D. Ling, D. J. Liaw, C. Zhu, D. S. H. Chan, E. T. Kang, K. G. Neoh, *Prog. Polym. Sci.*, 2008, **33**, 917.
30. S. Moller, C. Perlov, W. Jackson, C. Taussig, S. R. Forrest, *Nature*, 2003, **426**, 166.
31. J. Ouyang, C. W. Chu, C. R. Szmanda, L. P. Ma, Y. Yang, *Nat. Mater.*, 2004, **3**, 918.

32. Q. D. Ling, Y. Song, S. L. Lim, E. Y. H. Teo, Y. P. Tan, C. X. Zhu, *Angew. Chem. Int. Ed.*, 2006, **45**, 2947.

33. K. Ramanathan, M. A. Bangar, M. Yun, W. Chen, A. Mulchandani, N. V. Myung, *Nano Lett*., 2004, **4**, 1237.

34. Q. D. Ling, S. L. Lim, Y. Song, C. X. Zhu, D. S. H. Chan, E. T. Kang, *Langmuir*, 2007, **23**, 312.

35. R. J. Tseng, J. X. Huang, J. Ouyang, R. B. Kaner, Y. Yang, *Nano Lett.*, 2005, **5**, 1077.

36. Q. D. Ling, Y. Song, S. J. Ding, C. Zhu, D. S. H Chan, D. L. Kwong, E. T. Kang, K. G. Neoh, *Adv. Mater.*, 2005, **17**, 455.

37. P. K. C. Pillai, Polymeric electrets, H.S. Nalwa (Ed.), Ferroelectric polymers: chemistry, physics, and applications, Marcel Dekker, New York, 1995,p1-62.

38. G. Dearnaley, D. V. Morgan, A. M. Stoneham, *J. Non-Cryst. Solids*, 1970, **4**, 593.

39. G. Dearnaley, A. M. Stoneham, D. V. Morgan, *Rep. Prog. Phys*, 1970, **33**, 1129.

40. P. O. Sliva, G. Dir, C. Griffiths, *J. Non-Cryst. Solids*, 1970, **2**, 316.

41. J. Gazso, *Thin Solid Films*, 1974, **21**, 43.

42. H. K. Henisch, J. A. Meyers, *Thin Solid Films*, 1978, **51**, 265.

43. L. F. Pender, R. J. Fleming, *J. Appl. Phys*, 1975, **46**, 3426.

44. M. Siradjuddin, V. K. Raju, P. J. Reddy, *Phys. Status. Solidi. A*, 1984, **81**, K37.

45. J. Tyczkowski, *Thin Solid Films*, 1991, **199**, 335.

46. S. Sivaramakrishnan, P. J. Chia, Y. C. Yeo, L. L. Chua, P. K. Ho, *Nat. Mater.*, 2007, **6**, 149.

47. D. M. Taylor, *IEEE Trans. Dielect. Electr. Insulation*, 2006, **13**, 1063.

48. H. T. Lin, Z. Pei, Y. J. Chan, *IEEE Electron Device Lett*., 2007, **28**, 569.

49. A. Wilkinson, *Blackwell Science*, 2nd ed., Boston, 1997.

50. R. S. Potember, T. O. Poehler, D. O. Cowan, *Appl. Phys. Lett.*, 1979, **34**, 405.

51. K. Z. Wang, H. X. Zhang, D. W. Wang, Z. Q. Xue, *Vac. Sci. Technol*., 1996, **16**, 277.

52. J. P. Farges, *Marcel Dekker*, New York, 1994.

53. J. B. Torrance, *Acc. Chem. Res*., 1979, **12**, 79.

54. A. Dei, D. Gatteschi, C. Sangregorio, L. Sorace, *Acc. Chem. Res.*, 2004, **37**, 827.

55. S. H. Cheng, S. H. Hsiao, T. H. Su, G. S. Liou, *Macromolecules*, 2005, **38**, 307.

56. Q. D. Ling, F. C. Chang, Y. Song, C. X. Zhu, D. J. Liaw, D. S. H. Chan, E. T. Kang, K. G. Neoh, *J. Am. Chem. Soc*., 2006, **128**, 8732.

57. C. L. Liou, W. C. Chen, *Polym. Chem.*, 2011, **2**, 2169.

58. C. W. Chu, J. Ouyang, J. H. Tseng, Y. Yang, *Adv. Mater.*, 2005, **17**, 1440.

59. G. Liu, Q. D. Ling, E. Y. H. Teo, C. X. Zhu, D. S. H. Chan, K. G. Neoh, E. T. Kang, *ACS Nano*, 2009, **3**, 1929.

60. S. Song, B. Cho, T. W. Kim, Y. Ji, M. Jo, G. Wang, M. Choe, *Adv. Mater*., 2010, **22**, 5048.

61. Q. D. Ling, Y. Song, S. L. Lim, E. Y. H. Teo, Y. P. Tan, C. Zhu, D. S. H. Chan, D. L. Kwong, E. T. Kang, K. G. Neoh, *Angew. Chem. Int. Ed.*, 2006, **45**, 2947.

62. G. Liu, Q. D. Ling, E. T. Kang, K. G. Neoh, D. J. Liaw, F. C. Chang, C. X. Zhu, D. S. H. Chan, *J. Appl. Phys.*, 2007, **102**, 024502.

63. Q. D. Ling, E. T. Kang, K. G. Neoh, Y. Chen, X. D. Zhuang, C. Zhu, D. S. H. Chan, *Appl. Phys. Lett.*, 2008, **92**, 143302.

64. X. D. Zhuang, Y. Chen, G. Liu, P. P. Li, C. X. Zhu, E. T. Kang, K. G. Noeh, B. Zhang, J. H. Zhu, Y. X. Li, *Adv. Mater.*, 2010, **22**, 1731.

65. X. D. Zhuang, Y. Chen, B. X. Li, D. G. Ma, B. Zhang, Y. Li, *Chem. Mater.*, 2010, **22**, 4455.

66. T. J. Lee, S. Park, S. G. Hahm, D. M. Kim, K. Kim, J. Kim, W. Kwon, Y. Kim, T. Chang, M. Ree, *J. Phys. Chem.*, 2009, **113**, 3855.

67. Q. Ling, Y. Song, S. J. Ding, C. Zhu, D. S. H. Chan, D. L. Kwong, E. T. Kang, K. G. Neoh, *Adv. Mater.*, 2005, **17**, 455.

68. Q. D. Ling, W. Wang, Y. Song, C. X. Zhu, D. S. H. Chan, E. T. Kang, K. G. Neoh, *J. Phys. Chem. B*, 2006, **110**, 23995.

69. Y. K. Fang, C. L. Liu, W. C. Chen, *J. Mater. Chem.*, 2011, **21**, 4778.

70. Y. K. Fang, C. L. Liu, G. Y. Yang, P. C. Chen, W. C. Chen, *Macromolecules*, 2011, **44**, 2604.

71. G. Liu, B. Zhang, Y. Chen, C. X. Zhu, L. Zeng, D. S. H. Chan, K. G. Neoh, J. Chen, E. T. Kang, *J. Mater. Chem.*, 2011, **21**, 6027.

72. S. L. Lim, N. J. Li, J. M. Lu, Q. D. Ling, C. X. Zhu, E. T. Kang, K. G. Neoh, *ACS Appl. Mater. Interfaces*, 2009, **1**, 60.

73. N. Li, J. Lu, H. Li, E. T. Kang, *Dyes Pigm.*, 2011, **88**, 18.

74. Y. L. Liu, K. L. Wang, G. S. Huang, C. X. Zhu, E. S. Tok, K. G. Neoh, E. T. Kang, *Chem. Mater.*, 2009, **21**, 3391.

75. K. L Wang, Y. L. Liu, J. W. Lee, K. G. Neoh, E. T. Kang, *Macromolecules*, 2010, **43**, 7159.

76. K. L Wang, Y. L. Liu, I. H. Shih, K. G. Neoh, E. T. Kang, *J. Polym. Sci. Part A: Polym. Chem.*, 2010, **48**, 5790.

77. T. Kuorosawa, C. C. Chueh, C. L. Liu, T. Higashihara, M. Ueda, W. C. Chen, *Macromolecules*, 2010, **43**, 1236.

78. T. J. Lee, C. W. Chang, S. G. Hahm, K. Kim, S. Park, D. M. Kim, J. Kim, W. S. Kwon, G. S. Liou, M. Ree, *Nanotechnology*, 2009, **20**, 135204.

79. C. J. Chen, H. J. Yen, W. C. Chen, G. S. Liou, *J. Polym. Sci. Part A: Polym. Chem.*, 2011**, 49**, 3709.

80. C. J. Chen, H. J. Yen, W. C. Chen, G. S. Liou , *J. Mater. Chem.*, 2012, **22**, 14085.

CHAPTER 2

Electrically Bistable Memory devices Derived from Poly(triphenylamine)s Derivatives and its PCBM Hybrid Films

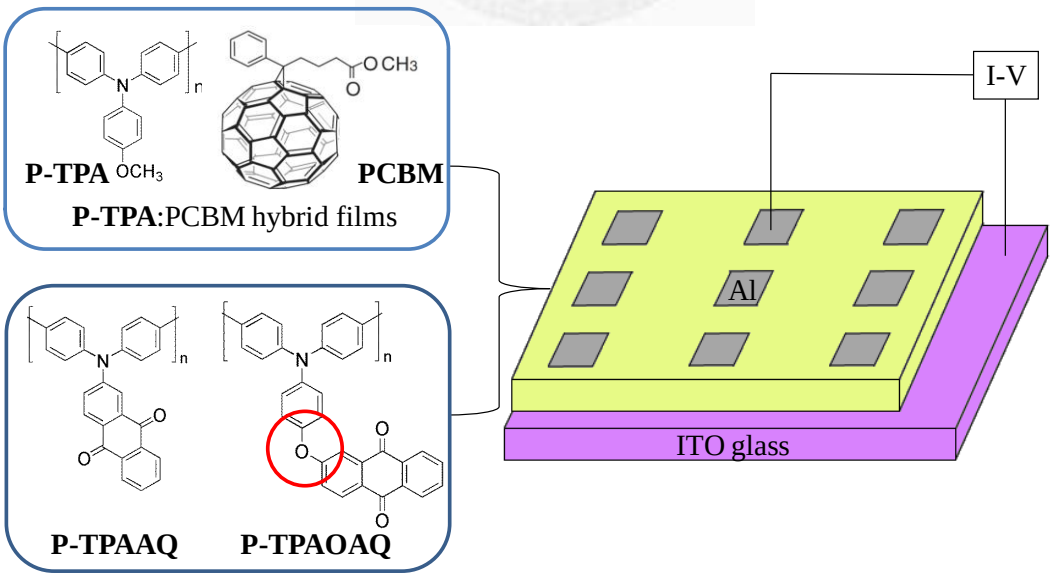

ABSTRACT OF CHAPTER 2

In this chapter, we explore the tunable memory characteristics due to the structural design of the electrical functionality and linkage group effect of the TPA-based polymer synthesized via oxidative coupling reaction or morphological control over the embedded PCBM. **P-TPA:PCBM** hybrid films exhibited dynamic random access memory (DRAM) and write-once-read-many times (WORM) behavior in the sandwich configuration of ITO/ **P-TPA:PCBM** /Al controlled by the concentration of PCBM. The switching behavior could be associated with the charge transfer effect between TPA and PCBM. The devices with the sandwich structure of ITO/**P-TPAAQ** and **P-TPAOAQ**/Al exhibited the volatile bistable electrical switching characteristics of DRAM and SRAM, respectively. The charge transfer effect between the TPA donor moiety and incorporated pendent anthraquinone acceptor moiety and the introduced isolated ether group stabilized the charge transfer complex then extend the retention time could explain the switching phenomenon.

2.1 INTRODUCTION

Differ from conventional memory devices, which were depended on semiconductor-based integrated circuits, new polymeric materials contains electrical bistability resulting from certain intrinsic properties, such as polarity, magnetism, conformation or especially conductivity, in response to the applied electric field. The resistive-type memory devices store data based on the high- and low-conductance response to an applied voltage using the simple sandwich device, consisting of metal as electrodes and polymer as data storage medium. Kinds of polymeric systems with electrical memory switching characteristics included conjugated polymers,[1] functional polyimides.[2]

Besides, the hybrid composites were extensively prepared for memory device applications. The supplementary component such as organic molecule or nano materials could be viewed as the data storage media or have the electronic activated domain which is dispersed in the polymer matrix. The operating mechanism of polymer hybrid composite can be attributed to charge transfer or trapping-detrapping for memory application. The domain size of the electronic activated material in the polymer matrix is the key issue for the nano-scale memory device. The well-dispersed capped-gold (Au) nano-particles and aromatic 8-hydroxy quinoline (8-HQ) compound or [6,6]-C_{61}-butyric acid methyl ester (PCBM) and tetrathiafulvalene (TTF) within a polystyrene (PS) matrix were reported as the WORM-type memory behavior due to the field induced charge transfer from the electron donor to electron acceptor.[3] Afterward, the electro-active molecules such as carbon nanotube (CNT),[4] fullerene,[5] were blended into the donor-containing polymer matrix and then explored its resulting memory behavior. In particular, PCBM containing hybrid films[6] were most widely used as the active layer in the memory application.

Meanwhile, a wide range of vinyl polymers consisted of side-chain donor–acceptor have been intensively investigated and used for memory applications. As the non-conjugated polymers generally exhibit greater solubility than conjugated polymers, which is facilitating their application to solution-processed memory devices. According to this view point, vinyl polymers containing charge transported pendent groups such as carbazole,[7] oxadiazole,[8] cyano,[9] and azobenzene[10]have been demonstrated the digital memory characteristic, attributed to the pendent donor or acceptor moieties played the roles in elucidating the mechanism of charge transfer or space charges and traps effect for the switchable polymers. TPA and its derivatives are well-known candidates for hole transport materials in organic photo-electronic devices due to their stable resulting radical cations, the well hole mobility.[11] However, TPA-based polymers are not only used as the hole-transport layer in electroluminescent devices but widely investigated in the field of electrochromic[12] and memory applications.[2a,2e,2g,13]

In this article, we report the two distinct approaches to fabricate the memory devices by blending the PCBM as the acceptor with the donor-containing poly-4-methoxytriphenylamine (**P-TPA**), and both donor/acceptor-containing poly-**2-**diphenylaminoanthracene-9,10-dione (**P-TPAAQ**) and poly-**2-**(4-diphenylaminophenoxy)anthracene-9,10-dione (**P-TPAOAQ**), respectively. All of the memory behaviors were obtained by the I–V characteristics using the device structure of ITO/polymer/Al. The blend system of the electron donor **P-TPA** with different electron acceptor PCBM concentration demonstrated the electrical field induced memory behaviors, and the experimental results suggested the memory characteristics were probably affected by the PCBM containing and corresponding PCBM aggregated size in the corresponding hybrid film. Furthermore, the isolated linkage effect which could affect the backward charge transfer[14] resulting from the

ether group between TPA donor and anthraquinone (AQ) acceptor was investigated by comparing the switching behavior of **P-TPAAQ** and **P-TPAOAQ**.

2.2 EXPERIMENTAL SECTION

2.2.1 Materials

4-Methoxytriphenylamine[15] **(1)** and 4-hydroxytriphenylamine[16] **(2)** were prepared according to the literature. 2-Amino-anthraquinone (ACROS), [6,6]-C_{61}-butyric acid methyl ester (PCBM), iodobenzene (TCI), potassuim carbonate (ACROS), *N*,*N*-dimethylformamide (DMF) (ACROS), dimethyl sulfoxide (DMSO) (TEDIA), chloroform (ECHO), and tetrahydrofuran (THF) (TEDIA) were used without further purification. Tetrabutylammonium perchlorate (TBAP) (ACROS) was recrystallized twice by ethyl acetate under nitrogen atmosphere and then dried *in vacuo* prior to use. All other reagents were used as received from commercial sources.

2.2.2 Monomer Synthesis

2-diphenylaminoanthracene-9,10-dione (3)

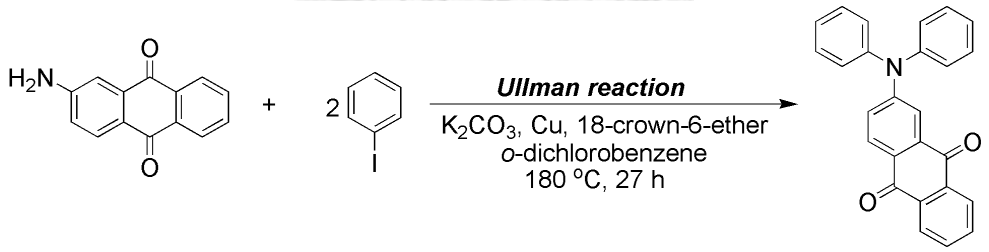

3

A mixture of 6.69 g (30.00 mmol) 2-amino-anthraquinone, 10.36 g (75.00 mmol) potassium carbonate, 4.82 g (75.00 mmol) copper at room temperature. 7.86 g (30.00 mmol), 15.30 g (75.00 mmol) of iodobenzene and 18-crown-6-ether 1.99 g (7.53 mmol) in 30 mL o-dichlorobenzene was added in 250 ml three-neck round-bottomed flask in sequence. The mixture was heated with stirring at 180 °C for 27 h under nitrogen atmosphere then poured slowly into 150 mL of stirred methanol, and the precipitated brown powders was collected by filtration and dissolved in toluene then filtrated for removing copper. The product was collected by concentration to afford

8.3902 g (74.5 % in yield) of brown powders. Mp: 190–193 ^{o}C measured by DSC at a scan rate of 10 ^{o}C/ min. IR (KBr): 1674 cm^{-1} (C=O stretch). ^{1}H NMR (500 MHz, DMSO-d_6, δ, ppm): 8.14-8.12 (d, 1H, H_f), 8.07-8.05 (d, 1H, H_i), 8.01-7.99 (d, 1H, H_e), 7.88-7.80 (m, 2H, H_g + H_h), 7.47-7.44 (t, 1H, H_a), 7.40-7.39 (d, 4H, H_c), 7.30-7.24 (m, 6H, H_j + H_b) , 7.14-7.11 (dd, 1H, H_d) .Anal. $C_{26}H_{17}NO_2$ (375.42): C, 83.18 %; H, 4.56 %; N, 3.73 %. Found: C, 83.21 %; H, 4.46 %; N, 3.70 %.

2-(4-diphenylaminophenoxy)anthracene-9,10-dione (4)

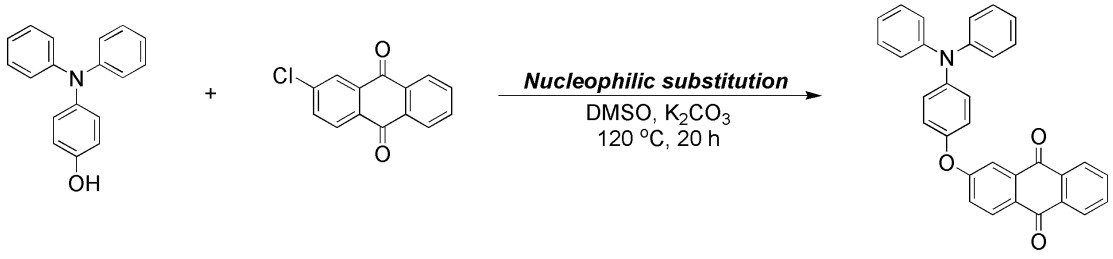

2 **4**

A mixture of 3.18 g (23.00 mmol) of potassium carbonate in 40 mL dimethyl sulfoxide (DMSO) was stirred at room temperature. To the mixture 3.82 g (15.70 mmol) of 2-chloroanthracene-9,10-dione and 3.96 g (15.00 mmol) of **2** were added in sequence. The mixture was heated with stirring at 120 ^{o}C for 20 h and slowly poured into 300 mL methanol/water (2:1). The product was purified by THF/ methanol to afford 5.56g (79.3 % in yield) of yellow powders with a mp of 177–179 ^{o}C (by Melting Point System at a scan rate of 5 ^{o}C /min). FT-IR (KBr): 1673 cm^{-1} (C=O stretch). ^{1}H NMR (500 MHz, DMSO-d_6, δ, ppm): 8.24-8.21 (d, H, H_e), 8.20-8.15 (m, 2H, H_a + H_b), 7.95-7.88 (m, 2H, H_b+ H_c), 7.56-7.55 (s, 1H, H_g), 7.52-7.49 (d, 1H, H_f), 7.34-7.30 (m, 4H, H_h + H_i), 7.16-7.03 (m, 10H, H_j + H_k + H_l). Anal. Calcd (%) for $C_{32}H_{21}NO_3$ (467.51): C, 82.21 %; H, 4.53 %; N, 3.00 %. Found: C, 81.87 %; H, 4.31 %; N, 2.62 %. ESI-MS: calcd for $(C_{32}H_{21}NO_3)^+$: m/z 467.5; found: m/z 468.2.

2.2.3 Polymer Synthesis

The polymerization procedure of the studying materials were synthesized via oxidative coupling reaction according to the previous literature.[17] **P-TPAOAQ** was used as an example to illustrate the general synthetic route of this kind of the oxidative coupling reaction. To a two-necked 50 mL flask equipped with a magnetic stirrer were placed 2-(4-diphenylaminophenoxy)anthracene-9,10-dione (1 mmol) and chloroform (3 mL) under nitrogen atmosphere. A quarter portion of $FeCl_3$ (1 mmol; total is 4 mmol) was added to the reaction mixture at the interval of 1 h. The solution was stirred at 45 ^oC for 48 h then poured into a mixture of methanol containing 10% hydrochloric acid to recover the product. Collected powder was washed in dilute ammonia aqueous solution. The resulting polymer was filtrated and dried in vacuo at 120 ^oC for 12 h (yield: 94%).

2.2.4 Measurements

The inherent viscosities were determined at 0.5 g/dL concentration using Tamson TV-2000 viscometer at 30 ^{o}C. Gel permeation chromatographic (GPC) analysis was carried out on a Waters chromatography unit interfaced with a Waters 2410 refractive index detector. Two Waters 5 μm Styragel HR-2 and HR-4 columns (7.8 mm I. D. × 300 mm) were connected in series with NMP as the eluent at a flow rate of 0.5 ml/min at 40 ^{o}C and were calibrated with polystyrene standards. DSC analyses were performed on a PerkinElmer Pyris 1 DSC in flowing nitrogen (20 cm^3/min). Thermogravimetric analysis (TGA) was conducted with a PerkinElmer Pyris 1 TGA. Experiments were carried out on approximately 6-8 mg samples heated in flowing nitrogen or air (flow rate = 20 cm^3/min) at a heating rate of 20 ^{o}C/min. Cyclic voltammetry (CV) was performed with a Bioanalytical System Model CV-27 and conducted with the use of a three-electrode cell in which ITO (polymer films area about 0.5 cm x 1.2 cm) was used as a working electrode and a platinum wire as an auxiliary electrode at a scan rate of 100 mV/s against a Ag/AgCl reference electrode in anhydrous DMF and CH_3CN, using 0.1 M of TBAP as a supporting electrolyte in nitrogen atmosphere. All cell potentials were taken by using a homemade Ag/AgCl, KCl (sat.) reference electrode. The ITO-coated glass slide was used as the working electrode, a platinum wire as the counter electrode, and a Ag/AgCl cell as the reference electrode. Fourier transform infrared (FT-IR) spectra were recorded on a PerkinElmer Spectrum 100 Model FT-IR spectrometer. ^{1}H spectra were measured on a JEOL JNMAL 300 MHz spectrometer in DMSO- d_6. The microstructure of the prepared films was examined by using a JOEL JEM-1230 transmission electron microscope (TEM). Photoluminescence (PL) spectra was measured with Fluorolog-3 spectrofluorometer.

2.2.5 Fabrication and Measurement of the Memory Device

The memory device was fabricated with the configuration of ITO/thin film/Al as shown in Figure 2.1. The ITO glass used for memory device was precleaned by ultrasonication with water, acetone, and isopropanol each for 15 min. The hybrid thin film was prepared by the chloroform solution of **P-TPA** containing calculated PCBM, which was stirred to form homogeneous solutions then filtrated by 0.45 μm pore size of PTFE membrane syringe filter and spin-coated at 1000 rpm for 30 seconds onto the ITO substrate and kept at 70 ^{o}C for 10 mins under nitrogen. The other thin films were prepared by 250 μl chloroform solution of **P-TPAAQ** or **P-TPAOAQ** (5 mg/ml) by above procedure. The film thickness was determined to be around 50 nm. Finally, a 300-nm-thick Al top electrode was thermally evaporated through the shadow mask (recorded device units of 0.5 × 0.5 mm^2 in size) at a pressure of 10^{-7} torr with a uniform depositing rate of 3-5 Å/s. The electrical characterization of the memory device was performed by a Keithley 4200-SCS semiconductor parameter analyzer equipped with a Keithely 4205-PG2 arbitrary waveform pulse generator. ITO was used as the cathode (maintained as common), and Al was set as the anode during the voltage sweep. The probe tip used 10 μm diameter tungsten wire attached to a tinned copper shaft with a point radius <0.1 μm (GGB Industries, Inc.).

2.2.6 Theoretical Calculation

The theoretical calculation in this study was performed by Gaussian 09 program package. The results of value and distributions of the corresponding energy levels within each basic unit of **P-TPAAQ** and **P-TPAOAQ** were investigated via density functional theory (DFT) method at the B3LYP level of theory (Beckesstyle three-parameter density functional theory using the Lee-Yang-Parr correlation functional) with the 6-31G(d) basic set.

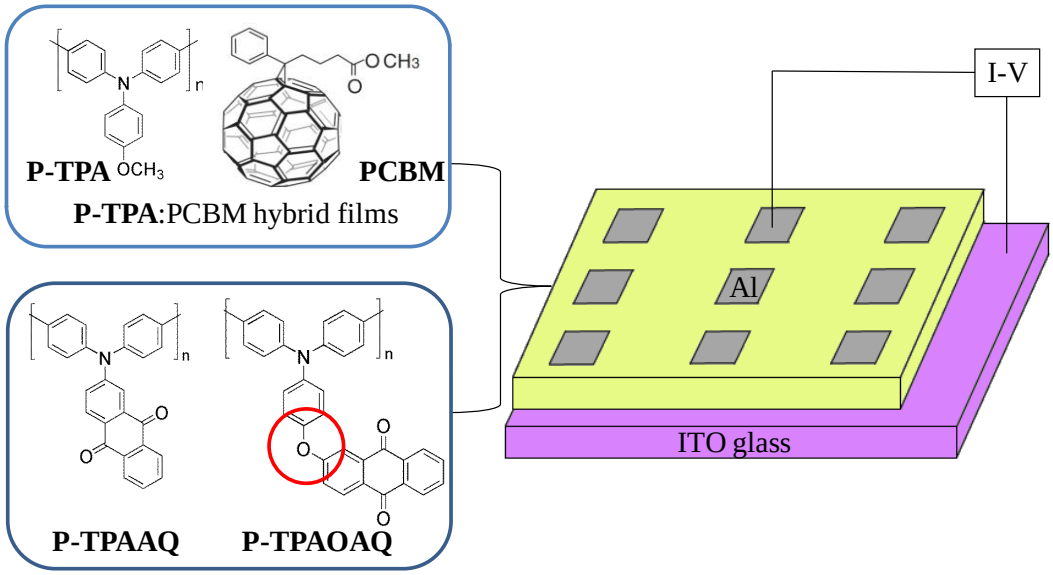

Figure 2.1. The schematic diagram of the memory device consisting of a polymeric active layer sandwiched between an ITO bottom electrode and an Al top electrode. The thickness of polymeric thin film is about 50 nm and the thickness of electrode is 300nm.

2.3 RESULTS AND DISCUSSION

2.3.1 Monomer Synthesis

2-Diphenylaminoanthracene-9,10-dione **(3)** was prepared by Ullman reaction of 2-amino-anthraquinone with iodobenzene according to the synthetic route outlined in Scheme 2.1. The novel aromatic pendent electro-active moiety containing compound 2-(4-diphenylaminophenoxy)anthracene-9,10-dione **(4)**, having a isolated ether linkage group between AQ unit and TPA unit was successfully synthesized by nucleophilic substitution of 2-chloroanthracene-9,10-dione and compound **(2)** the as shown in Scheme 2.1.

FT-IR and NMR spectroscopy were used to identify the structures of monomers **(3)** and **(4)**. The FT-IR spectra of the resulting monomers is demonstrated in Figure 2.2. The AQ-containing compound **(3)** and **(4)** exhibited the characteristic band at around 1674 and 1672 cm^{-1} could be attributed to the stretching of C=O, respectively, the absorption at 1213 cm^{-1} of compound **(4)** could be associate with the characteristic peak of C-O stretching was due to the presence of phenoxyl linkage group. However, the absence of the absorption band of amino and hydroxyl in **(3)** and **(4)** indicated the conversion from the precursor to the target compound, respectively. The ^{1}H NMR spectra results of compound **(3)** and **(4)** are illustrated in Figure 2.3 and Figure 2.4, respectively, and both of them are in good agreement with the proposed molecular structures.

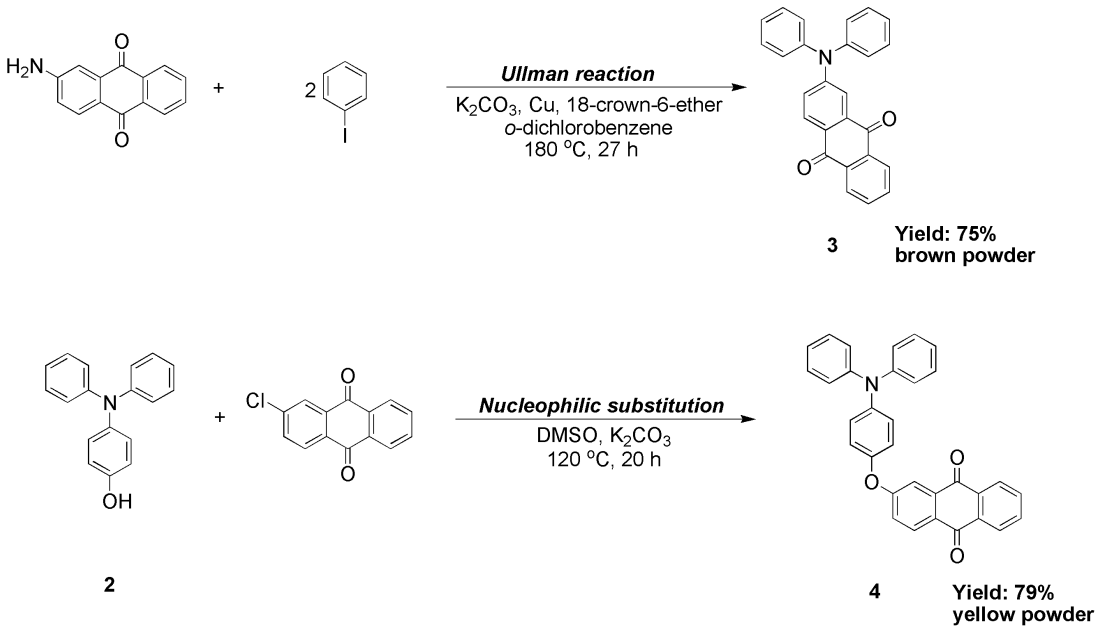

Scheme 2.1. Synthesis route to target compound **3** and **4**.

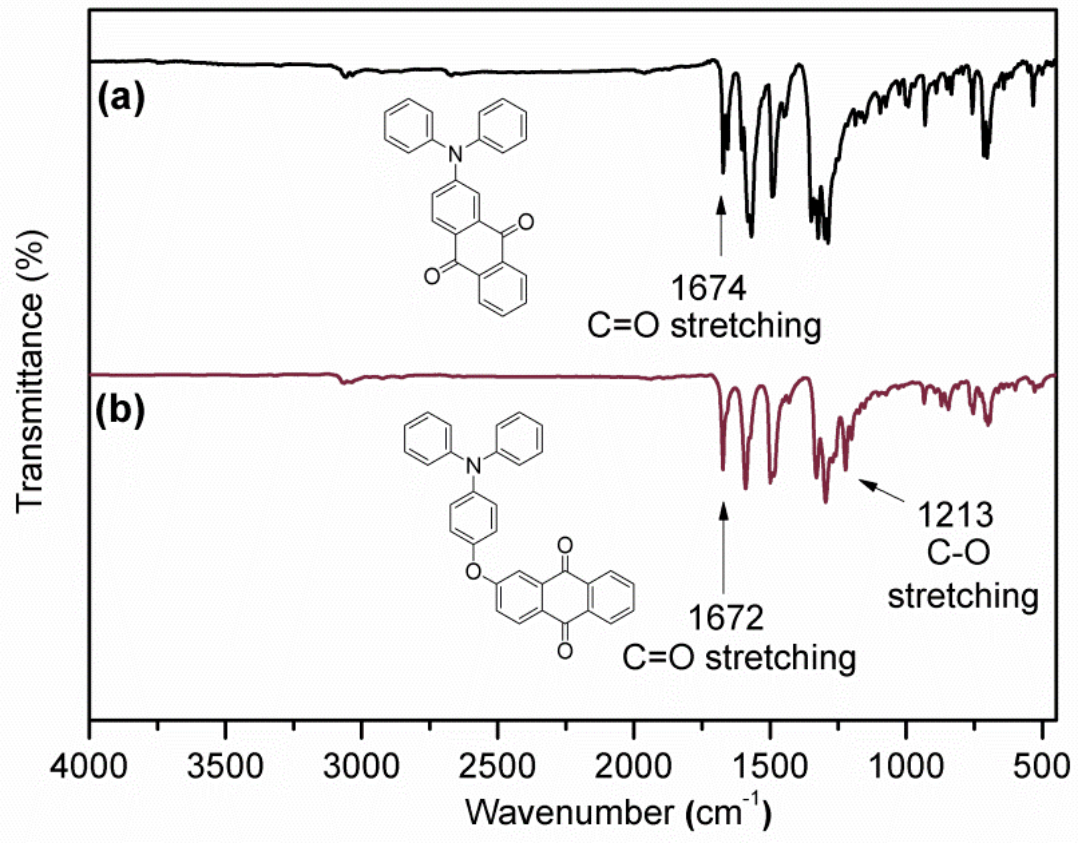

Figure 2.2. IR spectra of (a) compound **3** and (b) compound **4**.

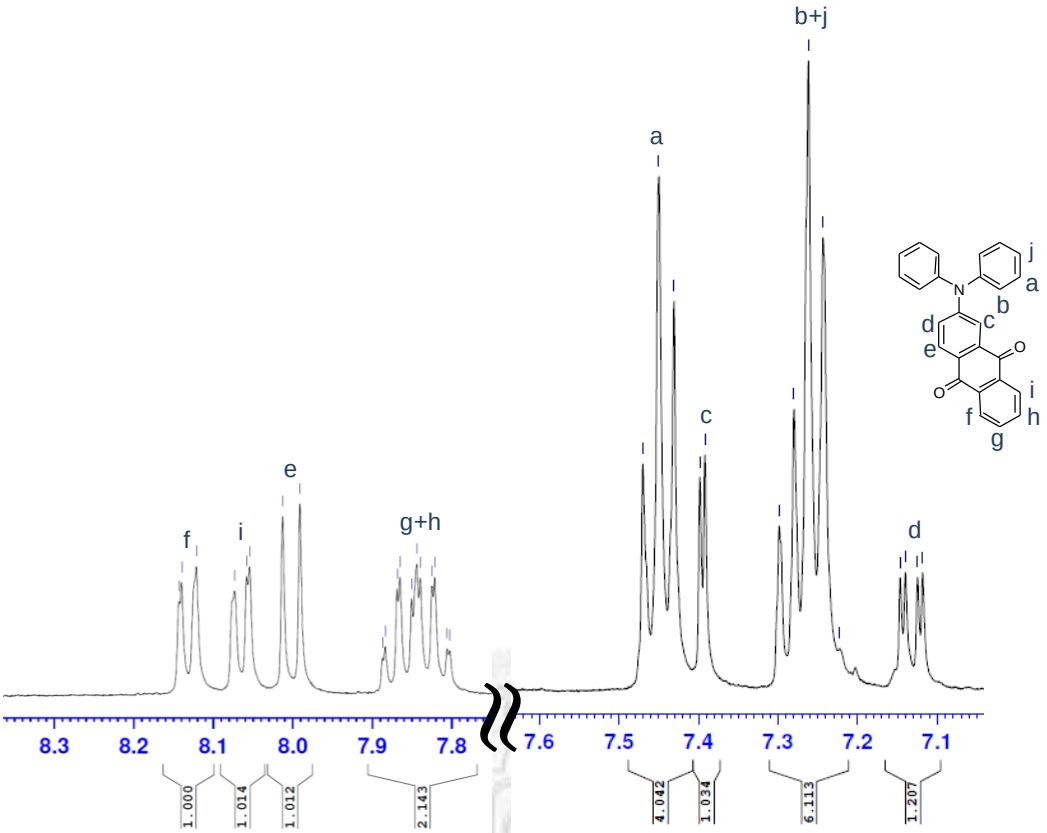

Figure 2.3. ^{1}H NMR spectra of compound **3** in DMSO-d_6.

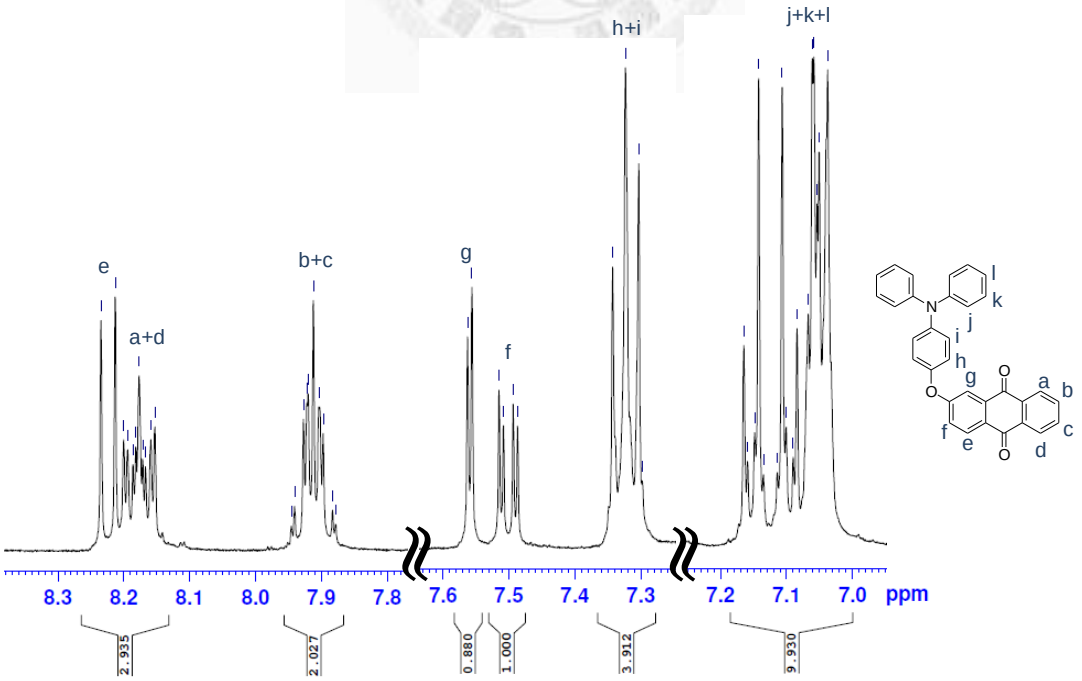

Figure 2.4. ^{1}H NMR spectra of compound **4** in DMSO-d_6.

2.3.2 Polymer Synthesis

P-TPA, **P-TPAAQ**, and **P-TPAOAQ** were synthesized via oxidative coupling reaction using $FeCl_3$ as catalyst from compound **(1)**, **(3)**, and **(4)**, respectively (Scheme 2.2), and all resulting products exhibited enough molecular weight to afford thin films by spin-coating. The inherent viscosities, weight-average molecular weights (*M*w), and polydispersity (PDI) of these resulting polymers are summarized in Table 2.1.

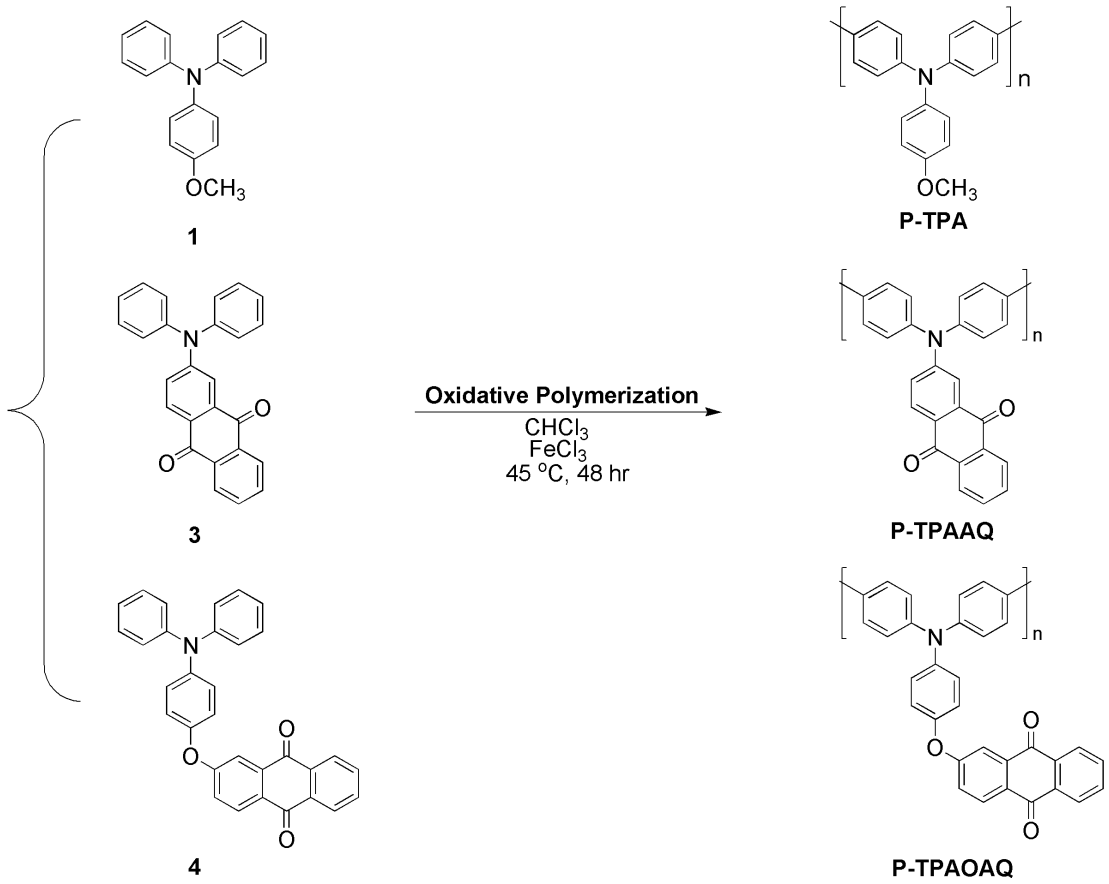

Scheme 2.2. Preparation procedure of **P-TPA**, **P-TPAAQ**, and **P-TPAOAQ**.

2.3.3 Basic Characteristic Polymer Properties

The solubility behavior of resulting polymers was investigated in some organic solvent qualitatively, and the results are also summarized in Table 2.1. Due to the highly chain packing and strong intermolecular interaction resulting from the rigidity of the high phenyl ring containing studying polymers, its only showed well solubility in few organic solvent such as *N*-methyl-2-pyrrolidinone (NMP) and $CHCl_3$. Thus, the low boiling temperature $CHCl_3$ was chosen as the processing solvent to fabricate high performance functional thin by spin-coating or inkjet-printing process for further application such as optoelectronic devices and digital memory devices.

The thermal properties of obtained polymers were recorded by TGA, and the thermal behavior data are summarized in Table 2.2. Typical TGA curves of **P-TPAAQ** and **P-TPAOAQ** are depicted in Figure 2.5. All the prepared polytriarylamine derivates exhibited good thermal stability with insignificant weight loss up to 500 ^{o}C under both nitrogen and air atmosphere. The decomposition temperature at a 10 % weight-loss of these polymers in nitrogen and air were recorded in the range of 580-630 and 540-590 ^{o}C, respectively. The amount of carbonized residue (char yield) of these polymers in a nitrogen atmosphere was more than 70 % at 800 ^{o}C, leading a high limiting oxygen index (LOI) in the range of 46-48. The high char yields of these polymers can be ascribed to their high aromatic content.

Table 2.1. Inherent Viscosity and Molecular Weights of Studied Materials

Code	yield	η_{inh}[a] (dL/g)	M_w[b]	M_n[b]	PDI[b]	Solvent[c]		
						DMAc	NMP	$CHCl_3$
P-TPA	88.1%	0.40	63000	40000	1.56	—	+	++
P-TPAAQ	79.1%	0.16	5100	2900	1.76	—	+	++
P-TPAOAQ	80.1%	0.15	4900	2700	1.81	—	+	++

[a] Measured at a polymer concentration of 0.5 g/dL in NMP at 30 °C.

[b] Calibrated with polystyrene standards, using NMP as the eluent at a constant flow rate of 1 ml/min at 40 °C. Polydispersity Index (M_w/M_n).

[c] The solubility was determined with a 5 mg sample in 1 ml of solvent. ++: soluble in room temperature; +: soluble in heating; —: partially soluble even in heating.

Table 2.2. Thermal Properties of Obtained Polymers

Polymer[a]	T_d^5 (°C)[b]		T_d^{10} (°C)[b]		R_{w800} (%)[c]	LOI[d]
	N_2	Air	N_2	Air		
P-TPA	440	500	500	530	76	48
P-TPAAQ	580	530	630	600	70	46
P-TPAOAQ	540	530	580	580	76	48

[a] The polymer samples were heated at 200 °C for 1 h prior to all the thermal analyses.

[b] Temperature at which 5 % and 10 % weight loss occurred, respectively, recorded by TGA at a heating rate of 20 °C/min and a gas flow rate of 20 cm^3/min.

[c] Residual weight percentages at 800 °C under nitrogen flow.

[d] LOI = Limiting Oxygen Index = (17.5 + 0.4 × char yield).[18]

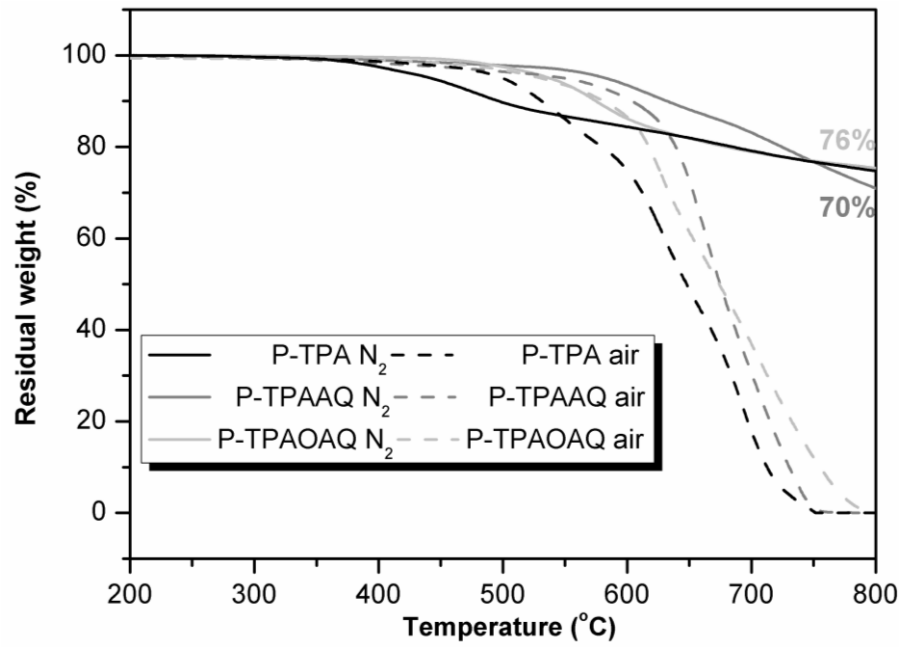

Figure 2.5. TGA thermograms of **P-TPA**, **P-TPAAQ**, and **P-TPAOAQ** at a scan rate of 20 °C/min.

2.3.4 Electrochemical Properties

The electrochemical behavior of the studied materials were investigated by cyclic voltammetry (CV) conducted for the cast film on an indium-tin oxide (ITO)-coated glass slide as working electrode in anhydrous acetonitrile and DMF, using 0.1 M of TBAP as a supporting electrolyte, and the results are summarized in Table 2.2. The typical CV diagrams of **P-TPA**, **P-TPAAQ**, and **P-TPAOAQ** are depicted in Figure 2.6, Figure 2.7, and Figure 2.8 for comparison research, respectively. There is one reversible oxidation redox couple for these three polymers, while the lower oxidation potential of **P-TPA** could be attributed to the *para*-position substituted electron-donating methoxyl group. On the other hand, **P-TPAAQ** and **P-TPAOAQ** required higher bias to overcome the energy barrier of oxidation due to the incorporation of the pendent AQ group. However, the higher oxidation potential of **P-TPAAQ** compared to **P-TPAOAQ** was resulted from the electron withdrawing AQ unit on TPA groups in polymer **P-TPAAQ**, indicating the ether linkage in polymer **P-TPAOAQ** can interdict the electron pathway and interrupt the conjugate behavior from TPA to AQ unit.

In case of reduction process, the CV diagram of **P-TPAAQ** (Figure 2.7) and **P-TPAOAQ** (Figure 2.8) revealed both two reversible reduce redox couples, and the corresponding redox reaction for AQ moiety shown in Scheme 2.3 represented a possible distribution of electron density for the reduction forms and described by other resonance forms, which contributed to the charge delocalization. The first reduce step at $E_{1/2}$ = -0.77 V and the second reduced couple at $E_{1/2}$= -1.53 V for **P-TPAAQ**; the reduce couple of **P-TPAOAQ** could be found at the $E_{1/2}$= -0.76 V and -1.53 V, respectively. The slightly lower reduce potential of the **P-TPAOAQ** could be attributed to the isolation effect of the ether linkage. The larger difference between first and second reduction process of **P-TPAAQ** and **P-TPAOAQ** from $E_{1/2}$ value (Δ

E) were 0.76 and 0.77 V, respectively, which was larger than Kapton (Δ E = 0.51 V), revealing the anthraquinone segment possessed stronger electron transfer capability than the pyromellitimide.[12r]

Moreover, the isolated effect which could stabilize the cation radical forming during oxidation procedure and therefore enhancing the reversibility continuous CV scans was shown in Figure 2.9. The redox potentials of the studied materials as well as their respective highest occupied molecular orbital (HOMO) and lowest unoccupied molecular orbital (LUMO) (versus vacuum) are calculated and summarized in Table 2.3.

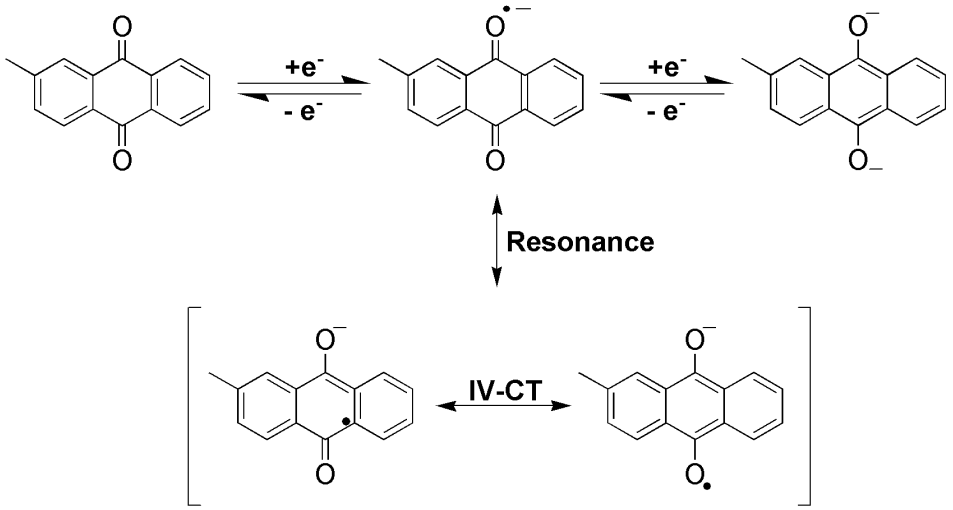

Scheme 2.3. Postulated redox chemistry of anthrquinone moiety.

Table 2.3. Redox Potentials and Energy Levels of Studying Polymers

Polymer	Oxidation (V)[a]		Reduction (V)[b]				
	E_{onset}	$E_{1/2}$	E_{onset}	$E_{1/2(re,1)}$	$E_{1/2(re,2)}$	HOMO[c]	LUMO[d]
P-TPA	0.62	0.85	-	-	-	5.17	1.87[e]
P-TPAAQ	0.99	1.17	-0.74	-0.77	-1.53	5.49	3.53
P-TPAOAQ	0.83	1.02	-0.65	-0.76	-1.53	5.34	3.51

[a]From cyclic votammograms versus Ag/AgCl in CH_3CN. $E_{1/2}$: average potential of the redox couple peaks.

[b]From cyclic votammograms versus Ag/AgCl in DMF.

[c]The HOMO energy levels were calculated from cyclic voltammetry and were referenced to ferrocene ($E_{1/2}$ = 0.48 V).

[d]The LUMO energy levels were calculated from cyclic voltammetry and were referenced to ferrocene ($E_{1/2}$ = 0.53 V).

[e]The LUMO energy levels were calculated from HOMO-gap (3.30) reported before.[17]

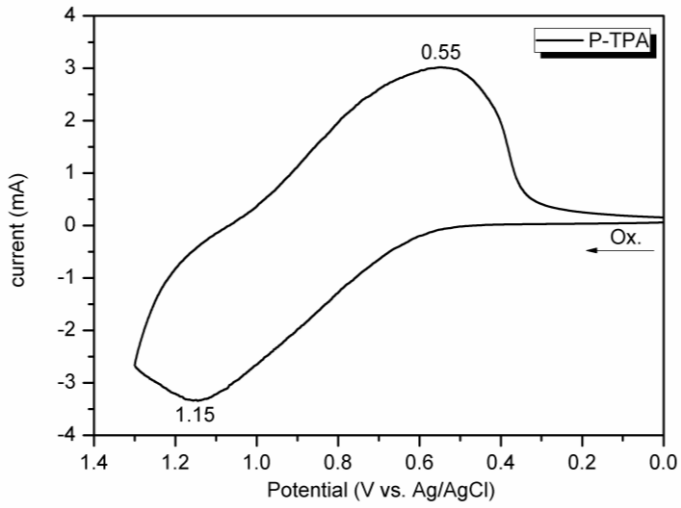

Figure 2.6. Cyclic voltammetric diagrams of **P-TPA** films on an ITO-coated glass substrate over cyclic scans in 0.1 M TBAP/CH_3CN at a scan rate of 100 mV/s.

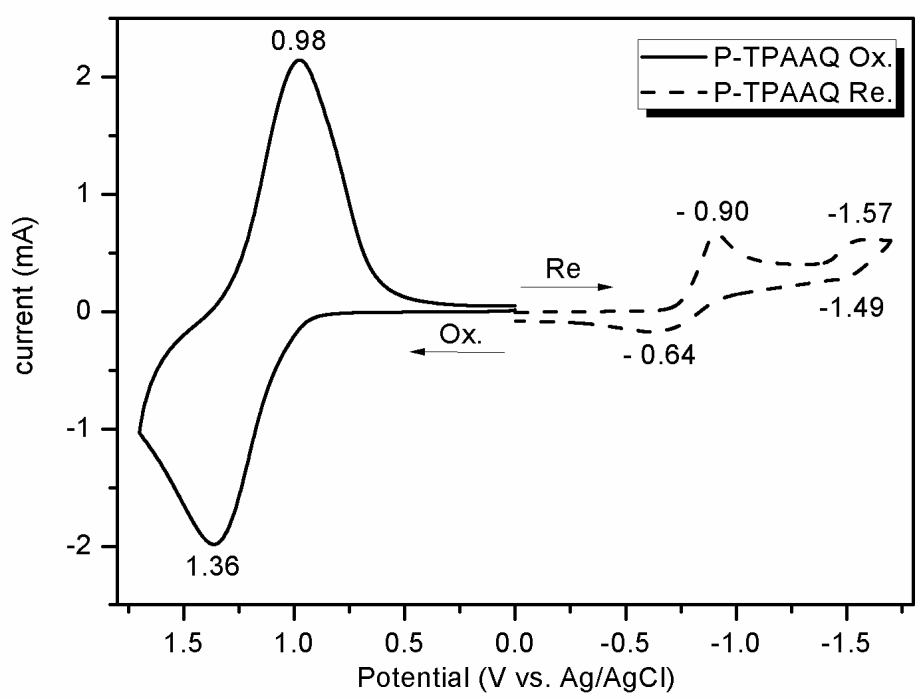

Figure 2.7. Cyclic voltammetric diagrams of **P-TPAAQ** film on an ITO-coated glass substrate over cyclic scans in 0.1M TBAP/CH_3CN for oxidation, in 0.1M TBAP/DMF for reduction at a scan rate of 100 mV/s.

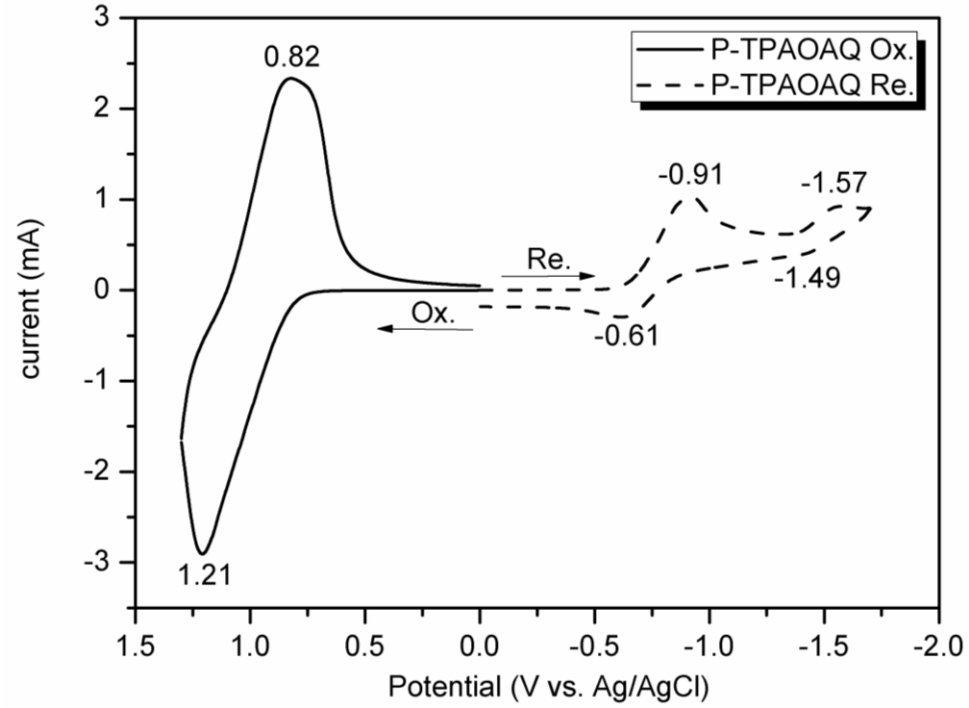

Figure 2.8. Cyclic voltammetric diagrams of **P-TPAOAQ** film on an ITO-coated glass substrate over cyclic scans in 0.1M TBAP/CH_3CN for oxidation, in 0.1M TBAP/DMF for reduction at a scan rate of 100 mV/s.

(a)

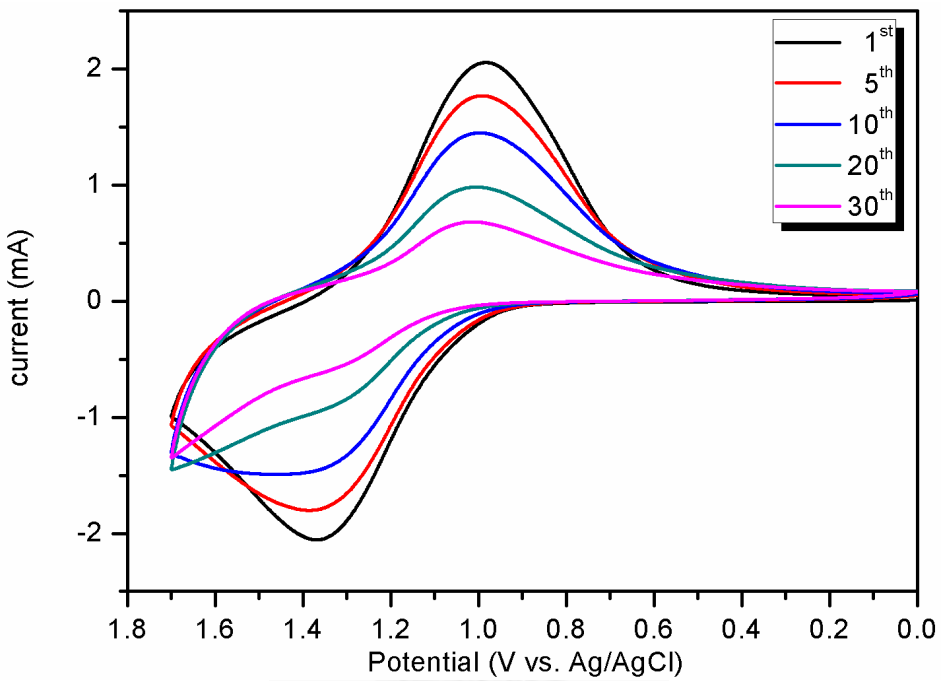

(b)

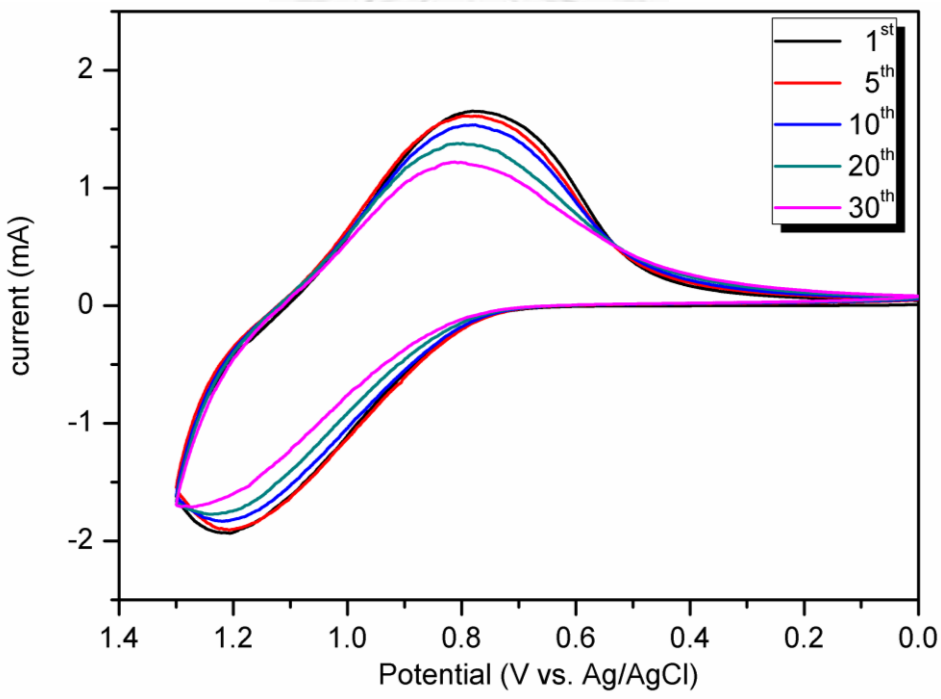

Figure 2.9. Continuous cyclic voltammetric diagrams of (a) **P-TPAAQ** and (b) **P-TPAOAQ** films on an ITO-coated glass substrate over cyclic scans in 0.1 M TBAP/CH_3CN at a scan rate of 100 mV/s.

2.3.5 Memory Device Characteristics of the P-TPA:PCBM Hybrid films

The resulting memory characteristics of these hybrid films were investigated by the current-voltage (I-V) characteristics of an ITO/hybrid film/Al sandwich device as shown in Figure 2.10. Within the sandwich device, hybrid film played the role as the active layer between the top and bottom electrodes Al and ITO, respectively.

Figure 2.10(a) and Figure 2.10(b) demonstrate the I-V result of pristine **P-TPA** and **1% P-TPA:PCBM**, which was conducted in the steps of 0.1V with a 0.01 A compliance current. The memory device of pristine **P-TPA** and **1% P-TPA:PCBM** kept at low-conductivity (OFF) state although **1% P-TPA:PCBM** exhibited a slightly higher off current due to the superadded **PCBM** during the positive and negative scan without any electrical switching capability, indicated the insulator behavior.

Figure 2.10(c) and Figure 2.10(d) despite the I-V results of **3% P-TPA:PCBM** and **5% P-TPA:PCBM**, respectively. During the first sweep from 0 V to -6 V, the devices maintained at the OFF state with a current range 10^{-12}-10^{-13} A in the beginning but increased abruptly to ON state with the current 10^{-3} A (high-conductivity state) at threshold voltage at -3.0 V (**3% P-TPA:PCBM**) and -2.8 V (**5% P-TPA:PCBM**), implying the writing process. In the case of **3% P-TPA:PCBM**, the ON state was instantly recovered to OFF state after removing the applied bias and switched to the ON state at the switch-on voltage of -3.1 V, the positive scan from 0 V to 6 V (line 3) shown no switching phenomena, indicating the negative-switchable DRAM behavior. On the contrary, the device fabricated by **5% P-TPA:PCBM** remained at the ON state during the subsequent negative scan (line 2) and then positive scan (line 3). Besides, the ON state could be kept even after turning off power for 30 minutes or longer time since it has been switched on. Thus, this I-V characteristic indicates that the memory device based on **5% P-TPA:PCBM** hybrid film reveal non-volatile WORM memory property.

In order to explore the effect results the transition from DRAM to WORN by increasing the PCBM containing from 3% to 5%, the intermediate **4% P-TPA:PCBM** hybrid film was prepared to fabricate the sandwich device for investigating the electrical characteristics, and the resulting I-V characteristic were interesting. Both the DRAM, as shown in Figure 2.10(e), and WORM, as shown in Figure 2.10(f), properties were present in the device. The current suddenly increased from 10^{-12}-10^{-13} A to 10^{-4} A at the switch-on voltage of -3.0 V during the negative swept (line 1), in some cases the ON state returned to OFF state as soon as turning of the power then could be turned to ON state at the same switch-on voltage again (line 2), the subsequent swept (line 3) implied this device could not be switched by positive bias, corresponding to negative-active DRAM which is similar to the device fabricated by **3% P-TPA:PCBM**; but in other cases, the ON state could be read by the subsequent ambipolar swept (line 2 and line 3), nevertheless, the ON state could be maintained even after 30 minutes without any electrical impulse, indicating the WORM behavior which is similar to the device based on **5% P-TPA:PCBM**, the probability of the resulting DRAM and WORM behaviors were 70% and 30%, respectively. These results indicated the **4% P-TPA:PCBM** is probably the critical concentration of the DRAM–WORM transition state of the memory device. Furthermore, the higher PCBM containing hybrid film such as **10% P-TPA:PCBM** device exhibited WORM property and the effects of increasing PCBM concentration were enhancing both of ON and OFF current and decreasing the switch-on voltage from about -3.0 V to -1.3 V as revealed by Figure 2.10(g).

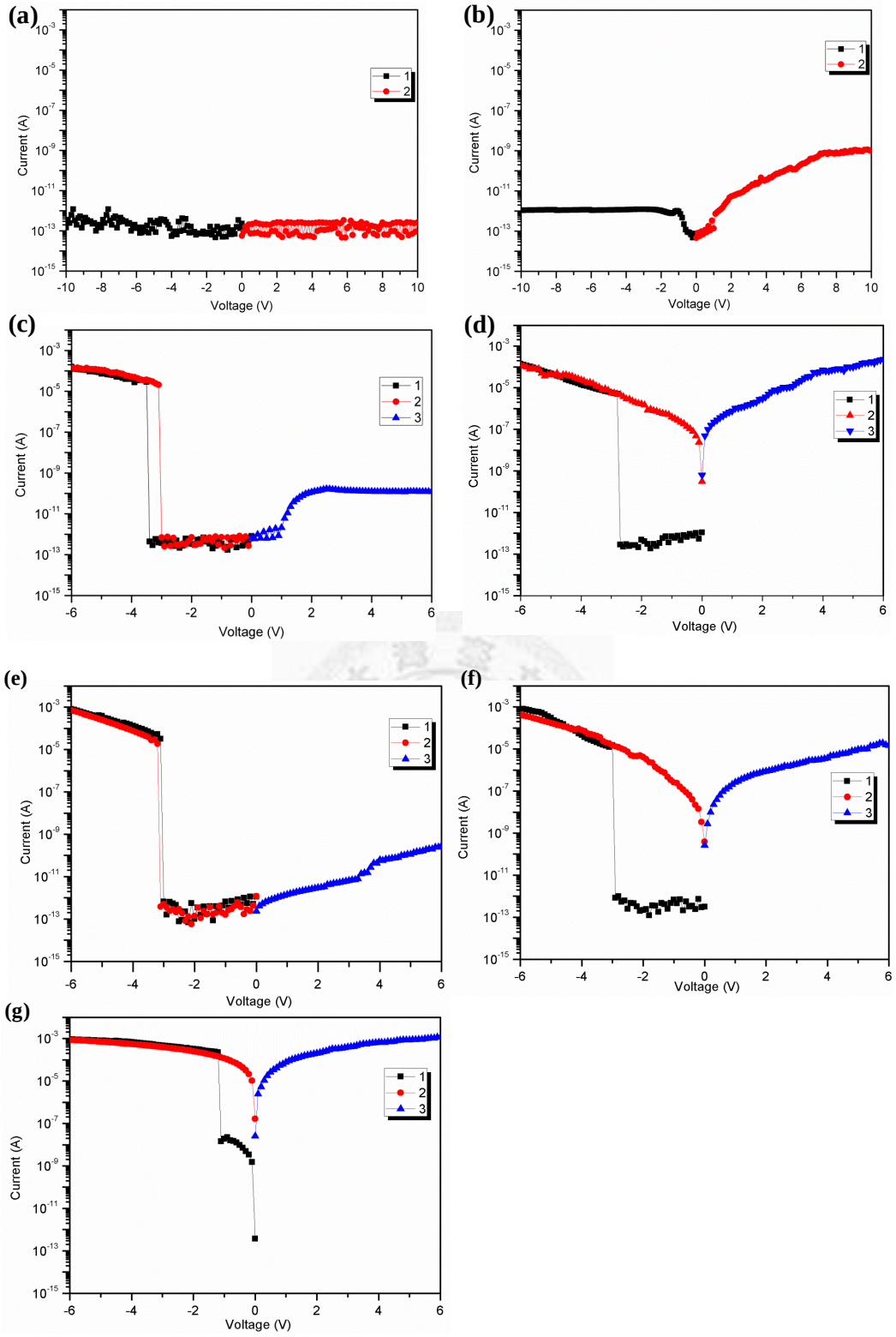

Figure 2.10. Current-voltage (I-V) characteristics of the ITO/**P-TPA:PCBM**/Al memory device with (a) 0%, (b) 1%, (c) 3%, (d) 5%, (e) 4%, (f) 4%, and (g) 10% PCBM weight fraction.

2.3.6 Memory Device Characteristics of the P-TPAAQ and P-TPAOAQ

The memory effects of **P-TPAAQ** and **P-TPAOAQ** were studied based on the current–voltage (I–V) characteristics of an ITO/polymer/Al sandwich device. The data was stored by the polymeric memory devices defined as the high- and low-conductivity response to external applied voltages, respectively. Figure 2.11 depicted the typical I–V curves of the memory devices fabricated with **P-TPAAQ** and **P-TPAOAQ**, respectively.

For the case of **P-TPAAQ**, as shown in Figure 2.11(a), the device is initially in the OFF state (defined as ‘‘0’’ signal in digital) with the current around 10^{-13} A, as the voltage sweeps from 0 to -2.8 V. When the applied voltage increased to the switch-on voltage at -2.9 V, an abrupt increase in the current could be found, indicating the transition from the OFF state to ON state (‘‘1’’ signal in data storage). The ON/OFF current ratio of the studied memory device is nearly up to 10^{8}, which could avoid misreading in the application of digital data storage. In addition, the device could retain in the ON state during the subsequent negative (line 2) and positive (line 3) sweep, indicating the reading process. The fourth sweep (line 4) was conducted after turning off the power for about 20 second. The device can be reprogrammed from the OFF state to the ON state again with the threshold voltage of -3.1 V. The ON state was found to relax to the OFF state without an erasing process but only removing the external applied bias. The short retention time of the ON state indicated that the memory device was volatile and could be performed as DRAM.

Figure 2.11(b) depicts the I-V results of **P-TPAOAQ**. The device could not be switched to the ON state and stayed in the OFF state with a current range 10^{-13} in the from 0 V up to -3.8 V, but a sharp increasing of the current in several orders of magnitude and changed to a high conduction state could be observed as the external applied voltage increased to its threshold voltage of -3.9 V during the first negative

sweep. The reading process of the device could be conducted by the subsequent negative (line 2) and positive scans (line 3) which were both read as the ON state, and implied the non-erasable characteristic of the device due to it could not reset to OFF state by the reverse scan. The device of **P-TPOAQ** retained in the ON state after turning off the power for a longer time interval than **P-TPAAQ**. The fourth sweep was measured after turning off the power for about 6 minutes (line 4); it was found that the ON state had relaxed to the OFF state without an erasing process, and programmed to ON state at the switch-on voltage of -4.0 V. The not only longer retention time at the ON state yet volatile but also the randomly accessible ON and OFF states is analogy to the data storage behavior of SRAM.

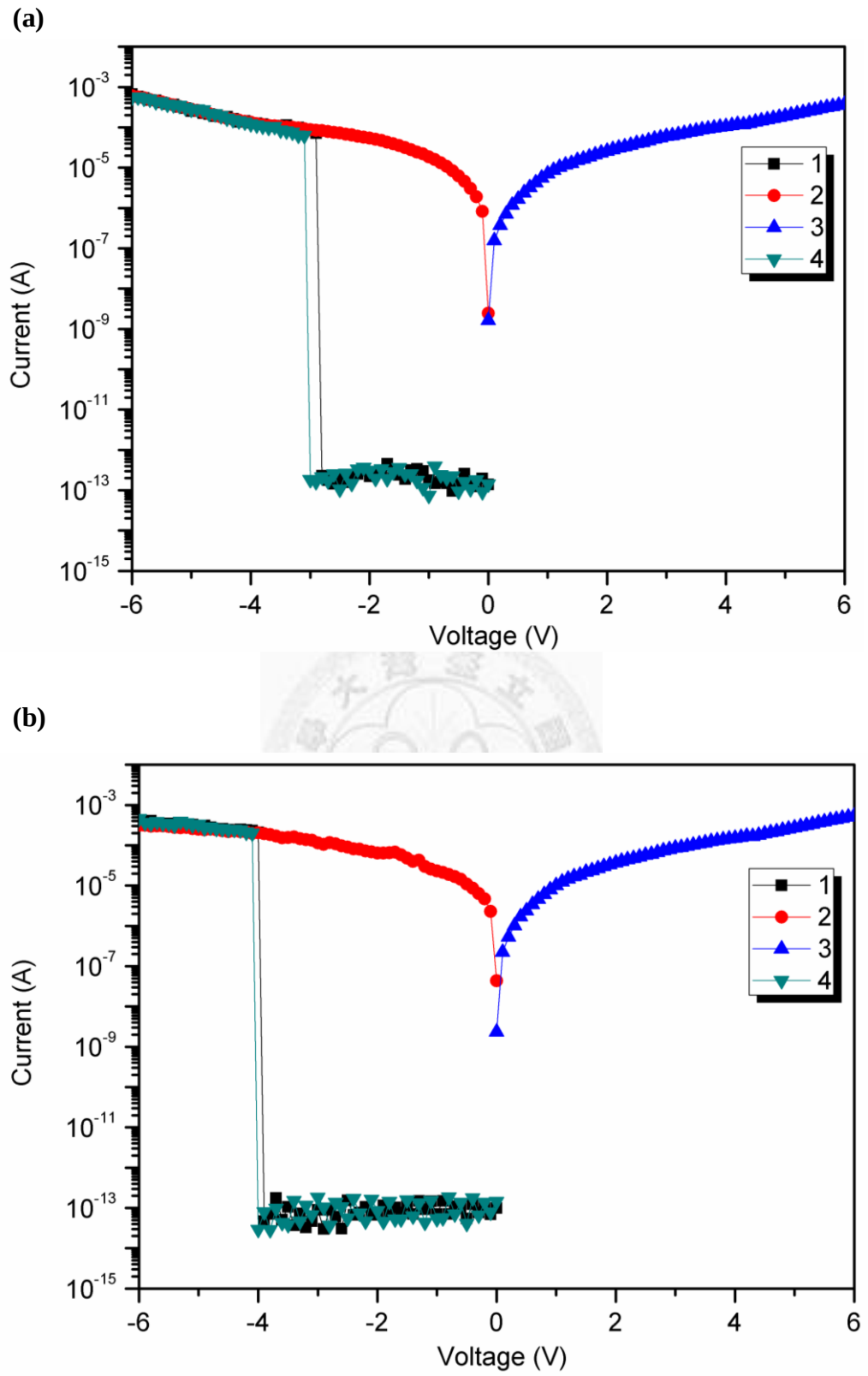

Figure 2.11. Current-voltage (I-V) characteristics of the (a) ITO/**P-TPAAQ**/Al and (b) ITO/**P-TPAOAQ**/Al memory device. The time interval between the third and fourth sweep is 20 seconds and 6 minutes, respectively.

2.3.7 Switching Mechanism of the P-TPA:PCBM, P-TPAAQ, and P-TPAOAQ

The memory device characteristics of the polymer hybrids are including insulator, DRAM, and even WORM type as the PCMB weight fraction changing from 1% to 10 wt% in **P-TPA** matrix. However, the high external applied electric potential may facilitate the electron transfer from the HOMO of the donor **P-TPA** to the LUMO of the acceptor PCBM. Hence, the partially filled LUMO and HOMO of PCBM and **P-TPA** resulted the hybrid film are negatively and positively charged, respectively. Therefore, carriers are generated within the device then brought out a tremendous decrease in electric resistance and an abrupt increase in the conductivity after charge transfer.[4b,6d]

The solid state photoluminescence (PL) spectra of the **P-TPA** and **P-TPA:PCBM** excited at the corresponding absorption λ_{max} (380 nm) of the studied polymers are presented in Figure 2.12. In comparison to pristine **P-TPA**, the fluorescence of **P-TPA:PCBM** is quenched obviously, decreased by 48% in PL intensity as the PCBM fraction increased to 10 wt%, as a indication of the charge transfer from the TPA within the **P-TPA** to the dispersed PCBM. As the applied voltage is overcome the energy barrier, the charge transfer phenomenon was probably occurred from electron-donating **P-TPA** to the electron acceptor PCBM and the generated carriers, charged moieties, consequently induce a sharp increase in the current.

The morphology of the **P-TPA:PCBM** hybrid films were further analyzed by TEM images. The TEM image of the **P-TPA:PCBM** spin-coating thin film were shown in Figure 2.13, the dark regions indicated the formation of denser PCBM clusters. The PCBM were well dispersed in the matrix **P-TPA** with the major diameter of about 40-80 nm, slightly increasing as enhancing the weight fraction of PCBM. The PCBM clusters with larger domain size may probably stabilize charge separation state then hinder from recombining even under the reverse bias and the high conductance state

can be retained for a long time, thus changing from DRAM to WORM type memory characteristic.

We next investigated the switching mechanism of **P-TPAAQ** and **P-TPAOAQ** by the theoretical calculations taken to analyze the molecular orbital and electrostatic potential surface (ESP) of the corresponding basic unit as shown in Figure 2.14. These two systems with analogous charge density distribution, indicated that similar charge transfer pathway from TPA donor to the pendent AQ acceptor could occur under the stimulation of the external applied electrcal field. As the applied potential reach the switching-on voltage, electrons at the HOMO may accumulate energy then overcome the band gap thus transit to the LUMO+2 resulting in an excited state. On the other hand, electrons at the HOMO could also be excited to LUMO+1 with lower energy barrier. Therefore, charge transfer could result from through several routes such as indirectly from the LUMO+2 through intermediate LUMO+1 and then to the LUMO, or from the intermediate LUMO+1 to the LUMO, and even directly from the HOMO to the LUMO to form the conductive charge transfer complexes. However, during the intra- or intermolecular charge transfer induced by the applied electric field, the generating holes can be delocalized to the conjugated TPA moieties arising in a conducting channel in the HOMO moieties within the polymer chain then facile the migration of the charge carriers (holes).[2a,14b] Therefore, the current increases rapidly and the memory device can be switched to the high conductivity state (ON state). The back charge transfer from AQ (LUMO) moiety to TPA (HOMO) could happen easily due to the overlapping of these two electrostatic potential surface distribution, impling the short life time of the high conductivity state of **P-TPAAQ** thus explaining the volatile DRAM behavior. On the contrary, the **P-TPAOAQ** exhibits a higher energy barrier of back charge transfer in comparing to **P-TPAAQ** causing by incorporating the ether group between TPA and AQ that isolates and reduces the coplainity the

electrostatic potential surface distribution of HOMO and LUMO, resulting the SRAM behavior.[14]

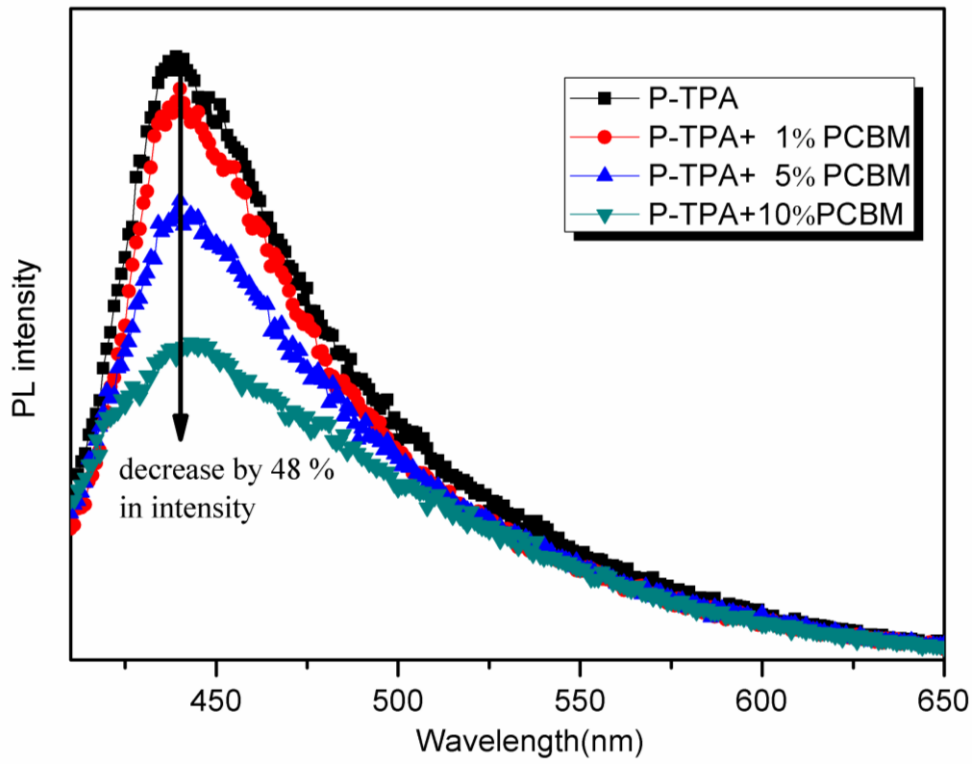

Figure 2.12. Photoluminescence spectra of **P-TPA:PCBM** hybrid thin films.

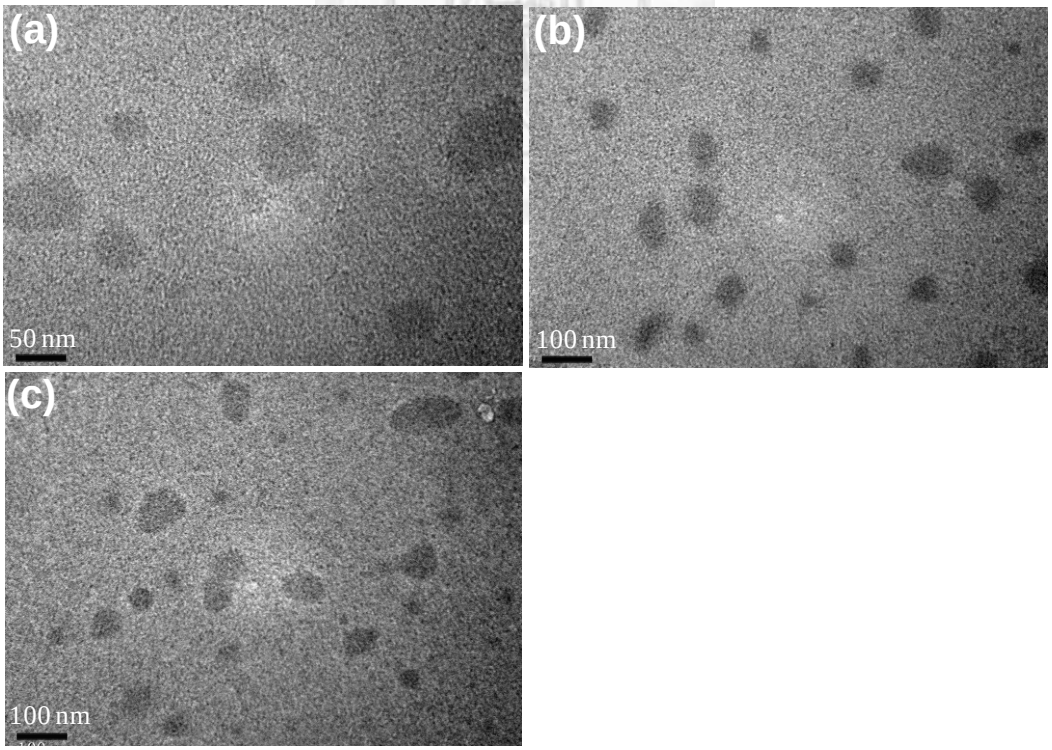

Figure 2.13. The TEM images of (a) 3 wt%, (b) 4 wt%, and (c) 5 wt% **P-TPA:PCBM** spin-coating films.

Basic Units:

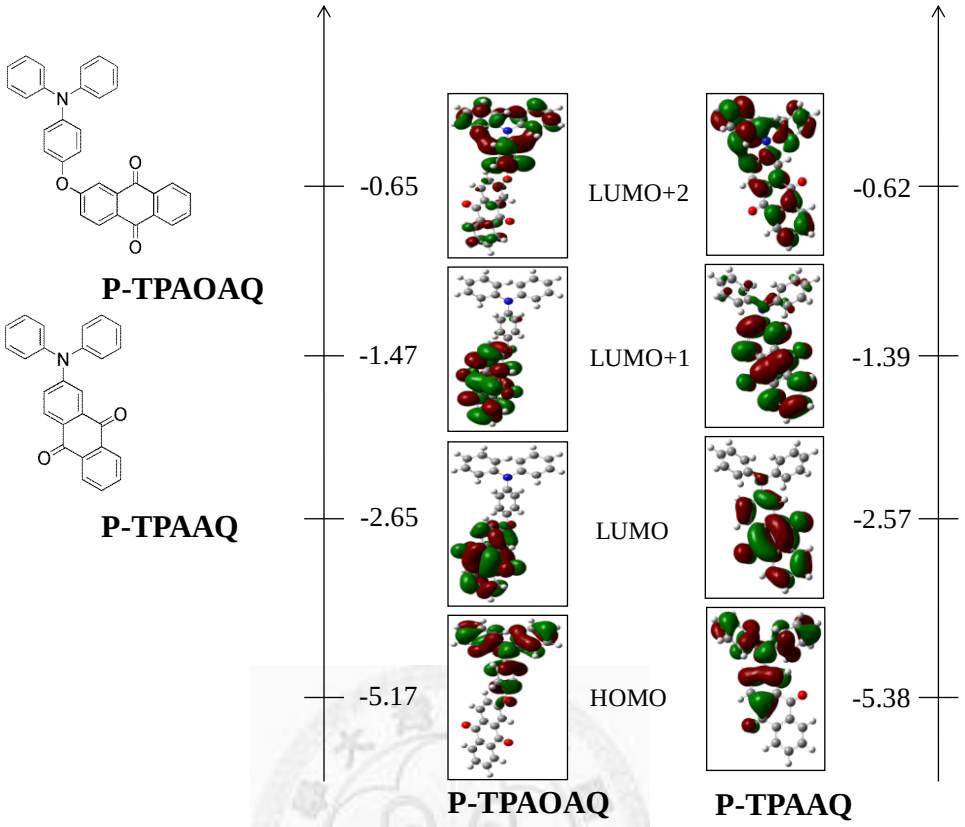

Figure 2.14. Calculated molecular orbitals and corresponding energy levels of the basic units (BU) for **P-TPAAQ** (left) and **P-TPAOAQ** (right).

2.4 SUMMARY

The high ON/OFF current ratio polymeric memory performance based on the TPA-based polymer with incorporating the electron donor via blending or covalent bond have been successfully prepared and investigated systematically. The memory devices with the configuration of ITO/**P-TPA:PCBM**/Al exhibited both DRAM and WORM controlled by the concentration of PCBM. The switching behavior could be attributed to the charge transfer effect between TPA and PCBM proved by the corresponding TEM images and photoluminescence of these hybrid thin films indicated the PCBM aggregation and the charge transfer formation. The devices with the sandwich structure of ITO/**P-TPAAQ** and **P-TPAOAQ**/Al exhibited the volatile bistable electrical switching characteristics due to the charge transfer effect between the TPA donor moiety and incorporated pendent AQ acceptor moiety. While the introduced isolated ether group stabilized the charge transfer complex then extend the retention time at the ON state leading the SRAM behavior of the device of ITO/ **P-TPAOAQ**/Al comparing to the DRAM characteristic of **P-TPAAQ**. The results of this study demonstrated the tunable memory characteristics due to the structural design of the electrical functionality and linkage group effect of the TPA-based polymer and concentration control over the embedded PCBM.

REFERENCES AND NOTES

1. (*a*) S. Baek, D. Lee, J. Kim, S. H. Hong, O. Kim, M. Ree, *Adv. Funct. Mater.*, 2007, **17**, 2637; *(b)* Y. K. Fang, C. L. Liu, C. X. Li, C. J. Lin, R. Mezzenga, W. C. Chen, *Adv. Funct. Mater.*, 2010, **20**, 3012 (*c*) T. W. Kim, S. H. Oh, H. Choi, G. Wang, H. Hwang, D. Y. Kim, T. Lee, *Appl. Phys. Lett.*, 2008, **92**, 253308 (*d*) S. J. Liu, Z. H. Lin, Q. Zhao, Y. Ma, H. F. Shi, M. D. Yi, Q. D. Ling, Q. L. Fan, C. X. Zhu, E. T. Kang, W. Huang, *Adv. Funct. Mater.*, 2011, **21**, 979.

2. *(a)* Q. D. Ling, F. C. Chang, Y. Song, C. X. Zhu, D. J. Liaw, D. S. H. Chan, E. T. Kang, K. G. Neoh, *J. Am. Chem. Soc.*, 2006, **128**, 8732; *(b)* N. H. You, C. C. Chueh, C. L. Liu, M. Ueda, W. C. Chen, *Macromolecules*, 2009, **42**, 4456; *(c)* S. G. Hahm, S. Choi, S. H. Hong, T. J. Lee, S. Park, D. M. Kim, W. S. Kwon, K. Kim, O. Kim, M. Ree, *Adv. Funct. Mater.*, 2008, **18**, 3276; *(d)* S. G. Hahm, S. Choi, S. H. Hong, T. J. Lee, S. Park, D. M. Kim, J. C. Kim, W. Kwon, K. Kim, M. J. Kim, O. Kim, M. Ree, *J. Mater. Chem.*, 2009, **19**, 2207. (*e*) D. M. Kim, S. Park, T. J. Lee, S. G. Hahm, K. Kim, J. C. Kim, W. Kwon, M. Ree, *Langmuir*, 2009, **25**, 11713; (*f*) Y. L. Liu, K. L. Wang, G. S. Huang, C. X. Zhu, E. S. Tok, K. G. Neoh, E. T. Kang, *Chem. Mater.*, 2009, **21**, 3391; (*g*) C. J. Chen, H. J. Yen, W. C. Chen, G. S. Liou, *J. Polym. Sci. Part A: Polym. Chem.*, 2011, **49**, 3709; (*h*) Y. Q. Li, R. C. Fang, A. M. Zheng, Y. Y. Chu, X. Tao, H. H. Xu, S. J. Ding, Y. Z. Shen, *J. Mater. Chem.*, 2011, **21**, 15643; (*i*) Y. Zhang, Y. W. Liu, Q. Lan, S. W. Liu, Z. X. Qin, L. H. Chen, C. Y. Zhao, Z. G. Chi, J. R. Xu and J. Economy, *Chem. Mater.*, 2012, **24**, 1212; (*j*) B. L. Hu, F. Zhuge, X. J. Zhu, S. S. Peng, X. X. Chen, L. Pan, Q. Yan, R. W. Li, *J. Mater. Chem.*, 2012, **22**, 520; (*k*) Y. Q. Li, Y. Y. Chu, R. C. Fang, S. J. Ding, Y. L. Wang, Y. Z. Shen, A. M. Zheng, *Polymer*, 2012, **53**, 229.

3. *(a)* J. Ouyang, C. W. Chu, C. R. Szmanda, L. Ma, Y. Yang, *Nat. Mater.*, 2004, **3**, 918; *(b)* C. W. Chu, J. Ouyang, J. H. Tseng, Y. Yang, *Adv. Mater.*, 2005, **17**, 1440.

4. G. Liu, Q. D. Ling, E. Y. H. Teo, C. X. Zhu, D. S. H. Chan, K. G. Neoh, E. T. Kang, *ACS Nano*, 2009, **3**, 1929.

5. *(a)* G. Liu, Q. D. Ling, E. T. Kang, K. G. Neoh, D. J. Liaw, F. C. Chang, C. X. Zhu, D. S. H. Chan, *J. Appl. Phys.*, 2007, **102**, 024502; *(b)* A. Laiho, H. S. Majumdar, J. K. Baral, F. Jansson, R. Osterbacka, O. Ikkala, *Appl. Phys. Lett.*, 2008, **93**, 203309/1; *(c)* J. Q. Liu, Z. Y. Yin, X. H. Cao, F. Zhao, A. P. Lin, L. H. Xie, Q. L. Fan, F. Boey, H. Zhang, W. Huang, *ACS Nano*, 2010, **4**, 3987.

6. *(a)* S. Song, B. Cho, T. W. Kim, Y. Ji, M. Jo, G. Wang, M. Choe, Y. H. Kahng, H. Hwang, T. Lee, *Adv. Mater*. 2010, **22**, 5048; *(b)* J. C. Hsu, C. L. Liu, W. C. Chen, K. Sugiyama, A. Hirao, *Macromol. Rapid Commun*., 2011, **32**, 528; *(c)* J. E. Park, J. H. Eom, T. Lim, D. H. Hwang, S. Pyo, *J. Polym. Sci. Part A: Polym. Chem*. 2012, **50**, 2188; *(d)* Y. C. Lai, K. Ohshimizu, W. Y. Lee, J. C. Hsu, T. Higashihara, M. Ueda, W. C. Chen, *J. Mater. Chem.*, 2011, **21**, 14502; *(e)*T. W. Kim, D. F. Zeigler, O. Acton, H. L. Yip, H. Ma, A. K. Y. Jen, *Adv. Mater.*, 2012, **24**, 828.

7. *(a)* Q. Ling, Y. Song, S. J. Ding, C. Zhu, D. S. H. Chan, D. L. Kwong, E. T. Kang, K. G. Neoh, *Adv. Mater.*, 2005, **17**, 455; *(b)* Q. D. Ling, W. Wang, Y. Song, C. X. Zhu, D. S. H. Chan, E. T. Kang, K. G. Neoh, *J. Phys. Chem. B*, 2006, **110**, 23995.

8. Y. K. Fang, C. L. Liu, W. C. Chen, *J. Mater. Chem.*, *2011*, **21**, 4778.

9. *(a)* Y. K. Fang, C. L. Liu, G. Y. Yang, P. C. Chen, W. C. Chen, *Macromolecules*, 2011, **44**, 2604; *(b)* G. Liu, B. Zhang, Y. Chen, C. X. Zhu, L. Zeng, D. S. H. Chan, K. G. Neoh, J. Chen, E. T. Kang, *J. Mater. Chem.*, 2011, **21**, 6027.

10. *(a)* S. L. Lim, N. J. Li, J. M. Lu, Q. D. Ling, C. X. Zhu, E. T. Kang, K. G. Neoh,

ACS Appl. Mater. Interfaces, 2009, **1**, 60; *(b)* N. Li, J. Lu, H. Li, E. T. Kang, *Dyes Pigm.*, 2011, **88**, 18; *(c)* G. Liu, B. Zhang, Y. Chen, C. X. Zhu, L. Zeng, D. S. H. Chan, K. G. Neoh, J. Chen, E. T. Kang, *J. Mater. Chem.*, 2011, **21**, 6027; *(d)* B. Zhang, G. Liu, C. Wang, K. G. Neoh, T. Bai, E. T. Kang, *ChemPlusChem*, 2012, **77**, 74.

11. *(a)* K. Y. Chiu, T. H. Su, C. W Huang, G. S. Liou, S. H. Cheng, *J. Electroanal Chem.*, 2005, **578**, 283; *(b)* M. H. Park, J. O. Huh, Y. Do, M. H. Lee, *J. Polym. Sci. Part A: Polym. Chem.*, 2008, **46**, 5816.

12. (*a*) S. H. Cheng, S. H. Hsiao, T. H. Su, G. S. Liou, *Macromolecules*, 2005, **38**, 307; (*b*) T. H. Su, S. H. Hsiao, G. S. Liou, *J. Polym. Sci. Part A:Polym. Chem*., 2005. **43**, 2085; (*c*) C. W. Chang, G. S. Liou, S. H. Hsiao, *J. Mater. Chem*., 2007, **17**, 1007; (*d*) G. S. Liou, C. W. Chang, *Macromolecules*, 2008, **41**, 1667; (*e*) S. H. Hsiao, G. S. Liou, Y. C. Kung, H. J. Yen, *Macromolecules*, 2008, **41**, 2800; (*f*) C. W. Chang, C. H. Chung, G. S. Liou, *Macromolecules*, 2008, **41**, 8441; (*g*) C. W. Chang, G. S. Liou, *J. Mater. Chem*., 2008, **18**, 5638; (*h*) C. W. Chang, H. J. Yen, K. Y. Huang, J. M. Yeh, G. S. Liou, *J.Polym. Sci. Part A: Polym. Chem*., 2008, **46**, 7937; (*i*) H. J. Yen, G. S. Liou, *Chem. Mater*., 2009, **21**, 4062; (*j*) S. H. Hsiao, G. S. Liou, H. M. Wang, *J. Polym. Sci. Part A: Polym. Chem*., 2009, **47**, 2330; (*k*) G. S. Liou, H. Y. Lin, H. J. Yen, *J. Mater. Chem*., 2009, **19**, 7666; (*l*) G. S. Liou, H. Y. Lin, *Macromolecules*, 2009, **42**, 125; (*m*) L. T. Huang, H. J. Yen, C. W. Chang, G. S. Liou, *J. Polym. Sci. Part A:Polym. Chem*., 2010, **48**, 4747; (*n*) H. J. Yen, S. M. Guo, G. S. Liou, *J. Polym. Sci. Part A: Polym. Chem*., 2010, **48**, 5271; (*o*) H. J. Yen, G. S. Liou, *J. Mater. Chem*., 2010, **20**, 9886; (*p*) H. J. Yen, H. Y. Lin, G. S. Liou, *Chem. Mater*., 2011, **23**, 1874; (*q*) H. J. Yen, S. M. Guo, G. S. Liou, J. C. Chung, Y. C. Liu, Y. F. Lu, Y. Z. Zeng, *J. Polym. Sci. Part A: Polym. Chem*., 2011, **49**, 3805; (*r*) L. T. Huang, H. J. Yen, G. S. Liou, *Macromolecules*, 2011, **44**,

9595; (*s*) H. J. Yen, G. S. Liou, *Polym. Chem*., 2012, **3**, 255; (*t*) L. T. Huang, H. J. Yen, J. H. Wu, G. S. Liou, *Org. Electron.*, 2012, **13**, 840.

13. (*a*) T. J. Lee, C. W. Chang, S. G. Hahm, K. Kim, S. Park, D. M. Kim, J. Kim, W. S. Kwon, G. S. Liou, M. Ree, *Nanotechnology*, 2009, **20**, 135204; *(b)* T. J. Lee, Y. G. Ko, H. J. Yen , K. Kim , D. M. Kim, W. Kwon , S. G. Hahm , G. S. Liou, M. Ree, *Polym. Chem.*, 2012, **3**, 1276; *(c)* Y. G. Ko, W. Kwon, H. J. Yen, C. W. Chang, D. M. Kim, K. Kim, S. G. Hahm, T. J. Lee, G. S. Liou, M. Ree, *Macromolecules*, 2012, **45**, 3749; *(d)* C. J. Chen, H. J. Yen, W. C. Chen, G. S. Liou , *J. Mater. Chem.*, 2012, **22**, 14085.
14. T. Kuorosawa, C. C. Chueh, C. L. Liu, T. Higashihara, M. Ueda, W. C. Chen, *Macromolecules*, 2010, **43**, 1236.
15. *(a)* G. S. Liou, Y. L. Yang, W. C. Chen, Y. L. O. Su, *J. Polym. Sci. Part A: Polym. Chem.*, 2007, **45**, 3292; *(b)* H. W. Chang, K. H. Lin, C. C. Chueh, G. S. Liou, W. C. Chen, *J. Polym. Sci. Part A: Polym. Chem*., 2009, **47**, 3292.
16. M. Faccini, M. Balakrishnan, B. J. Diemeer, R. Torosantucci, A. Driessen, D. N. Reinhoudt, W. Verboom, *J. Mater. Chem*., 2008, **18**, 5293.
17. *(a)* H. Y. Lin, G. S. Liou , *J. Polym. Sci. Part A: Polym. Chem.*, 2009, **47**, 285, *(b)* H. W. Chang, K. H. Lin, C. C. Chueh, G. S. Liou, W. C. Chen, *J. Polym. Sci. Part A: Polym. Chem.*, 2009, **47**, 4037.
18. D. W. van Krevelen, *Polymer*, 1975, **16**, 615.

CHAPTER 3

Memory Behaviors Resulted From Functional Polyimide Systems Containing Triphenylamine With Dual Competitive Electron Acceptors

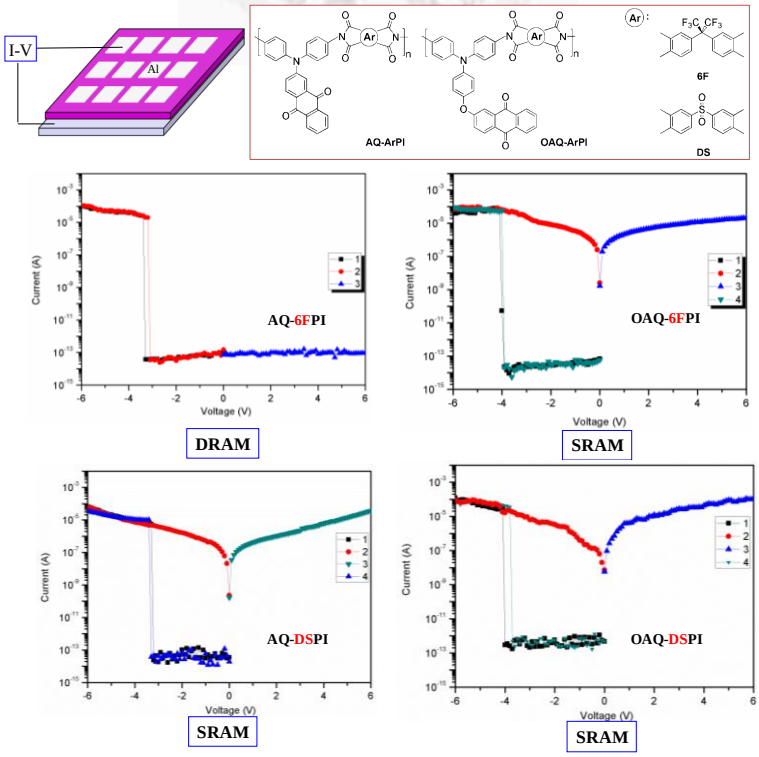

ABSTRACT OF CHAPTER 3

The novel electron-donating triphenylamine (TPA)-containing electroactive functional polyimides with electron-withdrawing pendent anthraquinone moiety were designed and prepared for memory device. These high-performance polymers exhibited two conductivity states and could be swept negatively with a high ON/OFF current ratio of 10^9. The ON state of polyimide **OAQ-6FPI** remained around 8 min after removing the applied voltage, while the polyimide **AQ-6FPI** quickly returned to the OFF state during the backward sweep in dual sweep process, implying that the devices based on **OAQ-6FPI** revealed static random access memory (SRAM); **AQ-6FPI** revealed dynamic random access memory (DRAM) behaviors resulting from the isolated donor-acceptor (D-A) and non-isolated D-A structures, respectively. On the other hand, both of **AQ-DSPI** and **OAQ-DSPI** possessed SRAM behavior and exhibited 8 to 10 minutes for returning from ON state to OFF state due to the strong charge-transfer effect between TPA donor and backbone sulfone-containing phthalimide acceptor moiety.

3.1 INTRODUCTION

Nowadays, the utilization of polymeric material in electronic devices have attracted tremendous attention, such as light-emtting diodes,[1] transistors,[2] and solar cells.[3] Donor-acceptor (D-A) containing polymers include both electron donor and acceptor moieties within a repeating unit, which can be switched between two conductive states via electrical field are widely researched recently for resistive switching memory applications.[4] Based on the advantages of convenient and low-cost device fabrication by using solution process, three-dimensional stacking capability and well structural flexibility,[5] electrically bistable resistive switching device based on polymeric materials have significant advantages over inorganic silicon- and metal-oxide-based memory materials. Among the researched polymeric systems, charge transfer (CT) effect is one of an interesting mechanism to induce the RRAM (resistor-type polymer memory) behavior. The electron donor and the electron acceptor moiety are introduced in the repeat unit of the polymer. Under an applied electric field, the charge transfer will occur which means a transfer of electronic charge from the donor to the acceptor moiety, and the resulting structure can be defined as CT complex (CTC).[6] The stsbility of the CTC is regarded as one of crucial factors on its memory behavior.

Aromatic polymers containing TPA moiety such as polyimide (PI) and polyamide (PA)[4j] are favorable functional materials not only for memory device due to their intrinsic excellent thermal dimensional and high ON/OFF ratio. The importance of structural effects tuned by incorperating different substituents into electron donating moieties on the relaxation time of the polymeric memory was investigated by Kang's and Ree's work; the devices fabricated by TPA-based polyimide **TPA-6FPI**[4a] exhibited volatile DRAM behavior but both phenylamine-substituded and

hydroxy-substituted TPA-containing polyimide (**6F-2TPA PI**)[7a] and (**6F-HTPA PI**)[7b] demostrated non-volatile write-once-read-mamy-times (WORM) property, respectively. Besides, the characteristic of polymer memory can transit from DRAM to SRAM and even become WORM or flash type non-volatile memory behavior by increasing the dipole moment of the polymers.[4j,8] Moreover, the linkage group effects between donor and acceptor moieties may be a key factor to influence the time interval from CT state to the original state due to the conformational changes between the donor and acceptor moiety induced by charge transfer could increase the torsional displacement and produce a potential energy barrier for the back charge transfer to ground state then extended the retention time of the ON state.[4j,8c,9] For example, both **OXTA-PI**[9a] and **AZTA-PI**[9b] containing pendent TPA donor exhibit WORM memory characteristic in Al/polymer/ITO sandwich devices due to the orthogonal overlap in orbitals between acceptor and pendent donor which could provide a higher energy barrier for back transfer further maintain the device in the ON state after removing the applied electrical field.

In this study, in order to obtain solution-processable highperformance polymers for polymeric memory applications, we synthesized two series of polyimides **AQ-PIs** and **OAQ-PIs** from diamines 2-(bis(4-aminophenyl)amino)anthracene-9,10-dione **(1)**, and 2-(4-(bis(4-aminophenyl)amino)phenoxy)anthracene-9,10-dione **(2)**. The resulting TPA-containing polyimides **AQ-PIs** and **OAQ-PIs** were used to fabricate the memory devices. In addition to the carbonyl or phthalimide acceptor moiety in main chain, the anthraquinone as pendent acceptor group was also introduced to TPA via ether linkage or directly attached into the backbone. It is different from the previous researches discussing about the memory effect only on donor acceptor moieties on the main chain of PI system but dual acceptors both in main chain and side chain. The electron charge withdrawing capability of this two acceptors could be verified by molecular

simulation, electrochemical, and spectroelectrochemical behaviors. The memory devices were prepared with the configuration of ITO/polymer/Al, and the memory properties were investigated by I-V measurements and compared with each other.

3.2 EXPERIMENTAL SECTION

3.2.1 Materials

2-(Bis(4-aminophenyl)amino)anthracene-9,10-dione (**1**) and 2-(4-(bis(4-aminophenyl)amino)phenoxy)anthracene-9,10-dione (**2**) were synthesized according to literature.[10] Acetonitrile (CH_3CN), *N*,*N*-dimethylformamide (DMF) (ACROS), dimethyl sulfoxide (DMSO), *N*,*N*-dimethylacetamide (DMAc) (TEDIA), and tetrahydrofuran (THF) (TEDIA) were used without further purification. 2,2-Bis(3,4-dicarboxyphenyl)hexafluoropropane dianhydride (6FDA) (Chriskev), 3,3',4,4'-diphenylsulfonetetracarboxylic dianhydride (DSDA) (TCI) was purified by vacuum sublimation. Tetrabutylammonium perchlorate (TBAP) (ACROS) was recrystallized twice by ethyl acetate under nitrogen atmosphere and then dried in vacuo prior to use. All other reagents were used as received from commercial sources.

3.2.2 Polymer Synthesis

According to the previous work from our lab, aromatic polyimides **AQ-PIs** and **OAQ-PIs** could be prepared by the one-step polycondensation of diamines **1** and **2** with 2-bis(3,4-dicarboxyphenyl)hexafluoropropane dianhydride and 3,3',4,4'-diphenylsulfonetetracarboxylic dianhydride, respectively, in *m*-cresol in the presence of isoquinoline (Scheme 3.1), all polymerization reactions proceeded homogenously and with high viscosity. The synthesis of polyimide **AQ-6FPI** was used as an example to illustrate the general synthetic route used to produce the polyimides. The homogeneous mixture of the diamine **1** (0.4055 g, 1.00 mmol), the dianhydride 6FDA (0.4442 g, 1.00 mmol), and 0.32ml isoquinoline in *m*-cresol (3 mL) were stirred at room temperature under nitrogen atmosphere for 10 h, then heated to 185 ℃ for 18 h. Then the mixture was allowed to cool to room temperature, and the

viscous solution was poured slowly into 200 mL of methanol with stirring. The precipitated polymer was collected by filtration, washed thoroughly with hot methanol and dried under vacuum at 100 ℃ for 15 h. The inherent viscosity of the obtained polyimide **AQ-6FPI** was 0.49 dL/g (measured at a concentration of 0.5 g/dL in DMAc at 30 ^{o}C). The formation of the polyimide was confirmed by IR spectroscopy (as shown in Figure 3.1). The IR spectra of **AQ-6FPI** exhibited characteristic imide absorption bands at around 1781 (asymetrical C=O), 1720 (symmetrical C=O), 1380 (C-N), and 738 cm^{-1} (imide ring deformation).

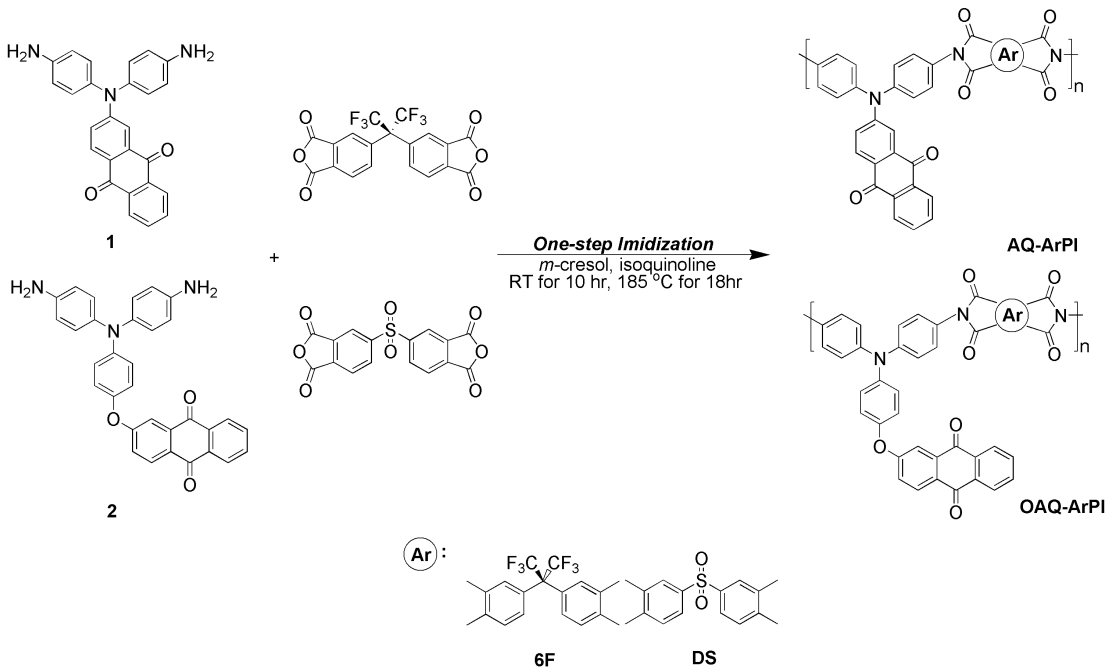

Scheme 3.1. Polymer synthesis of **AQ-PIs** and **OAQ-PIs.**

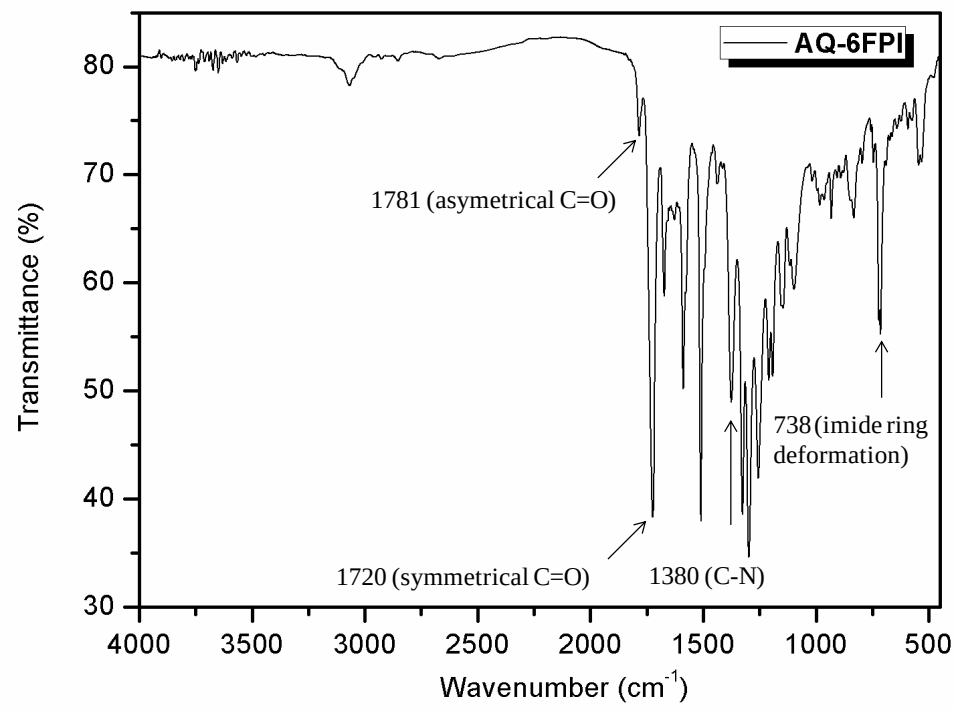

Figure 3.1. IR spectrum of polyimide **AQ-6FPI** film.

3.2.3 Measurements

The inherent viscosities were determined at 0.5 g/dL concentration using Tamson TV-2000 viscometer at 30 ^{o}C. Cyclic voltammetry (CV) was performed with a Bioanalytical System Model CV-27 and conducted with the use of a three-electrode cell in which ITO (polymer films area about 0.5 cm x 1.2 cm) was used as a working electrode and a platinum wire as an auxiliary electrode at a scan rate of 50 mV/s against a Ag/AgCl reference electrode in anhydrous DMF and CH_3CN, using 0.1 M of TBAP as a supporting electrolyte in nitrogen atmosphere. All cell potentials were taken by using a homemade Ag/AgCl, KCl (sat.) reference electrode. Spectroelectrochemical experiments were carried out in a cell built from a 1 cm commercial UV-visible cuvette using Hewlett-Packard 8453 UV-Visible diode array spectrophotometer. The ITO-coated glass slide was used as the working electrode, a platinum wire as the counter electrode, and a Ag/AgCl cell as the reference electrode.

3.2.4 Fabrication and Measurement of the Memory Device

The memory device was fabricated with the configuration of ITO/polymer/Al as shown in Figure 3.2. The ITO glass used for memory device was precleaned by ultrasonication with water, acetone, and isopropanol each for 15 min. A 250 μl DMAc solution of **AQ-6FPI** and **OAQ-6FPI** (23- 25 mg/ml) was first filtered through 0.45 μm pore size of PTFE membrane syringe filter. Then, the filtered solution was spin-coated onto the ITO glass at a rotation rate of 1000 rpm for 60 s and kept at 100 ^{o}C for 10 mins under nitrogen. The film thickness was determined to be around 50 nm. Finally, a 300-nm-thick Al top electrode was thermally evaporated through the shadow mask (recorded device units of 0.5 × 0.5 mm^2 in size) at a pressure of 10^{-7} torr with a uniform depositing rate of 3-5 Å/s. The electrical characterization of the memory device was performed by a Keithley 4200-SCS semiconductor parameter

analyzer equipped with a Keithely 4205-PG2 arbitrary waveform pulse generator. ITO was used as the cathode (maintained as common), and Al was set as the anode during the voltage sweep. The probe tip used 10 μm diameter tungsten wire attached to a tinned copper shaft with a point radius <0.1 μm (GGB Industries, Inc.).

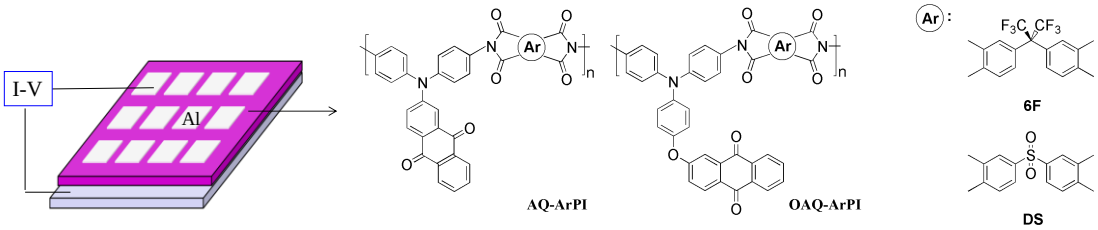

Figure 3.2. Molecular structure of **AQ-PIs** and **OAQ-PIs** and schematic diagram of the memory device consisting of a polymer thin film sandwiched between an ITO bottom electrode and an Al top electrode. The thickness of polymer film is about 50 nm and the thickness of electrode is 300nm.

3.2.5 Molecular Simulation

The Gaussian 09 program package is used for theoretical calculation in this research. And the basic units of **AQ-PIs** and **OAQ-PIs** were optimized by means of the density functional theory (DFT) method at the B3LYP level of theory (Beckesstyle three-parameter density functional theory using the Lee-Yang-Parr correlation functional) with the 6-31G(d) basic set.

3.3 RESULTS AND DISCUSSION

3.3.1 Polymer Synthesis

Polymers **AQ-6FPI**, **AQ-DSPI**, **OAQ-6FPI**, and **OAQ-DSPI** with high molecular weight were synthesized from diamine **1** and **2** *via* the low-temperature solution polycondensation and one-step high temperature polycondensation, respectively, and all obtained polymers having high enough molecular weight to afford flexible films. The inherent viscosities, weight-average molecular weights (*M*w), and polydispersity (PDI) of these resulting polyimides are summarized in Table 3.1.

Table 3.1. Inherent Viscosity and Molecular Weights of Polyimides

Code	η_{inh}[a] (dL/g)	M_w[b]	M_n[b]	PDI[c]
AQ-DSPI	0.56	159,000	70,000	2.27
AQ-6FPI	0.49	169,000	70,500	2.41
OAQ-DSPI	0.57	169,000	81,000	2.08
OAQ-6FPI	0.59	182,000	75,000	2.46

[a] Measured at a polymer concentration of 0.5 g/dL in DMAc at 30 °C.

[b] Calibrated with polystyrene standards, using NMP as the eluent at a constant flow rate of 1 ml/min at 40 °C.

[c] Polydispersity Index (M_w/M_n).

3.3.2 Electrochemical Properties

The electrochemical behavior of the polyimides **AQ-PIs** and **OAQ-PIs** series was investigated by cyclic voltammetry (CV) conducted for the cast film on an indium-tin oxide (ITO)-coated glass slide as working electrode in anhydrous acetonitrile and DMF, using 0.1 M of TBAP as a supporting electrolyte under a nitrogen atmosphere, and the results are summarized in Table 3.2. The typical reduction cyclic voltammograms for polyimides **AQ-6FPI and OAQ-6FPI** are depicted in Figure 3.3(a) and Figure 3.3(b), respectively. The first half-wave potentials ($E_{1/2}$) of the reduction process were -0.79 and -0.80 V for **OAQ-6FPI** and **AQ-6FPI,** respectively, which could be attributed to the reduction of anthraquinone unit.[10] Then, the second half-wave potentials ($E_{1/2}$) of the reduction process were -1.17 and -1.28 V for **OAQ-6FPI** and **AQ-6FPI,** respectively which were derived from the phthalimide ring moiety. Furthermore, the third half-wave potentials ($E_{1/2}$) of the reduction process for **OAQ-6FPI** was -1.49 V, implying the second reduction of anthraquinone unit.

Meanwhile, the results of the corresponding result of **DSPIs** are demonstrated in Figure 3.4 for comparison. However, only two redox couple, with the half-wave potentials of -0.76 V and -0.53 V for the first and second one respectively, and lower onset value in comparison to **OAQ-6FPI** could be observed during the reduction process for **OAQ-DSPI**, as shown in Figure 3.4(a). The different result comparing to **OAQ-6FPI** might be attributed to the incorporation of sulfone unit replaces 6F unit in the backbone of the polymer then enhanced the electron-withdrawing capability and lower the reduction potential of the phthalimide ring moiety and then resulted the overlap of the redox couple of anthraquinone unit and phthalimide ring moiety. Besides, the lower onset value could be viewed as a indication of the electron-withdrawing capability of sulfone-containing phthalimide is stronger than anthraquinone unit. The cyclic voltammetry diagram of Figure 3.4(b) revealed the

electrochemical behavior of **AQ-DSPI**. the one redox couple with the half-wave potentials of -0.84 V and lower onset value comparing to corresponding **AQ-6FPI** could be found during the measurement. As the similar phenomenon discovered from **OAQ-DSPI**, this redox couple could be attributed to the both of anthraquinone unit and phthalimide ring moiety.

Table 3.2. Redox Potentials and Energy Levels of Polyimides

Code	Thin films (nm)		Oxidation[a]	Reduction[b]		E_g^{EC}	E_g^{Opt}	Energy Level		
	λ_{max}	λ_{onset}	$E_{1/2}$ (V)	E_{onset}	$E_{1/2}$ (V)	(eV)	(eV)	$HOMO^{EC}$ (eV)[c]	$LUMO^{Opt}$ (eV)	$LUMO^{EC}$ (eV)
AQ-DSPI	308	566	1.29	-0.65	-0.84	2.08	2.19	5.65	3.46	3.44
AQ-6FPI	314	563	1.31	-0.70	-0.80	2.11	2.20	5.67	3.48	3.48
OAQ-DSPI	309	582	1.09	-0.59	-0.76	1.87	2.13	5.45	3.32	3.44
OAQ-6FPI	317	566	1.11	-0.68	-0.78	1.89	2.19	5.47	3.28	3.46

E_g^{EC} (Electrochemical band gap): Difference between $HOMO^{EC}$ and $LUMO^{EC}$.

E_g^{Opt} (Optical band gap): Calculated from polymer films (E_g=1240/λ_{onset}).

$LUMO^{Opt}$ (LUMO energy levels calculated from optical method): Difference between $HOMO^{EC}$ and E_g^{Opt}.

[a] vs. Ag/AgCl in CH_3CN.

[b] vs. Ag/AgCl in DMF.

[c] The HOMO and LUMO energy levels were calculated from cyclic voltammetry and were referenced to ferrocene (4.8 eV; $E_{1/2}$= 0.44 V in CH_3CN; $E_{1/2}$= 0.52 V in DMF).

(a)

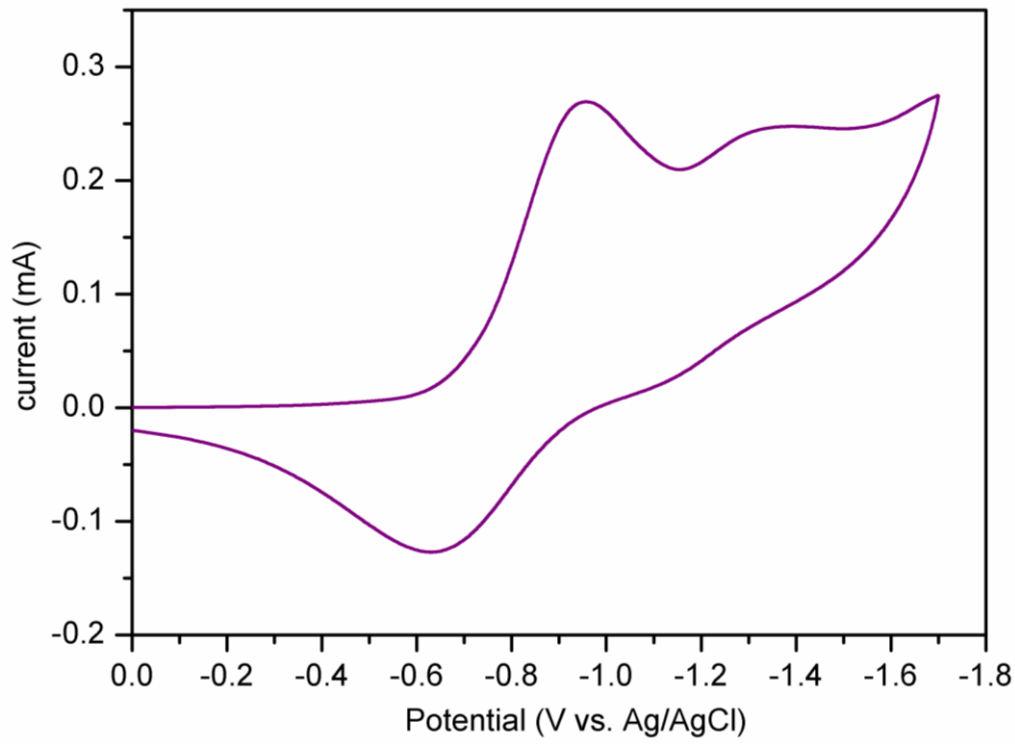

(b)

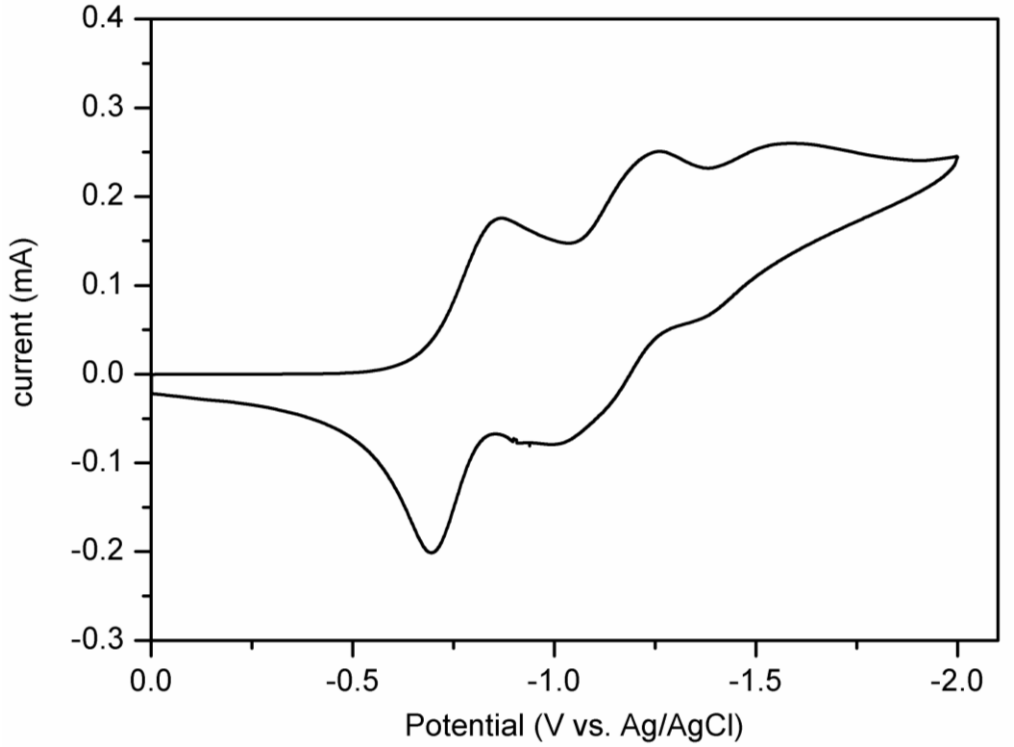

Figure 3.3. Cyclic voltammetric diagrams of polyimide (a) **AQ-6FPI** and (b) **OAQ-6FPI** films on an ITO-coated glass substrate over cyclic scans in 0.1M TBAP/DMF at a scan rate of 50 mV/s.

(a)

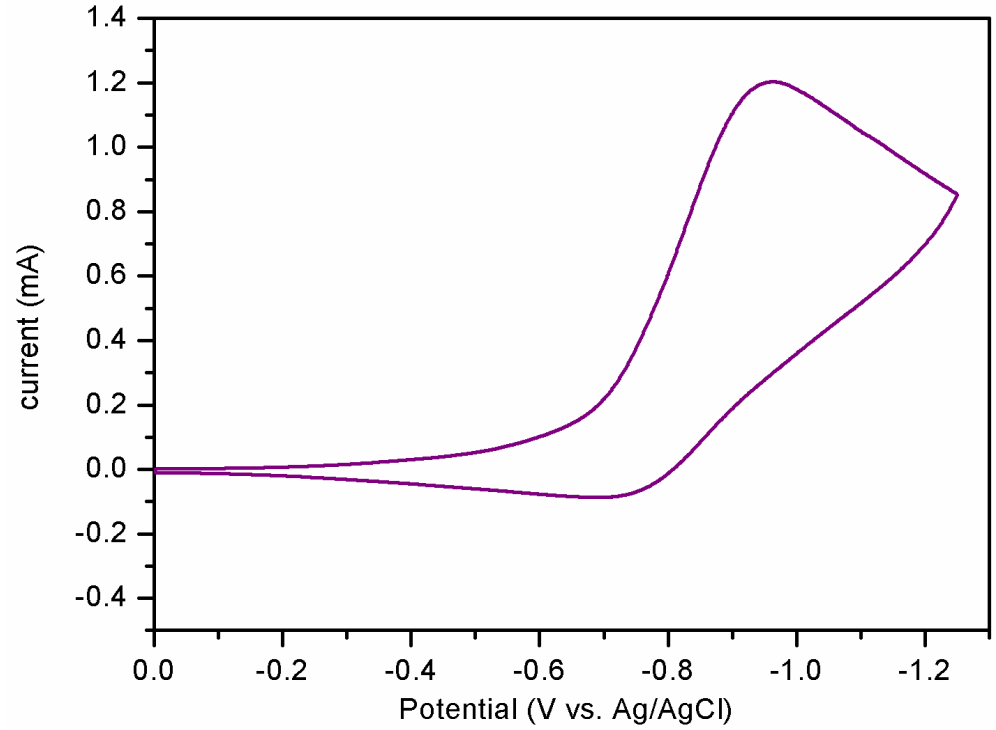

(b)

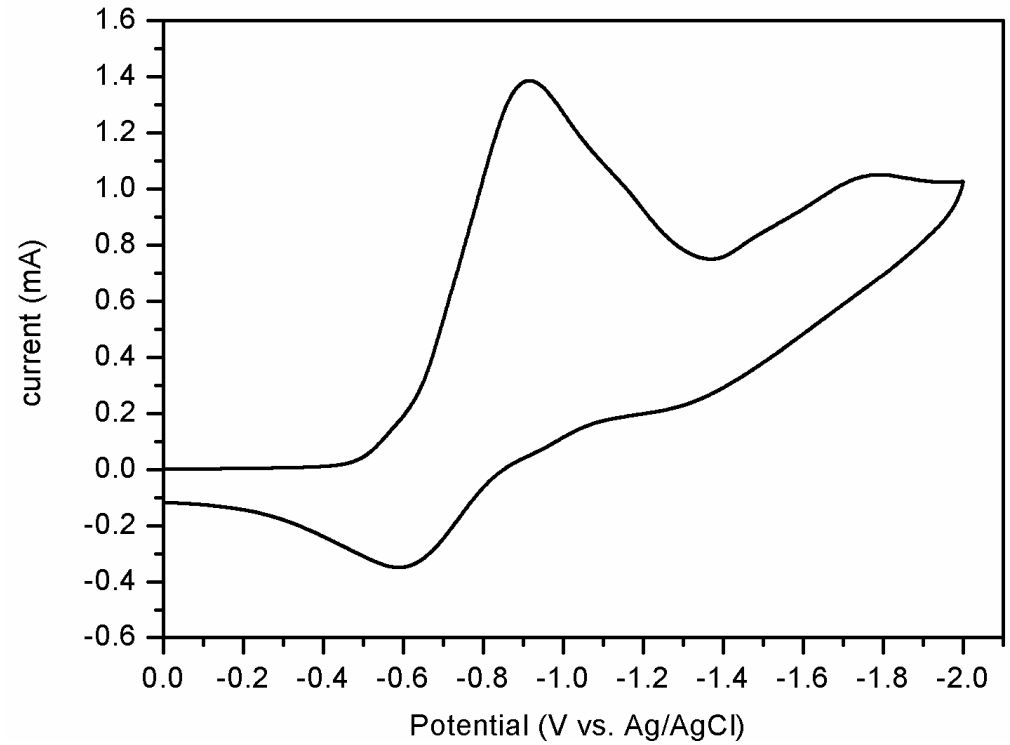

Figure 3.4. Cyclic voltammetric diagrams of polyimide (a) **AQ-DSPI** and (b) **OAQ-DSPI** films on an ITO-coated glass substrate over cyclic scans in 0.1M TBAP/DMF at a scan rate of 50 mV/s.

3.3.3 Memory Device Characteristics of the AQ-PIs and OAQ-PIs

Figure 3.5(a) exhibits the current-voltage result of **AQ-6FPI**; the device switched to ON state at threshold voltage about -3.5 V (line 1) and subsequently reset to OFF state just after removing the applied electrical field without any erasing process, and then the device could be turned on again at threshold voltage about -3.4 V during the second negative sweep (line 2), indicating that this polymer memory device showed DRAM property. Besides, the device kept at at low-conductivity (OFF) state when it was conducted with positive bias.

Moreover, the behavior of dual sweep current-voltage of **AQ-6FPI** is depicted in Figure 3.6(a); the device could be set to ON state at threshold voltage about -3.5 V and reset to OFF state at around -1.9 V during the backward sweep of the dual sweep process indicated the instability of the CT state of **AQ-6FPI**. Figure 3.5(b) demonstrates the current-voltage result of **OAQ-6FPI**, the current increased from 10^{-13}-10^{-14} to 10^{-4}-10^{-5} (high-conductivity state) instantaneously at the threshold voltage of -3.9 V in the first negative sweep (line 1) indicating the writing process for the transition from the OFF state to the ON state. The device remained in the ON state during the subsequent negative scan (line 2) and the subsequent positive scan (line 3), which could be defined as the reading process. After turning off the power for 8 minutes, the memory device returned to OFF state without any erasing process and could be turned on again at threshold voltage -3.9 V (line 4); this phenomenon implied that the memory device possessed SRAM property. Moreover, the effect of operation time on the ON and OFF states of the ITO/**OAQ-6FPI**/Al device with continuous -2 V was investigated as shown in Figure 3.6(b), and no obvious degradation in current could be observed at both ON and OFF states for at least 10^4 s in the readout test, revealing the excellent stability of this device.

Figure 3.7 (a) and Figure 3.7 (b) depicts the I-V characteristics of **AQ-DSPI** and

OAQ-DSPI, respectively. As shown in Figure 3.7 (a), a instantaneously increasing of the current could be observed at -3.2 V during the first negative sweep (line 1). The device also could remain in the ON state during the subsequent negative (line 2) and positive scans (line 3). Besides, the similar characteristics could be found in Figure 3.7 (b). The writing process could be performed at -4.0 V under negative bias (line 1) and the reading process could be performed by both of negative (line 2) and positive (line 3) swept. The results indicated both of these two memory devices could not be reset to the initial OFF state by the introduction of a reverse scan and is thus non-bias-erasable. The device of **AQ-DSPI** and **OAQ-DSPI** maintained in the ON state after turning off the power for 10 and 8 minutes, respectively. However, it was found that the ON state had relaxed to the steady OFF state without an erasing process. The re-writing process could be conducted (line 4 in both Figure 3.7(a) and (b)) at the threshold voltage of -3.3 V and -3.7 V, respectively. The volatile behavior with longer retention time at the ON state thus could be defined as the SRAM characteristic.

(a)

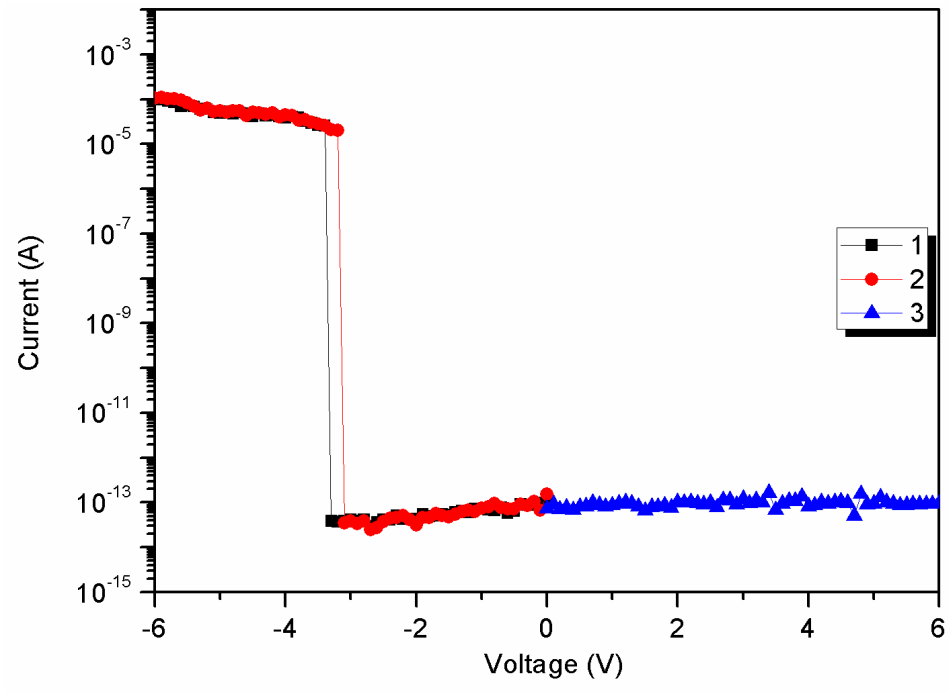

(b)

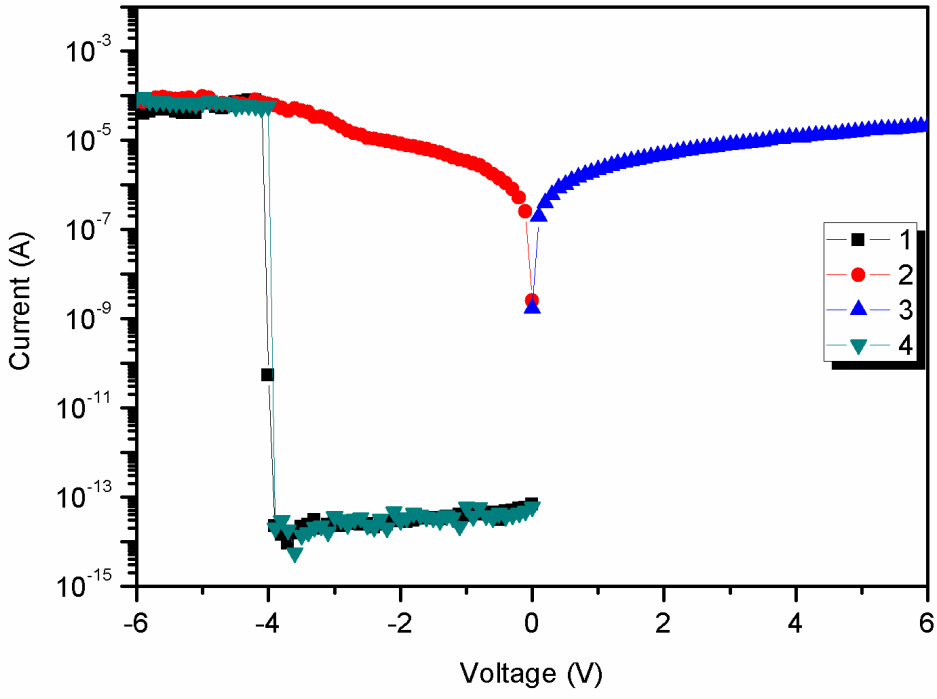

Figure 3.5. (a) Current-voltage (I-V) characteristics of the ITO/**AQ-6FPI**/Al memory device (The time interval between the first and second sweep is less than 5 seconds), (b) Current-voltage (I-V) characteristics of the ITO/**OAQ-6FPI**/Al memory device (The time interval between the third and fourth sweep is 8 minutes).

(a)

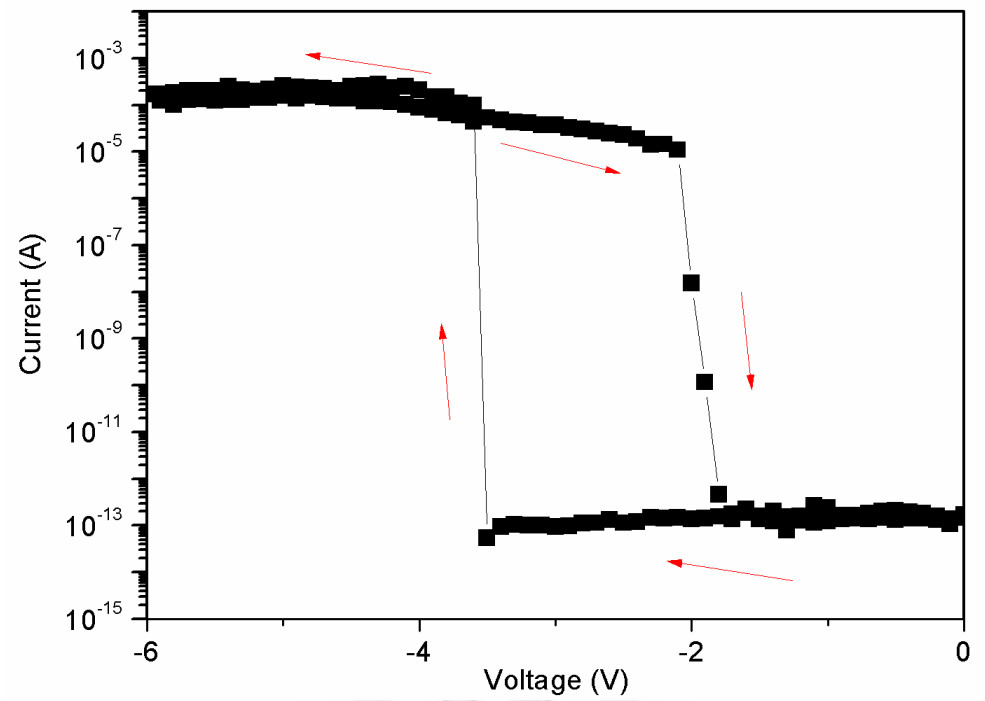

(b)

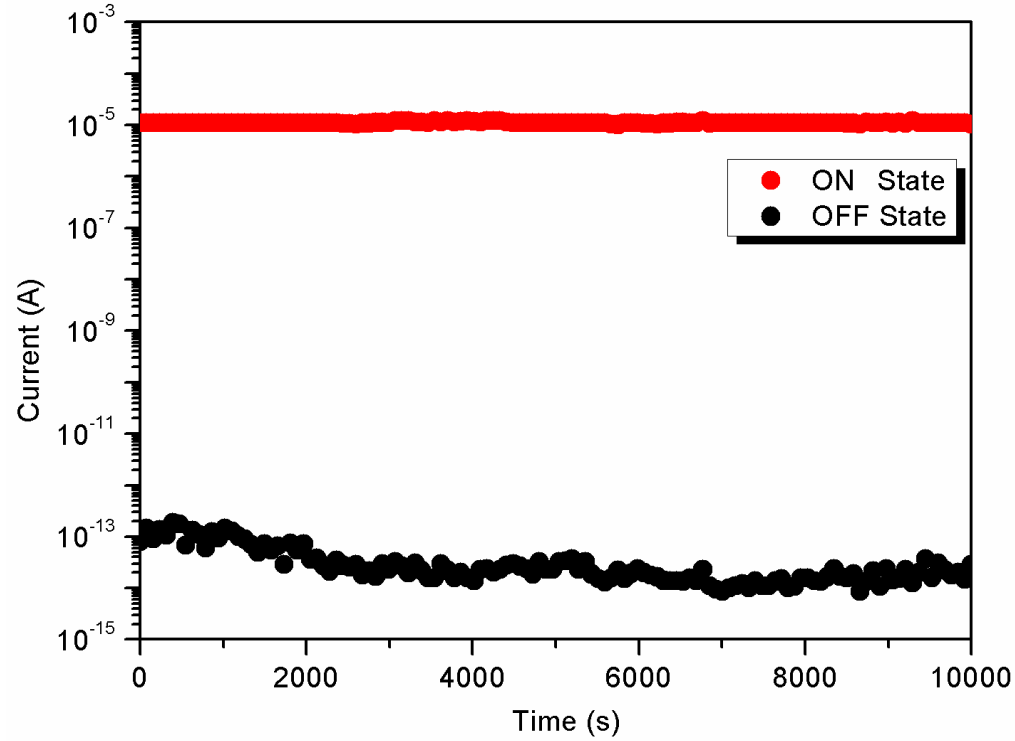

Figure 3.6. (a) Dual sweep current-voltage (I-V) characteristics of the ITO/**AQ-6FPI**/Al memory device. Each dual sweep process will turn to off state during the backward sweep. (b) Effect of operation time on the ON and OFF states of the ITO/**OAQ-6FPI**/Al device with a continue -2 V.

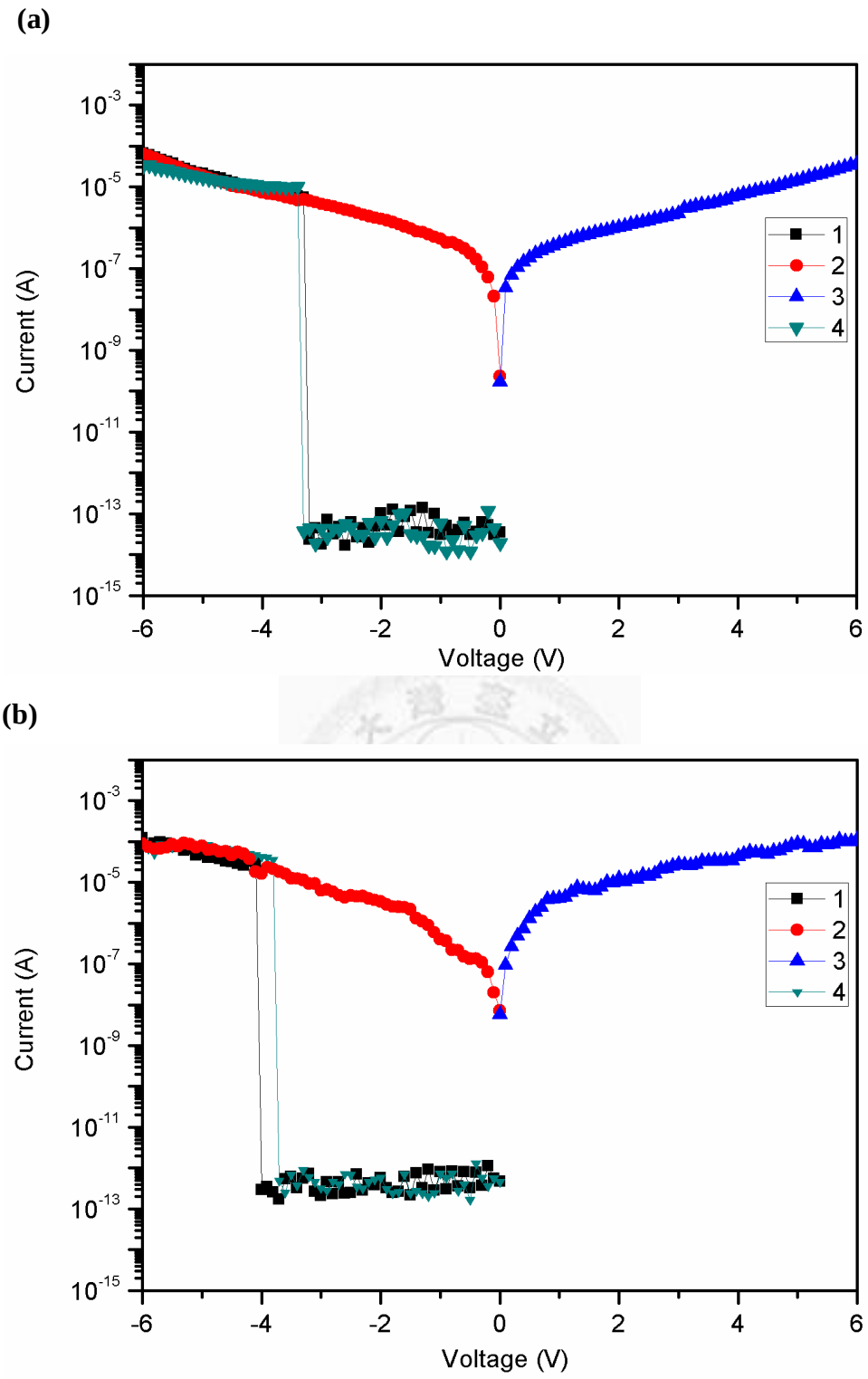

Figure 3.7. (a) Current-voltage (I-V) characteristics of the ITO/**AQ-DSPI**/Al memory device and (b) Current-voltage (I-V) characteristics of the ITO/**OAQ-DSPI**/Al memory device. The time interval between the third and fourth sweep is 10 and 8 minutes, respectively.

3.3.4 Switching Mechanism of the AQ-PIs and OAQ-PIs

For getting more understanding to the memory behaviors of the present **OAQ-6FPI** and **AQ-6FPI** devices, the molecular orbital and electrostatic potential surface (ESP) of the basic units were estimated by taking molecular simulation, and the results are illustrated in Figure 3.8. These two systems with similar molecular orbital location (charge density distribution) shown in Figure 3.8 indicated that these two systems could proceed similar charge transfer route from TPA donor to the pendent anthraquinone acceptor. However, the different memory properties of these two systems could be contributed to the isolated effect and the non-coplanar geometry of CT complex between the TPA donor and the acceptor occured in **OAQ-6FPI** structure by the phenoxy linkage between donor and acceptor moieties when compared with **AQ-6FPI**. The ether linkage between donor and pendent anthraquinone acceptor in **OAQ-6FPI** can efficiently prevent the intramolecular backward route therefore stabilize the CT complex, resulting a much longer retention time than **AQ-6FPI** system.

The same approching method was performed for invesgating the switching behavior of **AQ-DSPI** and **OAQ-DSPI**, and the outcome of theoretical analysis are demostrated in Figure 3.9. Comparing to aboved **AQ-6FPI and OAQ-6FPI**, it revealed an unexpectedly result in the different distribution of the LUMO energy level. In **6FPI** system, the LUMO energy levels were located mainly at the pendent anthraquinone moieties, while it were located at the sulfone-containing phthalimide units in **DSPI** system. According to this result and the charge transfer theory, the electrons at the HOMO could accumulate energy then transit to the higher LUMOs (LUMO+1 ~ LUMO+4) then result the excited state then transfer to the steady LUMO (sulfone-containing phthalimide units) or directly migrate to LUMO for a conversion into CT state then cause an tremendous decrease in the electric resistance

of the polymer films. Nevertheless, although these two devices possess a longer retention time than DRAM, the above hypothesis of linkage effect between the donor and the acceptor affecting the retention time of **AQ-6FPI** and **OAQ-6FPI** could not elucidate the long retention time here, but the stronger electron-withdrawing capability of the backbone phthalimide units which could result a stronger charge-transfer effect between donor and acceptor might probably induce some effect on memory behavior for extending the relaxation time.[11] The effects of electron-withdrawing phthalimide units within polyimide backbone on memory properties are interesting and worth to be further investigated.

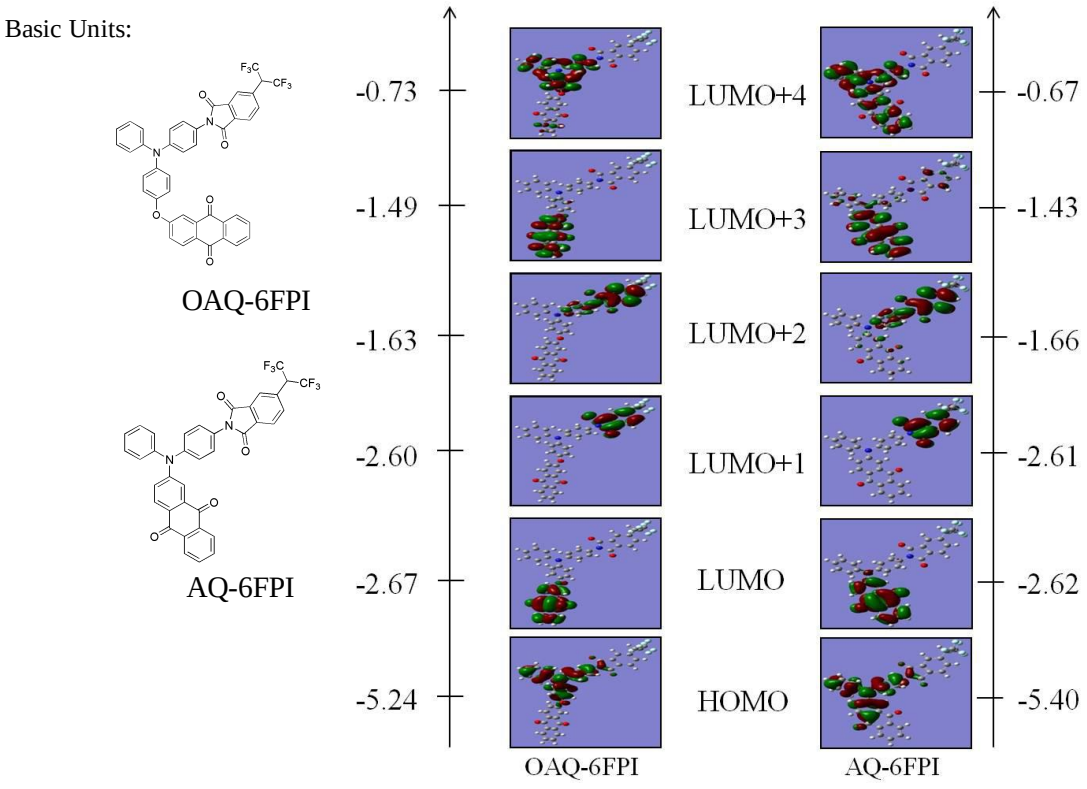

Figure 3.8. Calculated molecular orbitals and corresponding energy levels of the basic units (BU) for **OAQ-6PFI** and **AQ-6FPI**.

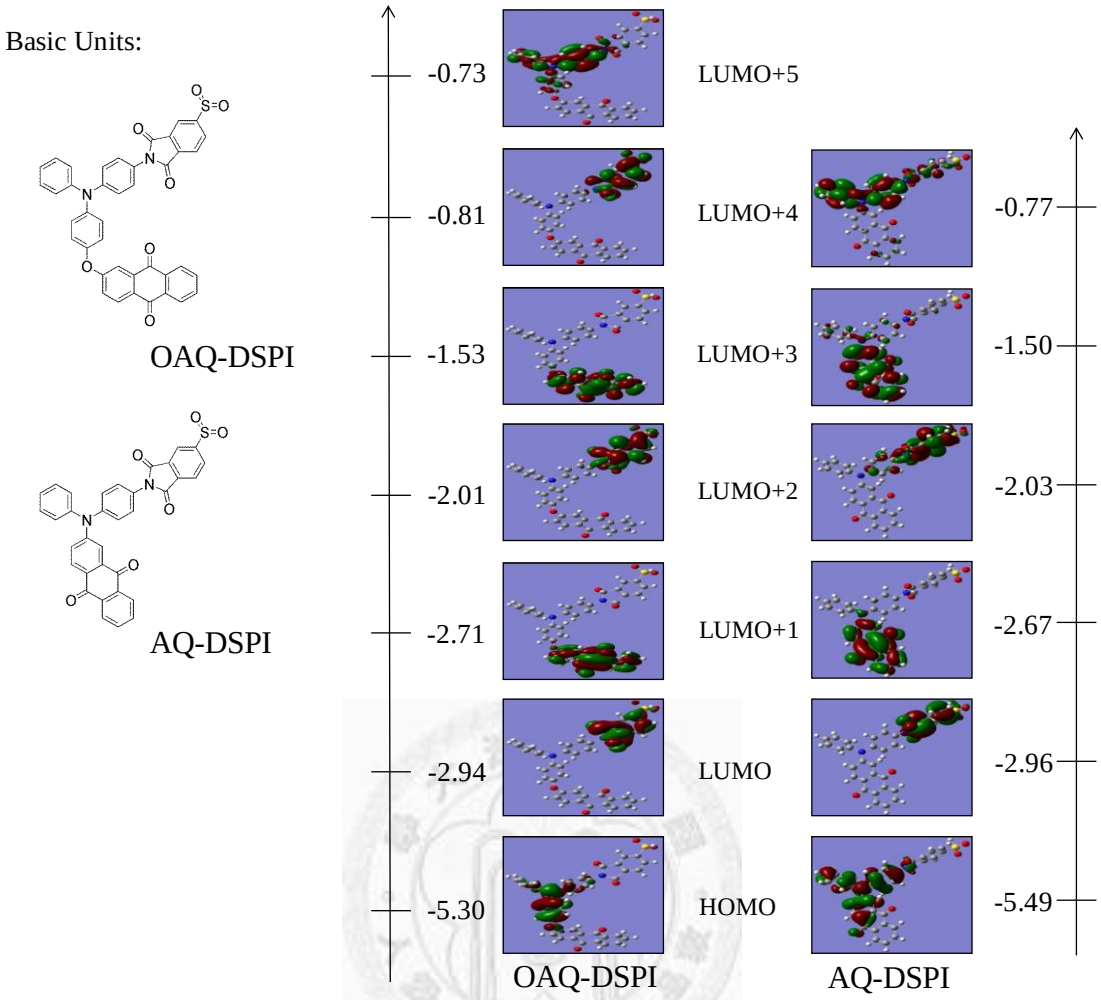

Figure 3.9. Calculated molecular orbitals and corresponding energy levels of the basic units (BU) for **OAQ-DSPI** and **AQ-DSPI**.

3.3.5 Spectroelectrochemistry

Because of the energy levels of LUMO+1 (phthalimide moiety) and LUMO (anthraquinone moiety) were too close to be distinguished from the result of simulation (as shown in Figure 3.8), the spectroelectrochemical measurements were used to evaluate and compare the electron-withdrawing capability between the two moieties for demonstrating the above switching mechanism. The spectroelectrochemical behavior of polyimide **OAQ-6FPI** film is presented in Figure 3.10(a) as UV-vis-NIR absorbance curves correlated to applied potentials. By applying the reduction potential of -0.8 V (the first stage reduction potential of polyimide **OAQ-6FPI**), the increasing intensity of the absorption peaks at 555 nm and 894 nm could be observed. For comparison, the corresponding polyimide **TPA-6FPI**[12] shown in Figure 3.10(b) was used to get more conclusive evidence about the reductive capability between anthraquinone and phthalimide moieties. At the reduction potential of -0.8 V, there is no obvious UV-vis-NIR absorbance change could be observed. An apparent absorption change in the UV-vis region from 300 nm to 450 nm could be found only until the reduction potential was at -1.3 V, implying the reduction of the imide ring requires a higher electrical potential. Thus, we confirmed the first stable anion radical from UV-vis-NIR spectral changes should be derived from anthraquinone moiety for **OAQ-6FPI**.[10]

The same approching way was executed for studying the switching behavior of the **DSPIs** and confirning the reductivie capability of anthraquinone unit and sulfone-containing phthalimide ring moiety. The spectroelectrochemical behavior of polyimide **OAQ-DSPI** film is presented in Figure 3.11 as UV-vis absorbance curves correlated to applied potentials. By applying the reduction potential of -0.65 V ,below the onset value -0.68 V of polyimide **OAQ-6FPI** but higher the onset value -0.59 V of polyimide **OAQ-DSPI**, the increasing intensity of the absorption peaks of imide ring

at 306 nm could be observed. An typical absorption change of anthraquinone moiety in the UV-vis region at 554 nm could be observed at the reduction potential was at -0.80 V, implying the reduction of the anthraquinone unit requires a higher electrical potential than sulfone-containing phthalimide .

(a)

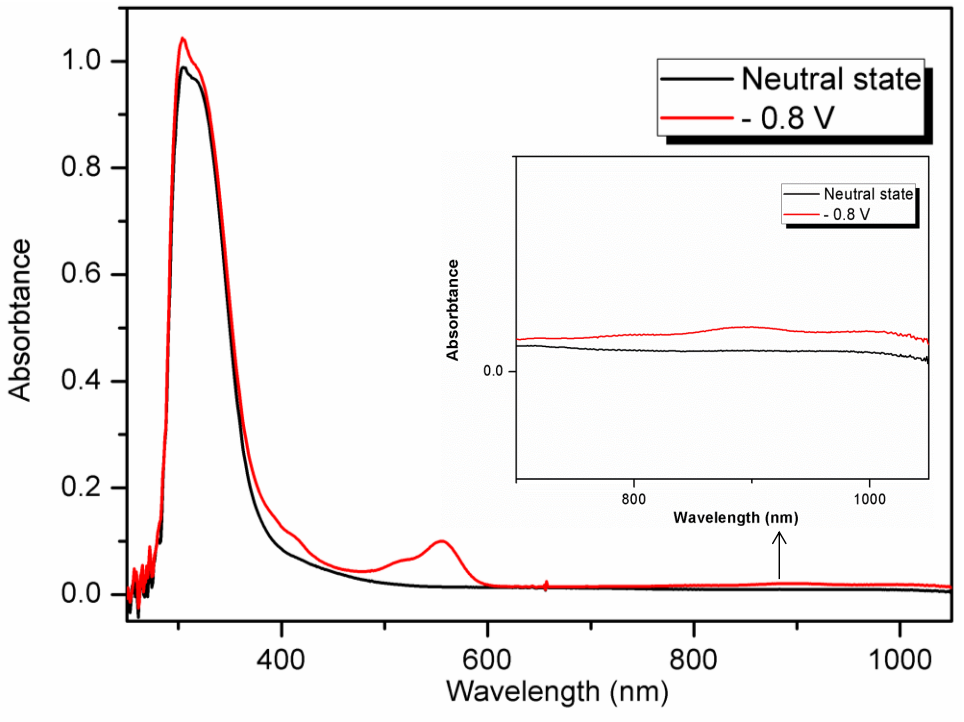

(b)

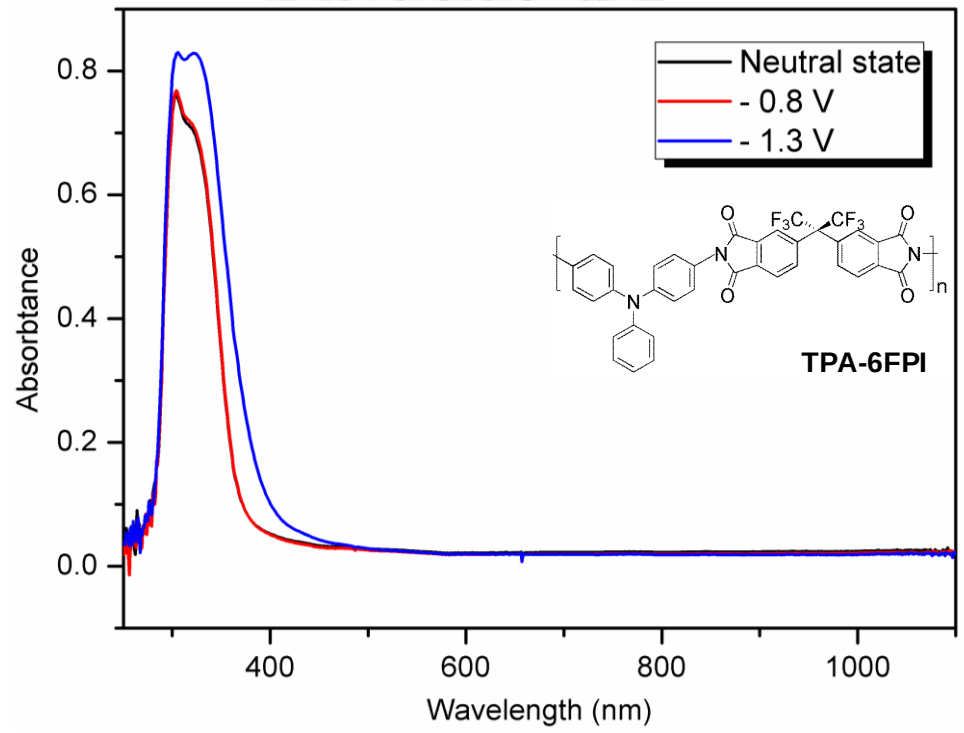

Figure 3.10. UV-vis-NIR spectra of polyimide (a) **OAQ-6FPI** (b) **TPA-6FPI** thin film on the ITO-coated glass substrate in 0.1 M TBAP/DMF.

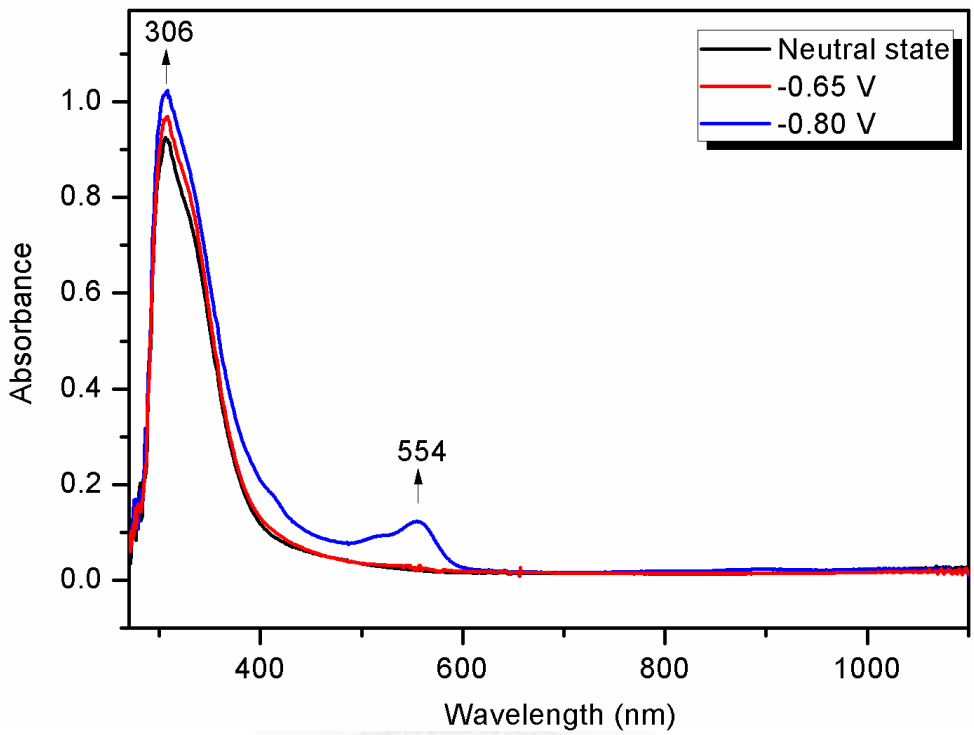

Figure 3.11. UV-vis-NIR spectra of polyimide **OAQ-DSPI** thin film on the ITO-coated glass substrate in 0.1 M TBAP/DMF.

3.4 SUMMARY

TPA-based aromatic polyimides containing pendent anthraquinone both directly attached to and incorporated via ether linkage into backbone as electron acceptor have been successfully synthesized for memory device applications. The memory devices with the configuration of ITO/**AQ-6FPI**/Al exhibited distinct volatile memory characteristics of DRAM while the ITO/**OAQ-6FPI**/Al showed volatile SRAM memory property. Thus, these results indicated the isolated D-A system could effectively extend the retention time in the memory device application. The ON/OFF current ratios of these memory devices are up to 10^9. The theoretical analysis results, electrochemical and spectroelectrochemical studies suggest that the CT mechanism could be used to explain the memory characteristics of these polyimides and confirmed the linkage effect between the donor and acceptor.

Both of ITO/**AQ-DSPI**/Al and ITO/**OAQ-DSPI**/Al show volatile SRAM memory property, high ON/OFF current ratio, and exhibit the retention time for 10 and 8 minutes, respectively. The SRAM behavior could be attributed to the strong charge-transfer effect between donor and acceptor result from TPA donor and backbone sulfone-containing phthalimide units which is deduced from the theoretical analysis results, electrochemical, spectroelectrochemical studies and charge transfer mechanism.

REFERENCES AND NOTES

1. (*a*) R. H. Friend, R. W. Gymer, A. B. Holmes, J. H. Burroughes, R. N. Marks, C. Taliani, D. D. C. Bradley, D. A. Dos Santos, J. L. Bredas, M. Logdlund, W. R. Salaneck, *Nature*, 1999, **397**, 121; *(b)* Q. Peng, E. T. Kang, K. G. Neoh, D. Xiaob, D. Zou, *J. Mater. Chem.*, 2006, **16**, 376; (*c*) K. Lee, J. Y. Kim, S. H. Park, S. H. Kim, S. Cho, A. J. Heeger, *Adv. Mater.*, 2007, **19**, 2445; (*d*) Y. Shao, G. C. Bazan, A. J. Heeger, *Adv. Mater.*, 2008, **20**, 1191; (*e*) Y. Shao, X. Gong, A. J. Heeger, M. Liu, A. K. Y. Jen, *Adv. Mater.*, 2009, **21**, 1972.
2. (*a)* H. Sirringhaus, N. Tessler, R. H. Friend, *Science*, 1998, **280**, 1741; (*b*) L. L. Chua, J. Zaumseil, J. F. Chang, E. C. W. Ou, P. K. H. Ho, H. Sirringhaus, R. H. Friend, *Nature*, 2005, **434**, 194; (*c*) A. Babel, Y. Zhu, K. F. Cheng, W. C. Chen, S. A. Jenekhe, *Adv. Funct. Mater.*, 2007, **17**, 2542; (*d*) M. Morana, M. Wegscheider, A. Bonanni, N. Kopidakis, S. Shaheen, M. Scharber, Z. Zhu, D. Waller, R. Gaudiana, C. Brabec, *Adv. Funct. Mater.*, 2008, **18**, 1757; (*e*) H. Yan, Z. H. Chen, Y. Zheng, C. Newman, J. R. Quinn, F. Dotz, M. Kastler, A. Facchetti, *Nature*, 2009, **457**, 679-U1; (*f*) J. H. Tsai, W. Y. Lee, W. C. Chen, C. Y. Yu, G. W. Hwang, C. Ting, *Chem. Mater.*, 2010, **22**, 3290; (*g*) C. J. Lin, W. Y. Lee, C. Lu, H. W. Lin, W. C. Chen, *Macromolecules*, 2011, **44** , 9565.
3. (*a*) G. Yu, J. Gao, J. C. Hummelen, F. Wudl, A. J. Heeger, *Science*, 1995, **270**, 1789; (*b*) C. J. Brabec, N. S. Sariciftci, J. C. Hummelen, *Adv. Funct. Mater.*, 2001, **11**, 15; (*c*) M. H. Chen, J. Hou, Z. Hong, G. Yang, S. Sista, L. M. Chen, Y. Yang, *Adv. Mater.*, 2009, **21**, 4238; (*d*) J. H. Hou, T. L. Chen, S. Q. Zhang, L. J. Huo, S. Sista, Y. Yang, *Macromolecules*, 2009, **42**, 9217; (*e*) A. Kumar, H. H. Liao, Y. Yang, *Org. Electron.*, 2009**, 10**, 1615; (*f*) S. Sista, Z. R. Hong, M. H. Park, Z. Xu, Y. Yang, *Adv. Mater.*, 2010, **22**, E77.

4. (*a*) Q. D. Ling, F. C. Chang, Y. Song, C. X. Zhu, D. J. Liaw, D. S. H. Chan, E. T. Kang, K. G. Neoh, *J. Am. Chem. Soc.*, 2006, **128**, 8732; (*b*) S. G. Hahm, S. Choi, S. H. Hong, T. J. Lee, S. Park, D. M. Kim, W. S. Kwon, K. Kim, O. Kim, M. Ree, *Adv. Funct. Mater.*, 2008, **18**, 3276; (*c*) S. G. Hahm, S. Choi, S. H. Hong, T. J. Lee, S. Park, D. M. Kim, J. C. Kim, W. Kwon, K. Kim, M. J. Kim, O. Kim, M. Ree, *J. Mater. Chem.*, 2009, **19**, 2207; (*d*) K. Kim, S. Park, S. G. Hahm, T. J. Lee, D. M. Kim, J. C. Kim, W. Kwon, Y. G. Ko, M. Ree, *J. Phys. Chem.B*, 2009, **113**, 9143; (*e*) Y. L. Liu, Q. D. Ling, E. T. Kang, K. G. Neoh, D. J. Liaw, K. L. Wang, W. T. Liou, C. X. Zhu, D. S. H. Chan, *J. Appl. Phys.*, 2009, **105**, 044501; (*f*) Y. L. Liu, K. L. Wang, G. S. Huang, C. X. Zhu, E. S. Tok, K. G. Neoh, E. T. Kang, *Chem. Mater.*, 2009, **21**, 3391; (*g*) Y. Q. Li, R. C. Fang, A. M. Zheng, Y. Y. Chu, X. Tao, H. H. Xu, S. J. Ding, Y. Z. Shen, *J. Mater. Chem.*, 2011, **21**, 15643; (*h*) Y. Q. Li, R. C. Fang, S. J. Ding, Y. Z. Shen, *Macromol. Chem. Phys.* 2011, **212**, 2360; (*i*) C. L. Liu, W. C. Chen, *Polym. Chem.*, 2011, **2**, 2169; (*j*) C. J. Chen, H. J. Yen, W. C. Chen, G. S. Liou, *J. Polym. Sci. Part A: Polym. Chem.*, 2011, **49**, 3709; (*k*) Y. Q. Li, Y. Y. Chu, R. C. Fang, S. J. Ding, Y. L. Wang, Y. Z. Shen, A. M. Zheng, *Polymer*, 2012, **53**, 229; (*l*) B. L. Hu, F. Zhuge, X. J. Zhu, S. S. Peng, X. X. Chen, L. Pan, Q. Yan, R. W. Li, *J. Mater. Chem.*, 2012, **22**, 520; (*m*) Y. G. Ko, W. Kwon, H. J. Yen, C. W. Chang, D. M. Kim, K. Kim, S. G. Hahm, T. J. Lee, G. S. Liou, M. Ree, *Macromolecules*, 2012, **45**, 3749.

5. D. W. Mosley, K. Auld, D. Conner, J. Gregory, X. Q. Liu, A. Pedicini, D. Thorsen, M. Wills, G. Khanarian, E. S. Simon, *Proc. SPIE.*, 2008, **6910**, 691017.

6. A. Wilkinson, *Blackwell Science*, 2nd ed., Boston , **1997**.

7. (*a*) T. J. Lee, C. W. Chang, S. G. Hahm, K. Kim, S. Park, D. M. Kim, J. Kim, W. S. Kwon, G. S. Liou, M. Ree, *Nanotechnology*, 2009, **20**, 135204; *(b)* D. M. Kim,

S. Park, T. J. Lee, S. G. Hahm, K. Kim, J. C. Kim, W. Kwon, M. Ree, *Langmuir*, 2009, **25**, 11713.

8. (*a*) Q. D. Ling, D. J. Liaw, E. Y. H. Teo, C. X. Zhu, D. S. H. Chan, E. T. Kang, K. G. Neoh, *Polymer*, 2007, **48**, 5182; (*b*) N. H. You, C. C. Chueh, C. L. Liu, M. Ueda, W. C. Chen, *Macromolecules*, 2009, **42**, 4456; (*c*) T. Kuorosawa, C. C. Chueh, C. L. Liu, T. Higashihara, M. Ueda, W. C. Chen, *Macromolecules*, 2010, **43**, 1236.
9. (*a*) K. L. Wang, Y. L. Liu, J. W. Lee, K. G. Neoh, E. T. Kang, *Macromolecules*, 2010, **43**, 7159; (*b*) K. L. Wang, Y. L. Liu, I. H. Shih, K. G. Neoh, E. T. Kang, *J. Polym. Sci. Part A Polym. Chem.*, 2010, **48**, 5790.
10. H. J. Yen, K. Y. Lin, G. S. Liou, *J. Polym. Sci. Part A: Polym. Chem*., 2012, **50**, 61.
11. (*a*) Y. Q. Li, H. H. Xu, X. Tao, K. J. Qian, S. Fu, S. J. Ding, Y. Z. Shen, *Polym. Int.*, 2011, **60**, 1679; (*b*) Y. Zhang, Y. W. Liu, Q. Lan, S. W. Liu, Z. X. Qin, L. H. Chen, C. Y. Zhao, Z. G. Chi, J. R. Xu, J. Economy, *Chem. Mater.*, 2012, **24**, 1212.
12. S. H. Cheng, S. H. Hsiao, T. H. Su, G. S. Liou, *Macromolecules*, 2005, **38**, 307.

CHAPTER 4

High Performance Polymers With Different D-L-A Containing for Memory Application

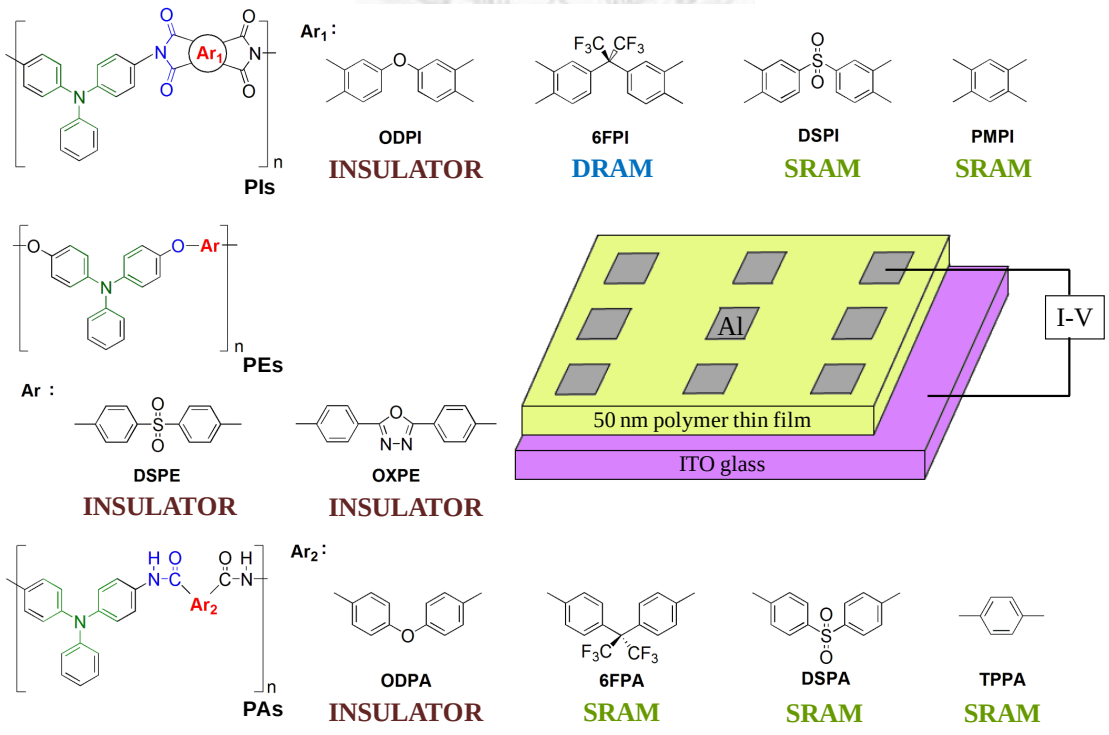

ABSTRACT OF CHAPTER 4

The memory device derived from the structural related triphenylamine-based polyimides **(PIs)**, polyamides **(PAs)**, and polyethers **(PEs)** have been successfully fabricated for comparison research. The differences of HOMO energy levels, LUMOs energy levels among these polymers with different electron-withdrawing moiety or linkage were investigated and demonstrated the effect on the memory behavior systemically. With the electron-withdrawing moiety intensity increasing, the retention time of corresponding memory device increases, while reducing the coplainity could provide the same contribution. **ODPI**, **ODPA**, and **PEs** demonstrated no memory but insulator behaviors, **6FPI** exhibited DRAM characteristic, and the stronger acceptor containing **DSPI** and **PMPI** showed SRAM behavior with 4 and 8 minutes of retention time, respectively. **TPPA**, **6FPA**, and **DSPA** all possessed SRAM characteristic with the retention time of 2, 5, and 8 minutes. **6FPA** and **DSPA** showed longer retention time than corresponding **6FPI** and **DSPI** due to the non-coplainity amide linkage group.

4.1 INTRODUCTION

In addition to light-emtting diodes,[1] transistors,[2] and solar cells,[3] bistable electrical resistive switching memory devices (RRAM) based on polymeric materialrials[4] have attracted tremendous attention and been widely investigated recently. Especially for donor-acceptor (D-A) containing polymers, which can be switched between two conductive states in response to the external electrical field attracted tremendous attention due to the facile structural design and synthesis thus affect the resulting switching behavior.[4] Aromatic high-performance polymers such as polyimde and polyamide thin film are competitively candidates as the active layer in memory device applications[5] among all the studied D-A systems because of the excellent thermal dimensional stability, chemical resistance, and high ON/OFF current ratio resulted from the insulator nature in the initial OFF state. Besides, the introduction of triphenylamine (TPA) group into polymer backbone could not only improve the solubility but also provide an excellent electro-active behavior thus explored for electrochromic[6] resulting from the electron-rich triarylamines which can be easily oxidized to form stable radical cations, and the oxidation process is always associated with a noticeable change of coloration.and memory device applications.[7]

The crucial factors on the memory property, in particular retention time, were structural effect (different donor or acceptor), dipole moment effect, and linkage group effect summarized from previous published literature. The donor effect resulted from incorperating different substituents into electron donating moieties on the relaxation time of the polymeric memory was investigated by Kang's and Ree's work. The devices fabricated by TPA-based polyimide **TPA-6FPI**[7a] exhibited volatile DRAM behavior, while the structural related but phenylamine-substituded or hydroxy-substituted TPA-containing polyimide (**6F-2TPA PI)**[7b] and (**6F-HTPA PI)**[7c]

demostrated non-volatile write-once-read-mamy-times (WORM) property. However, the electron acceptor effect was investigated in our recently work,[7g] which demonstated the retention time of corresponding memory device increased as the electron-withdrawing moiety intensity of polyimides increased. Besides, the higher dipole moment characteristic of polymer can transit from DRAM to SRAM and even become WORM or flash type non-volatile memory behavior.[5b,8] Furthermore, the linkage group effects between donor and acceptor moieties influence the time interval from CT state to the initial ground state due to low co-plainity and the conformational changes between the donor and acceptor moiety induced by charge transfer, that could increase the torsional displacement and produce a potential energy barrier for the back charge transfer to ground state thus extended the retention time of the ON state.[4o,9]

In this study, we prepared the memory device derived from the structural related donor-linkage-acceptor (D-L-A) containing TPA-based polyimide**s (PIs)**, polyamides **(PAs)**, and polyethers **(PEs)** for comparison and systematical research on both linkage and acceptor effect. These polymeric memory devices were fabricated with the sandwich configuration of ITO/polymer thin film/Al as shown in Figure 4.1, and the memory properties were characterized by I-V measurements. The corresponding HOMO energy level, and LUMOs energy level analyzed by electrochemical properties, optical properties, and molecular simulation on the basic unit carried out by DFT/B3LYP/6-31G(d) with the Gaussian 09 program arose from different linkage group and acceptor moiety implying donor-acceptor charge-transfer interaction among these polymers was demonstrated to affect the volatile memory behavior.

4.2 EXPERIMENTAL SECTION

4.2.1 Materials

4,4'-Diaminotriphenylamine **(1)**, 4,4'-dihydroxyltriphenyamine **(2)**, 2,5-bis(4-fluorophenyl)-1,3,4-oxadiazole (**OXA-DF**) were synthesized according to the literature.[10] The electroactive TPA-based aromatic **PAs** and **PIs** was prepared according to previous research[6a,6b,10a] from the diamine monomer **(1)**. Acetonitrile (CH_3CN), *N*,*N*-dimethylformamide (DMF) (ACROS), *N*,*N*-dimethylacetamide (DMAc) (TEDIA), and tetrahydrofuran (THF) (TEDIA) were used without further purification. 2,2-Bis(3,4-dicarboxyphenyl)hexafluoropropane dianhydride (6FDA) (Chriskev), oxydiphthalic dianhydride (ODPA) (Chriskev), 3,3',4,4'-diphenylsulfonetetracarboxylic dianhydride (DSDA) (TCI), and pyromellitic dianhydride (PMDA) (Chriskev) were purified by recrystallization from acetic anhydride. Tetrabutylammonium perchlorate (TBAP) (ACROS) was recrystallized twice by ethyl acetate under nitrogen atmosphere and then dried in vacuo prior to use. All other reagents were used as received from commercial sources.

4.2.2 Polymer Synthesis

Preparation of Polyimide PMPI by Two-step Method *via* Thermal Imidization Reaction

To a solution of 0.7 mmol of diamine (**1**) in 3mL of DMAc, 0.7 mmol of dianhydride PMDA was added in one portion. The mixture was stirred at room temperature for 2 h to afford a viscous poly(amic acid) (PAA) solution. The poly(amic acid) was subsequently converted to polyimide film *via* a thermal imidization process (100 ^{o}C 1 h, 200 ^{o}C 0.5 h, and 350 ^{o}C 1 h) in vacuum oven. The inherent viscosity of the corresponding PAA film was 0.43 dL/g in DMAc at a concentration of 0.5 g/dL at

30 ^{o}C.

Preparation of Polyehter PEs

The synthesis of **OXPE** according to published procedure[11] was used as an example to illustrate the general synthetic procedure. To a three necked 50 ml glass reactor was charged with diol monomer **2** (0.14 g, 0.5 mmol), **OXDF** (0.13 g, 0.5 mmol), and 1.5 ml NMP, 1 ml of toluene, and an excess of potassium carbonate (0.15 g, 0.75 mmol). The reaction mixture was heated at 150 ^{o}C for 3 h for removing water during the formation of phenoxide anions, anf then heated at 170 ^{o}C for 1 h, 180 ^{o}C for 3 h, and finally heated at 190 ^{o}C for 1 h. After the reaction, the obtained polymer solution was poured slowly into 300 ml of acidified methanol/water (v/v = 1/1). The precipitate was collected by filtration, washed thoroughly with hot water and methanol, and dried under vacuum at 100 ^{o}C. The inherent viscosity and weight-average molecular weights (Mw) of the obtained polyether **OXPE** was 0.29 dL/g (measured at a concentration of 0.5 g/dL in DMAc at 30 ^{o}C) and 62,000, respectively. The FT-IR spectrum of **OXPE** film exhibited characteristic C=N stretching absorption bands at around 1500-1600, and 1232 cm^{-1} (C-O-C stretching).

4.2.3 Measurements

The inherent viscosities were determined at 0.5 g/dL concentration using Tamson TV-2000 viscometer at 30 ^{o}C. Gel permeation chromatographic (GPC) analysis was carried out on a Waters chromatography unit interfaced with a Waters 2410 refractive index detector. Two Waters 5 μm Styragel HR-2 and HR-4 columns (7.8 mm I. D. × 300 mm) were connected in series with NMP as the eluent at a flow rate of 0.5 ml/min at 40 ^{o}C and were calibrated with polystyrene standards. DSC analyses were performed on a PerkinElmer Pyris 1 DSC in flowing nitrogen (20 cm^{3}/min). Thermogravimetric analysis (TGA) was conducted with a PerkinElmer Pyris 1 TGA.

Experiments were carried out on approximately 6-8 mg samples heated in flowing nitrogen or air (flow rate = 20 cm^3/min) at a heating rate of 20 ^oC/min. Cyclic voltammetry (CV) was performed with a Bioanalytical System Model CV-27 and conducted with the use of a three-electrode cell in which ITO (polymer films area about 0.5 cm x 1.2 cm) was used as a working electrode and a platinum wire as an auxiliary electrode at a scan rate of 50 mV/s against a Ag/AgCl reference electrode in anhydrous CH_3CN, using 0.1 M of TBAP as a supporting electrolyte in nitrogen atmosphere. All cell potentials were taken by using a homemade Ag/AgCl, KCl (sat.) reference electrode. The ITO-coated glass slide was used as the working electrode, a platinum wire as the counter electrode, and a Ag/AgCl cell as the reference electrode. UV-visible absorption was recorded on UV-visible spectrophotometer (Hitachi U-4100).

4.2.4 Fabrication and Measurement of the Memory Device

The memory device was fabricated with the configuration of ITO/thin film/Al as shown in Figure 4.1. The ITO glass used for memory device was precleaned by ultrasonication with water, acetone, and isopropanol each for 15 min. The solution of **PIs** (25 mg/mL in NMP for **ODPI**, 25 mg/mL in DMAc for others), **PAs** (25 mg/mL in DMAc), and **PEs** (5 mg/mL in $CHCl_3$) were first filtered through 0.45 μm pore size of PTFE membrane syringe filter. Then, 250 μL of the filtered solution was spin-coated onto the ITO glass at a rotation rate of 1000 rpm for 60 s and kept at 100 ^oC for 10 min under nitrogen (150 ^oC for **ODPI**). **PMPI** memory device was prepared by PAA solution in DMAc and then followed above procedure, then thermal imidization was performed as mentioned before to convert the PAA into PI. The film thickness was determined to be around 50 nm. Finally, a 300-nm-thick Al top electrode was thermally evaporated through the shadow mask (recorded device units

of 0.5 × 0.5 mm^2 in size) at a pressure of 10^{-7} torr with a uniform depositing rate of 3-5 Å/s. The electrical characterization of the memory device was performed by a Keithley 4200-SCS semiconductor parameter analyzer equipped with a Keithely 4205-PG2 arbitrary waveform pulse generator. ITO was used as the cathode (maintained as common), and Al was set as the anode during the voltage sweep. The probe tip used 10 μm diameter tungsten wire attached to a tinned copper shaft with a point radius <0.1 μm (GGB Industries, Inc.).

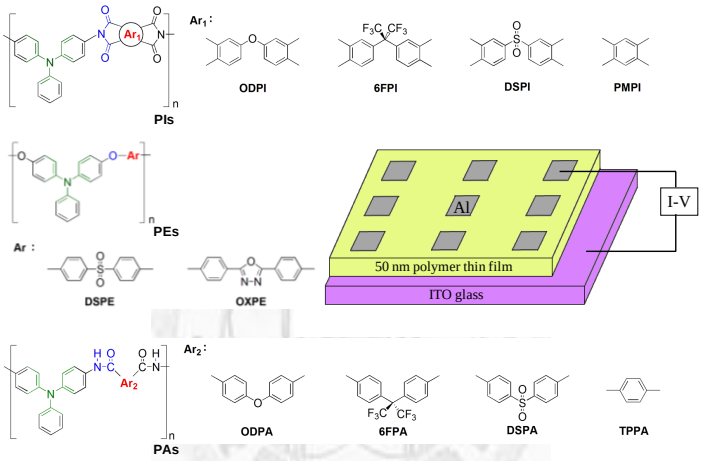

Figure 4.1. Molecular structure of **PIs**, **PAs**, and **PEs**, and schematic diagram of the memory device consisting of a polymer thin film sandwiched between an ITO bottom electrode and an Al top electrode. The thickness of polymer film is about 50 nm and the thickness of electrode is 300nm.

4.2.5 Theoretical Calculation

The theoretical calculations in this study were performed by Gaussian 09 program package. The results of value and distributions of the corresponding energy levels within each basic unit of the studying polymer were investigated via density functional theory (DFT) method at the B3LYP level of theory (Beckesstyle three-parameter density functional theory using the Lee-Yang-Parr correlation functional) with the 6-31G(d) basic set.

4.3 RESULTS AND DISCUSSION

4.3.1 Polymer Synthesis

PMPI was prepared by the reaction of diamine (**1**) with a commercially available dianhydride **PMDA** in DMAc at room temperature to obtain the precursor poly(amic acid), then proceeded thermal imidization to obtain the **PMPI**. TPA-based poly(aryl-ether)s **PEs** were synthesized from the diol monomer **2** with corresponding difluoro compounds (Scheme 4.1). The polymerization was carried out via potassium carbonate-mediated high temperature solution polycondensation. All polymerization reactions proceeded homogenously and gave high molecular weights.

The obtained PAA of **PMPI** had inherent viscosities of 0.43 dL/g with weight-average molecular weights (Mw) of 177,000 daltons (Table 4.1), and the **PEs** had inherent viscosities in the range of 0.27–0.29 dL/g with Mw and polydispersity index (PDI) ranged of 62,000–65,000 daltons and 2.56–2.60, respectively, relative to polystyrene standards.

The formation of the obtained polymers was confirmed with IR spectroscopy. The IR spectra of **PMPI** as shown in Figure 4.2(a) exhibited characteristic imide absorption bands at around 1781 (symmetrical C=O), 1725 (symmetrical C=O), 1379 (C–N), and 731 cm^{-1} (imide ring deformation). Besides, the **OXPE** exhibited the characteristic C=N stretching absorption bands at around 1500-1600 cm^{-1}, and ether absorption (C-O-C stretching) at 1232 cm^{-1} (Figure 4.2 (b)).

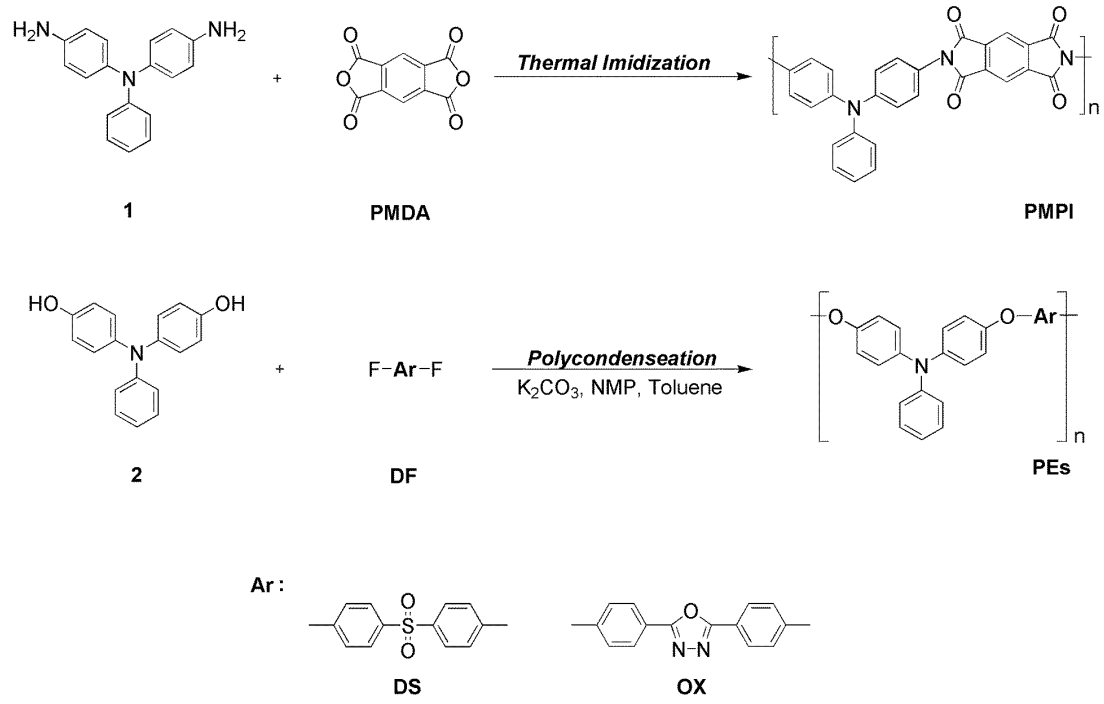

Scheme 4.1. Synthesis of the **PMPI**, **DSPE**, and **OXPE**.

Table 4.1. Inherent Viscosity and Molecular Weights of Polymers

Polymer	η_{inh}[a] (dL/g)	M_w[b]	M_n[b]	PDI[c]
ODPI	0.45 [e]	147,000	86,000	1.70
6FPI	0.57	166,000	93,000	1.78
DSPI	0.31	109,000	52,000	2.10
PMPI[d]	0.43	167,000	92,000	1.82
ODPA	0.45	64,500	33,000	1.95
6FPA	0.75	123,500	67,000	1.84
DSPA	0.35	61,700	34,500	1.79
TPPA	0.62	123,500	57,000	2.17
DSPE	0.29	65,000	25,000	2.60
OXPE	0.27	62,000	24,000	2.58

[a] Measured at a polymer concentration of 0.5 g dL^{-1} in DMAc at 30 ℃.

[b] Calibrated with polystyrene standards, using NMP as the eluent at a constant flow rate of 0.5 ml/min at 40 ^{o}C.

[c] Polydispersity Index (M_w/M_n).

[d] The data was measured from its corresponding PAA film

[e] Measured at a polymer concentration of 0.5 g dL^{-1} in NMP at 30 ℃.

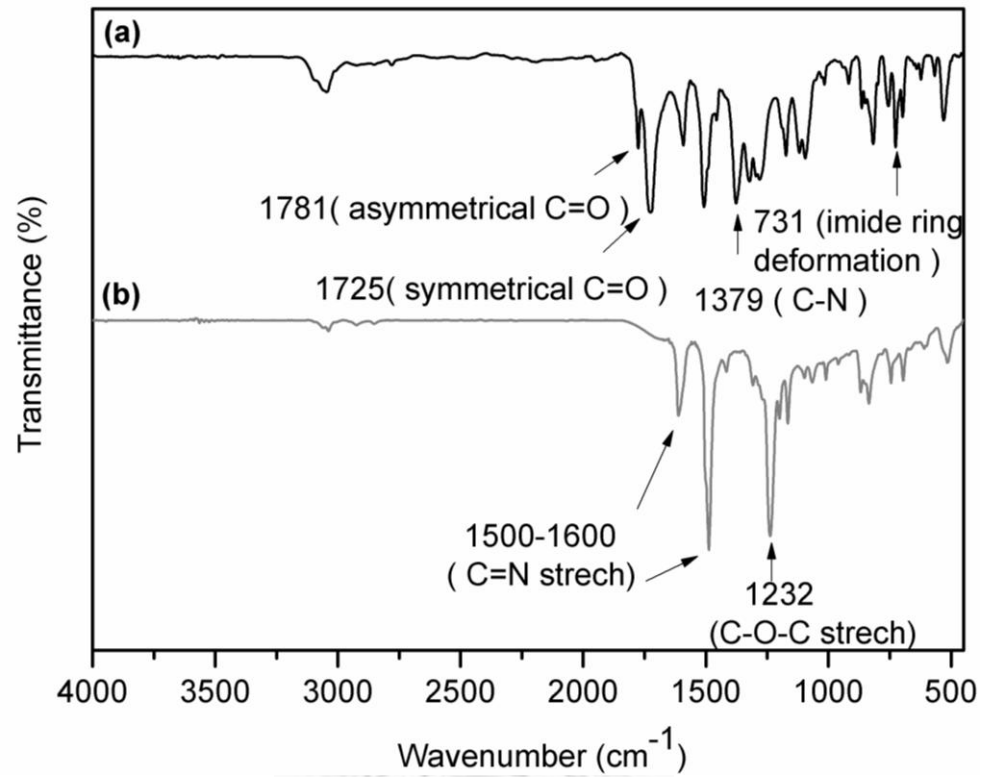

Figure 4.2. IR spectra of (a) **PMPI**, and (b) **OXPE**.

4.3.2 Thermal Properties and Solubility Behavior of the Polymers

The thermal properties of polymers were recorded by TGA, DSC, and TMA, and the resulting thermal behavior data are summarized in Table 4.2. Typical TGA curves of **PMPI**, **DSPE**, and **OXAE** are depicted in Figure 4.3. All the prepared polymers exhibited good thermal stability with insignificant weight loss up to 350 ^{o}C under nitrogen or air atmosphere. The decomposition temperature at a 10 % weight-loss of these polymers in nitrogen and air were recorded in the range of 500-645 and 500-550 ^{o}C, respectively. The amount of carbonized residue (char yield) of these polymers in a nitrogen atmosphere was more than 47 % at 800 ^{o}C. The highest char yields of PMPI can be ascribed to their high aromatic content, and leading a high limiting oxygen index (LOI) value of 46. The glass-transition temperature (T_g) of **PEs**, as shown in Figure 4.4, could be easily measured in the DSC thermograms; they were observed in

the range of 189-206 ^{o}C, depending upon the stiffness of the polymer chain. The TMA curves of **PMPI** is shown in Figure 4.4. The **PMPI** showed the higher T_g value of 327 ^{o}C could be explained by the rigidity and the higher intermolecular force providing strong dipole interactions and restricting rotation of the aromatic units relative to other connecting group comparing to **PEs**. Besides, the resulting CTE value of **PMPI** was 31 ppm/^{o}C determined over a 50-200 ^{o}C range showed the excellent dimension stability, leading an advantageous position in the field of electronic devices application. The solubility properties of the polymers were investigated qualitatively, and the results are also listed in Table 4.3. The polyether **DSPE** showed higher solubility than **OXPE** with co-planar oxadiazole groups in polar aprotic organic solvents such as NMP, DMAc, DMF, and THF. Thus, the result good solubility makes these polymers as potential candidates for practical applications by spin-coating or inkjet-printing processes to afford high performance thin films for electronic devices. On the contrary, the poor solubility of **PMPI** leads the device could only be fabricated by its PAA film.

Table 4.2. Thermal Properties of Obtained Polymers

Polymer	T_g (°C)[a]	T_d at 5 % weight loss (°C)[b]		T_d at 10 % weight loss (°C)[b]		char yield (wt%)[c]	CTE (ppm/°C)[d]	LOI[e]
		N_2	Air	N_2	Air			
PMPI	327	610	500	645	550	72	31	46
DSPE	189[f]	485	450	530	500	47	—	36
OXPE	206[f]	460	460	500	500	49	—	37

[a] Glass transition temperature measured by TMA with a constant applied load of 100 mN at a heating rate of 10 °C/min by film-fiber mode.

[b] Temperature at which 5% and 10% weight loss occurred, respectively, recorded by TGA at a heating rate of 20 °C min^{-1} and a gas flow rate of 30 cm^3 min^{-1}.

[c] Residual weight percentage at 800 °C in nitrogen.

[d] The CTE data was determined over a 50-200 °C range by film-fiber probe with expansion mode.

[e] LOI = Limiting Oxygen Index = (17.5+0.4×char yield).[12]

[f] Midpoint temperature of baseline shift on second DSC heating trace (rate 20˚C/min) of the sample after quenching from 350˚C.

Table 4.3. Solubility Behavior of Prepared Polymers

Code	Solubility in various Solvent[a]						
	NMP	DMAc	DMF	THF	$CHCl_3$	THF	CH_3CN
PMPI	—	—	—	—	—	—	—
DSPE	++	++	+	++	++	++	—
OXPE	++	++	+	+	++	++	—

[a] Qualitative solubility was tested with 10 mg of a sample in 1 mL of solvent. ++, soluble at room temperature; +, soluble on heating; —, insoluble even on heating.

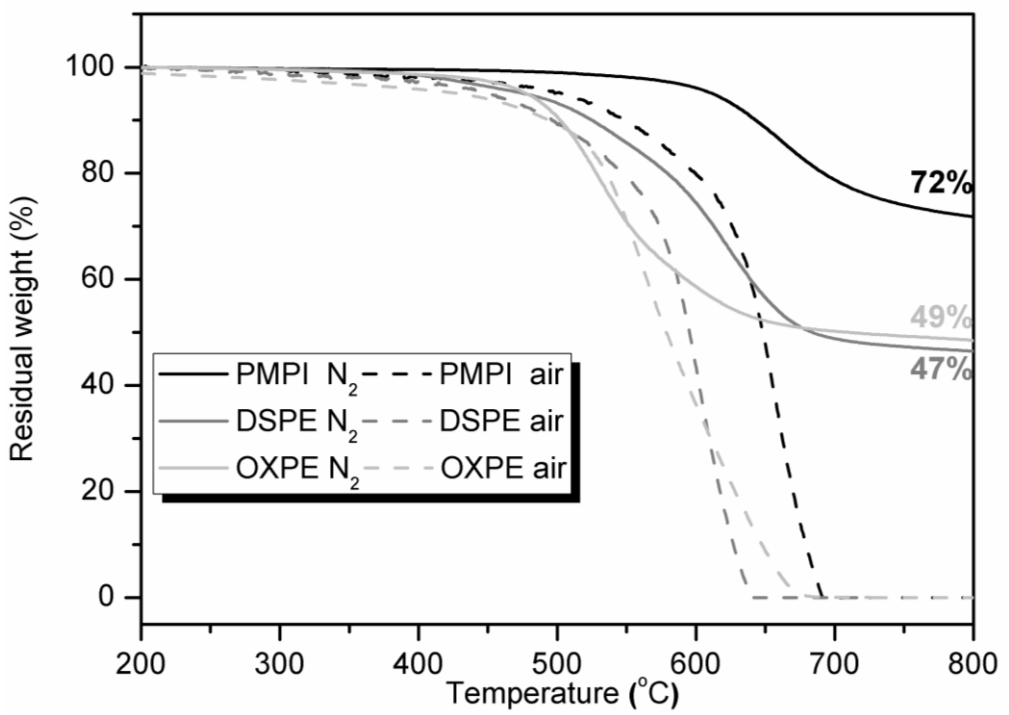

Figure 4.3. TGA thermograms of **PMPI**, **DSPE**, and **OXPE** at a scan rate of 20 ^{o}C/min.

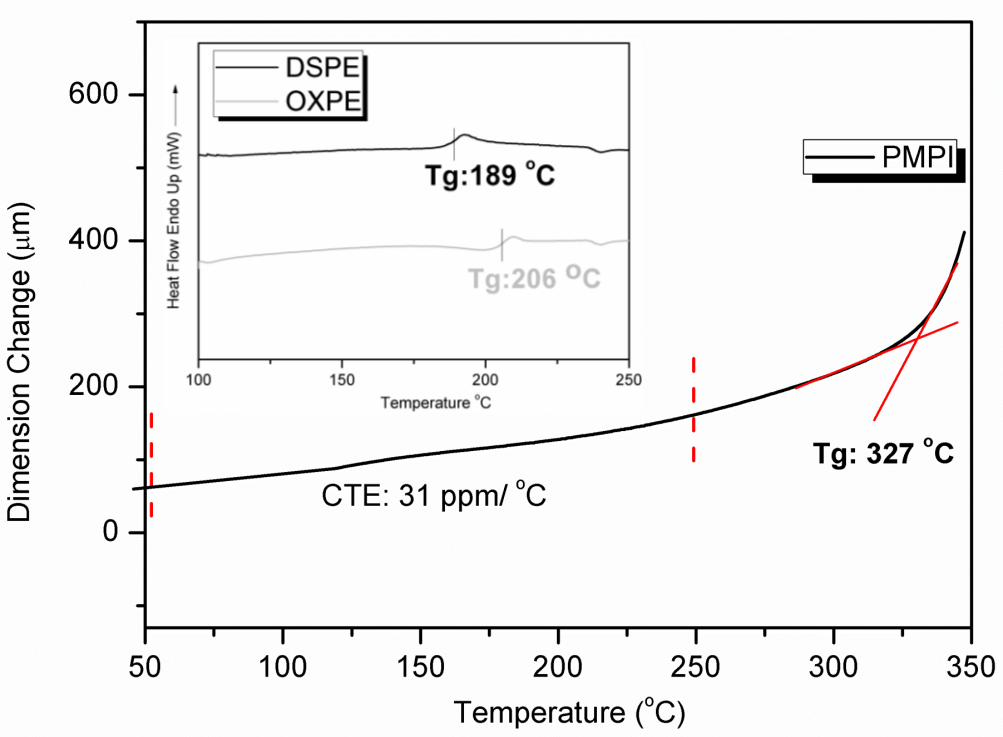

Figure 4.4. TMA curve of **PMPI**, and DSC traces of **DSPE** and **OXPE**.

4.3.3 Optical and Electrochemical Properties

UV-vis absorption spectra of **PIs**, **PAs**, and **PEs** are shown in Figure 4.5, the onset wavelength of optical absorption was utilized to obtain the optical energy band gap (E_g) of these polymers. The electrochemical behavior of these polymers was investigated by cyclic voltammetry conducted by film cast on an ITO-coated glass substrate as the working electrode in dry acetonitrile (CH_3CN) containing 0.1 M of TBAP as an electrolyte under nitrogen atmosphere. The typical cyclic voltammograms for these polymers are demonstrated in Figure 4.6. There is one reversible oxidation redox couple for all polymers, and the onset oxidation values of **PIs** ranged from 0.81 to 0.89 V, 0.69 to 0.74 V for **PAs**, and 0.68 to 0.69 V for **PEs**. The sequences of the onset values for each series imply the electron-withdrawing capability of the corresponding acceptor moiety. Besides, **PIs** exhibit the highest onset value elucidate the imide linkage possesses the stronger interaction between the TPA and the acceptor while **PEs** exhibit the lowest onset value due to the ether linkage could interrupt the interaction between TPA and the acceptor. The optical energy band gaps (E_g) estimated from the onset optical absorption are in the range of 2.12 to 3.43 eV, affecting by the charge-transfer effect. The lowest energy gap of **PMPI** was an evidence for the strongest charge transfer capability. The LUMO energy levels of these polymers decrease with the donor-acceptor interaction enhance, and are in the order of **PEs**, **PAs**, and **PIs**. In each series, the acceptor effect could be also observed, take **PIs** for instance, the corresponding LUMO energy levels of these polyimides also decrease with the dianhydrides electron-withdrawing ability increasing, and are in the order of **ODPI**, **6FPI**, **DSPI**, and **PMPI**. Besides, the **ODPI** revealed lowest onset oxidation potential (0.81 V) could be also attributed to the weaker electron-withdrawing ability from the dianhydride moiety. The redox potentials of the polyimides as well as their respective highest occupied molecular orbital (HOMO)

and lowest unoccupied molecular orbital (LUMO) (versus vacuum) are calculated and summarized in Table 4.4.

Table 4.4. Redox Potentials and Energy Levels of Polymers

Polymer	Thin film (nm)	Oxidation potential (V)[a]		E_g (eV)[b]	HOMO (eV)[c]	$LUMO^{opt}$ (eV)
	λ_{onset}	$E_{1/2}$	E_{onset}			
ODPI	474	1.04	0.81	2.62	5.25	2.64
6FPI	497	1.11	0.84	2.50	5.28	2. 97
DSPI	516	1.12	0.86	2.40	5.30	2.90
PMPI	585	1.20	0.88	2.12	5.32	3.20
ODPA	417	0.84	0.69	2.97	5.13	2.16
6FPA	426	0.86	0.71	2.91	5.15	2.24
DSPA	496	0.87	0.74	2.50	5.18	2.68
TPPA	466	0.85	0.71	2.66	5.15	2.49
DSPE	361	0.93	0.68	3.43	5.12	1.69
OXPE	379	0.94	0.69	3.27	5.13	1.86

[a] From cyclic votammograms versus Ag/AgCl in CH_3CN. $E_{1/2}$: Average potential of the redox couple peaks.

[b] The data were calculated from polymer films by the equation: $E_g = 1240/\lambda_{onset}$ (energy gap between HOMO and LUMO).

[c] The HOMO energy levels were calculated from cyclic voltammetry and were referenced to ferrocene (4.8 eV; E_{onset} = 0.36 V).

$LUMO^{Opt}$ (LUMO energy levels calculated from optical method): Difference between $HOMO^{EC}$ and E_g^{Opt}.

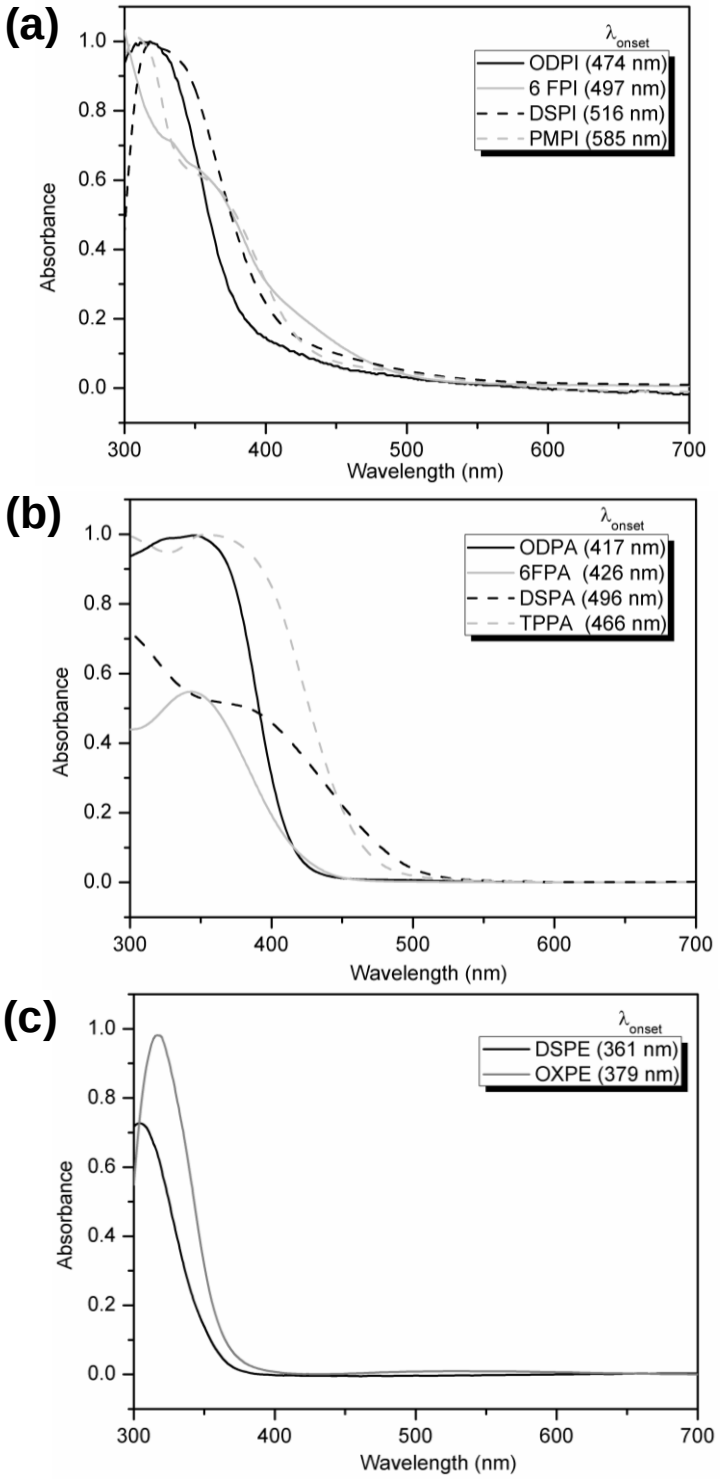

Figure 4.5. UV- visible absorption spectra of (a) **PIs**, (b) **PAs**, and (c) **PEs**.

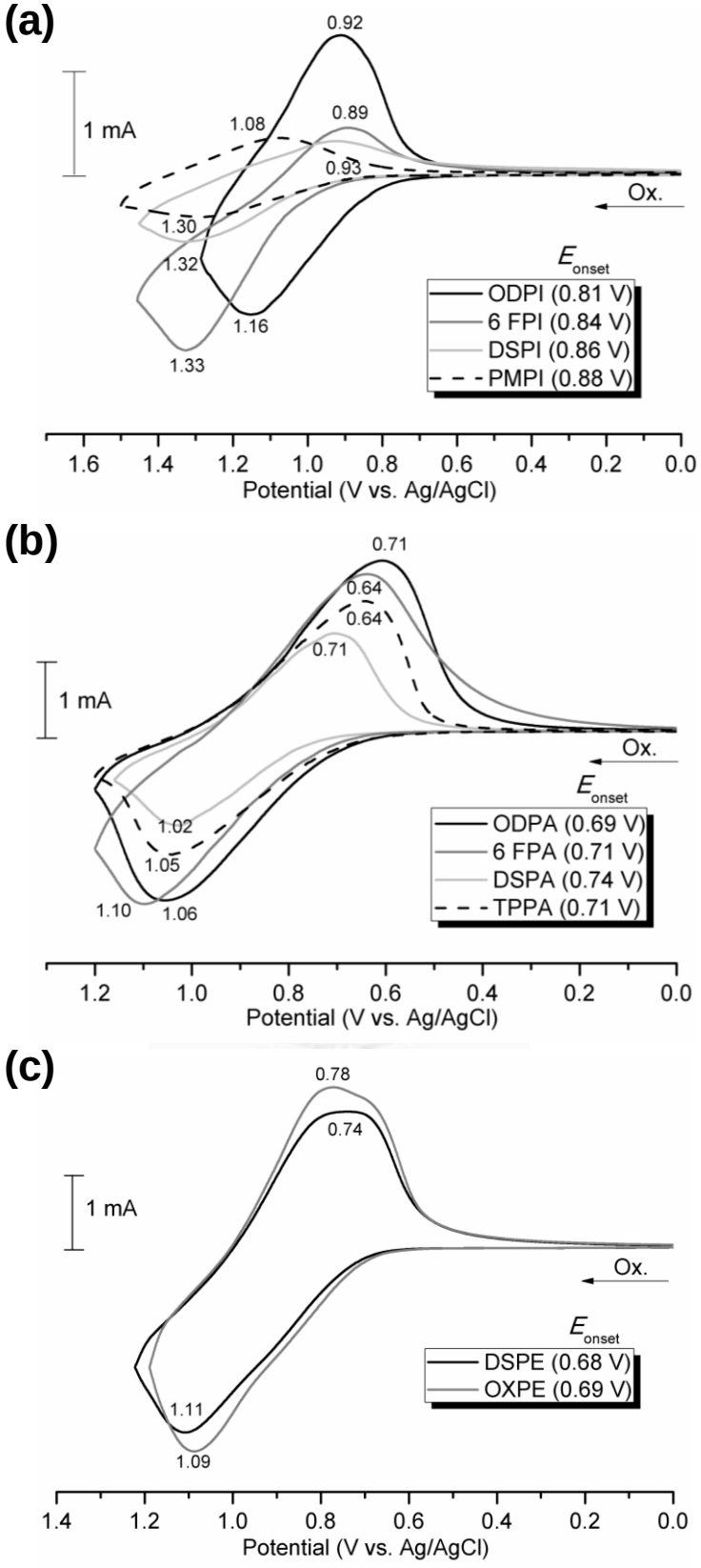

Figure 4.6. Cyclic voltammograms of **PIs**, **PAs**, and **PEs** films on an ITO-coated glass substrate in CH_3CN containing 0.1 M TBAP at the scan rate of 50 mV/s.

4.3.4 Switching Behaviors of These Polymeric Memory Devices

The resulting memory characteristics of these polymers were investigated by the current-voltage (I-V) characteristics of an ITO/polymer thin film/Al sandwich device, the 50 nm in thickness polymer thin film played the role as the active layer between the top and bottom electrodes Al and ITO within the sandwich device, respectively.

Figure 4.7(a) demonstrates the I-V result of **ODPI** which was conducted in the steps of 0.1V with a 0.01 A compliance current. The memory device of **ODPI** kept at low-conductivity (OFF) state and could not be switched to ON state during the applied bias scan from -10 V to 10 V, revealing an insulator behavior. For comparison study, the memory device behavior of the published **6FPI**[7a] and **DSPI**[7f] was also prepared and investigated on our own, and the corresponding I-V characteristics were depicted in Figure 4.7(b) and Figure 4.7(c), respectively. The memory device of **6FPI** switched from 10^{-13}-10^{-14} to 10^{-5} A at the threshold voltage of -3.5 V in the negative sweep and the ON state could be read by the subsequent negative (line 2) and positive scans (line 3). The ON state would return to OFF state in 1 min after removing the applied voltage then subsequently switch to ON state again at the threshold voltage of -3.4 V, implying the volatile DRAM behavior as published before. The device fabricated by DSPI also showed the switch behavior at the threshold voltage of -4.0 V (line 1), the corresponding ON state could be read by conducting the negative (line 2) and positive (line 3) subsequently. The ON state would relax to OFF state without any erasing program but after removing the electric field for 4 min, and the device transited to ON state again at the switch-on voltage of -3.9 V (line 4), resulting the SRAM behavior which is distinct from the published result. Figure 4.7(d) revealed the I-V characteristics of **PMPI**. The device exhibited a sharp increasing of the current once the external applied voltage reached -2.8 V during the negative scan (line 1), indicating the writing process. Besides, the reading process of the ON state could be

conducted by the subsequent negative (line 2) and positive scans (line 3). Thus, this **PMPI** memory device could not be reset to the initial OFF state by the introduction of a reverse scan, leading the non-erasable nature. The device of **PMPI** maintained in the ON state after turning off the power for a larger time interval than above mentioned **PIs**. The OFF state of this device was found after turning off the power for about 8 minutes, the ON state had relaxed to the steady OFF state without an erasing process. During the fourth sweep (line 4), the device could be switched to the ON state again at the threshold voltage of -2.7 V. The longer retention time at the ON state yet volatile, as well as the randomly accessible ON and OFF states is similar to the data remanence behavior of SRAM.

We next investigated the memory behavior of the structural related with different linkage group **PAs**. As the memory behavior of **ODPI**, the **ODPA** film exhibited the insulator behavior indicating by the non-switchable nature during the step voltage sweep in the range of -10 V to 10 V, as shown in Figure 4.8(a). However, Figure 4.8(b), Figure 4.8(c) and Figure 4.8(d) reveal the I-V characteristics of **6FPA**, **DSPA**, and **TPPA**. During the first negative sweep (line 1) from 0 V to -6 V, the tremendous and sharp increased in current indicating the switch phenomenon could be observed at the threshold voltage of -3.0 V, -3.2 V, and -2.7 V indicating the transition from the OFF state to high-conductivity (ON) state, defined as writing process. The device maintained at the ON state during the subsequent negative scan (line 2) and then positive scan line 3), defined as reading processing. The obtained ON state of these three devices could not erase by the reverse bias scan but relax to OFF state only if after stopping the electrical impulse for 5 minutes, 8 minutes, and 2 minutes, respectively. The longer retention time at the ON state yet volatile, leading the SRAM nature of these thin films while it were applied as the active layer in RRAM applications.

Furthermore, the structural related **PEs** were also prepared to fabricate the memory device for investigation, for organized research on both linkage and acceptor effect. The memory devices of both **DSPE** and **OXPE** did not possess the switch capability and retain at low-conductivity (OFF) state during the ambipolar scan, as shown in Figure 4.9. Therefore, **DSPE** and **OXPE** film exhibited no memory but insulator behavior.

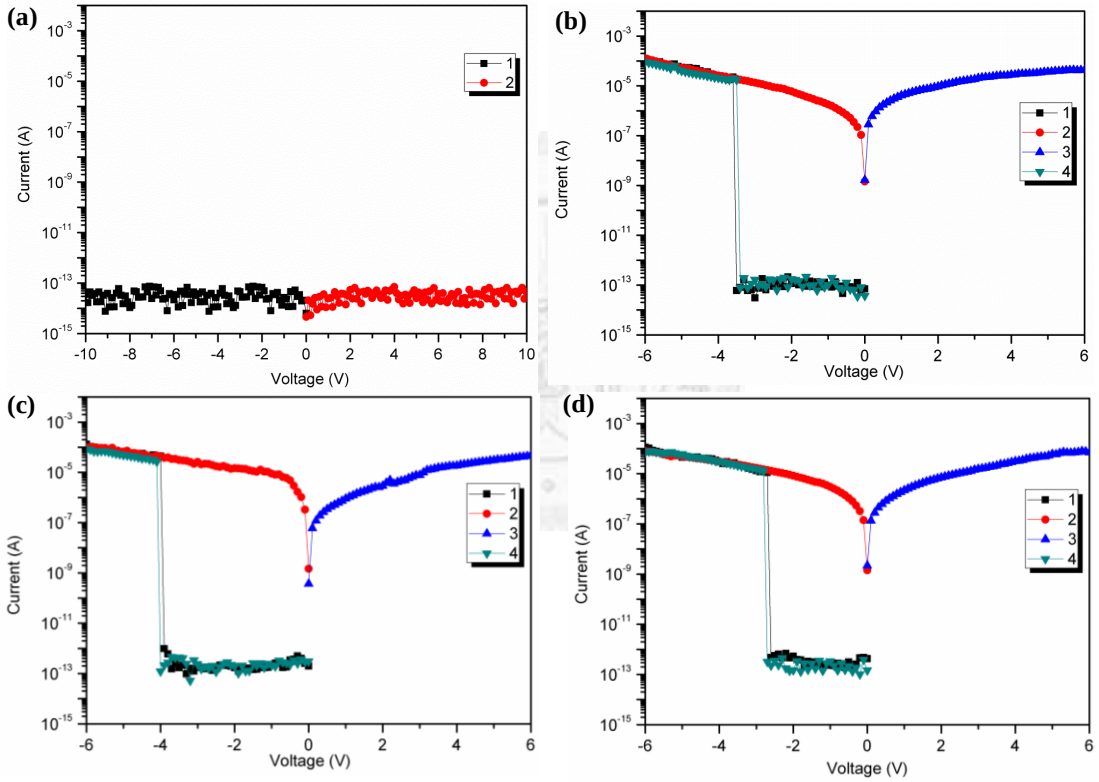

Figure 4.7. Current-voltage (I-V) characteristics of (a) **ODPI**, (b) **6FPI**, (c) **DSPI**, and (d) **PMPI**.

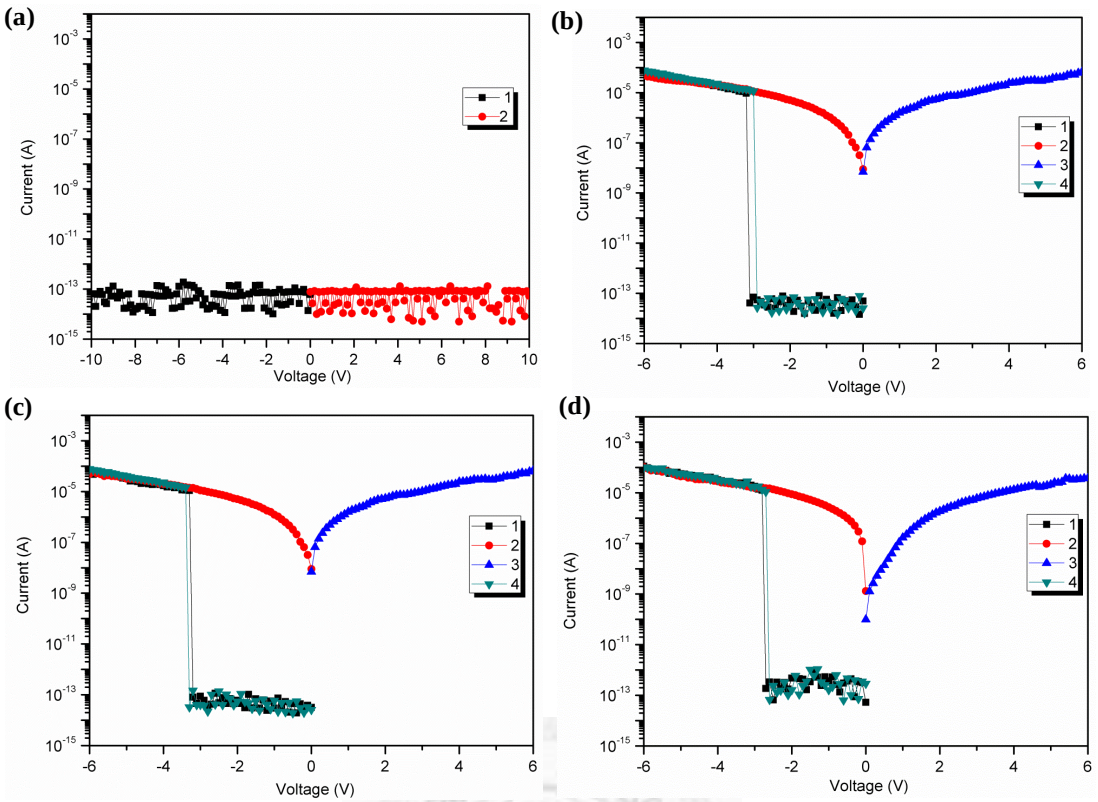

Figure 4.8. Current-voltage (I-V) characteristics of (a) **ODPA**, (b) **6FPA**, (c) **DSPA**, and (d) **TPPA**.

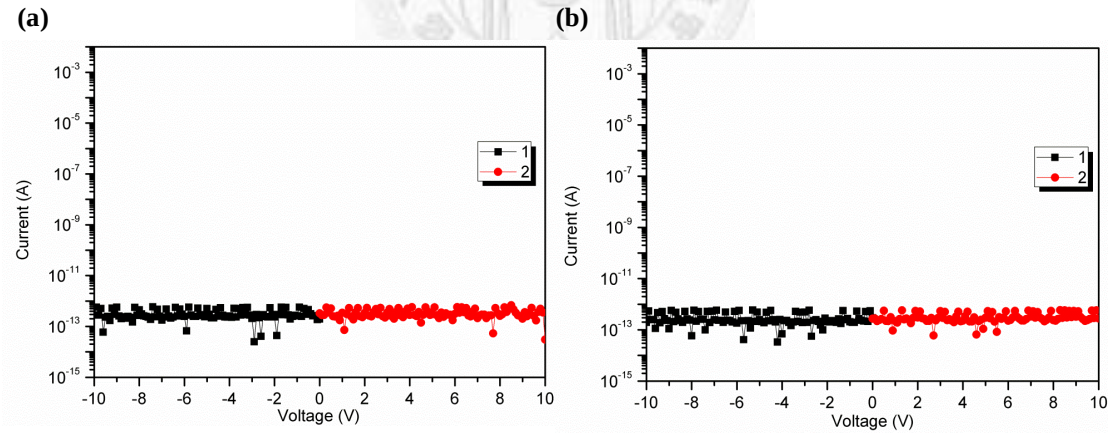

Figure 4.9. Current-voltage (I-V) characteristics of (a) **DSPE** and (b) **OXPE**.

4.3.5 Theoretical Analysis and Switching Mechanism

The molecular simulation on the basic unit which was carried out by DFT/B3LYP/6-31G(d) with the Gaussian 09 program was investigated to discuss the different memory behavior of the present devices based on **PIs**, **PAs**, and **PEs** further. The charge density isosurfaces and the electrostatic potential surface (ESP) of the basic unit are summarized in Figure 4.10, Figure 4.11, and Figure 4.12, respectively. The LUMO energy levels calculated by molecular simulation were in agreement with the experimental values tendency and could be utilized as an evidence to indicate the electron-withdrawing intensity of various acceptors and donor-acceptor interaction intensity via different linkage group. For these TPA-based polymer systems, the HOMO energy levels were located mainly at the electron-donating TPA moieties, while the LUMO energy levels were located at the corresponding electron-withdrawing moiety units. In the case of **PIs**, the distribution LUMO energy levels were within the dianhydride and imide ring moiety, due to its strong electron-withdrawing capability; the resulting LUMO energy levels of the **PAs** were found not only at the diacid and amide linkage group moiety but part of them at TPA donor moiety, related to the weaker electron-withdrawing effect leading the non-complete charge separation; the poorest charge separation phenomenon of **PEs** could be predicted and observed in the analysis of molecular simulation, indicating the weakest electron-withdrawing capability resulted from the non-elecreon-withdrawing capability isolated ether linkage group comparing to above electro-withdrawing linkage group both amide and imide. It was reported that the charge transfer happened once the external electric fields reach the switching-on voltage providing enough energy, some electrons at the HOMO accumulate energy and transit to the LUMO4 (LUMO5 for **DSPI**, LUMO3 for **PMPI**, LUMO2 for **TPPA**) with the highest probability because of overlapping of the HOMO and

LUMO4 resulting in an excited state. In addition, electrons at the HOMO can also be excited to the three intermediate LUMOs with lower energy barrier. Thus, charge transfer occurs through several courses to form the conductive charge transfer complexes: indirectly from the LUMO4 through intermediate LUMOs and then to the LUMO, or from the intermediate LUMOs to the LUMO, and directly from the HOMO to the LUMO. When the intra- or intermolecular charge transfer occurred by the external electric potential, the generating holes can be delocalized to the conjugated TPA moieties forming an open channel in the HOMO of the polymer chain providing a pathway the migrating charge carriers (holes), decreased the electrical resistance of the polymer tremendously leading the current increases rapidly and switched the memory device from OFF state (low conductivity state) to the high conductivity state (ON state).

Among the **PIs**, **ODPI** exhibit the largest energy band gap and the weakest charge-transfer capability which arise in no memory property. Comparing to the DRAM behavior of **6FPI**, the lower LUMO energy level of **DSPI** bring about the longer retention time and indicated as SRAM property. The lowest LUMO energy level and the strongest charge-transfer effect of **PMPI** also produce the SRAM behavior but possess much longer retention time of 8 minutes. Likewise, the **PAs** series show similar tendency in memory behavior, the retention time increase as the electron-withdrawing strength, resulting both SRAM behavior with from 2 to 8 minutes of retention time except for insulator **ODPA**. Interestingly, the **PAs** possess a weaker electron acceptor but surprisingly exhibit a longer retention time comparing to the structural related **PIs**, which could be contributed to the reduced co-planarity between donor and acceptor resulted from the amide linkage, providing a higher energy barrier for back charge transfer, thus extend the retention time. **PEs** exhibit the insulator behavior due to the analogous reason with both **ODPI** and **ODPA**, large

band gap and weak charge transfer capability.

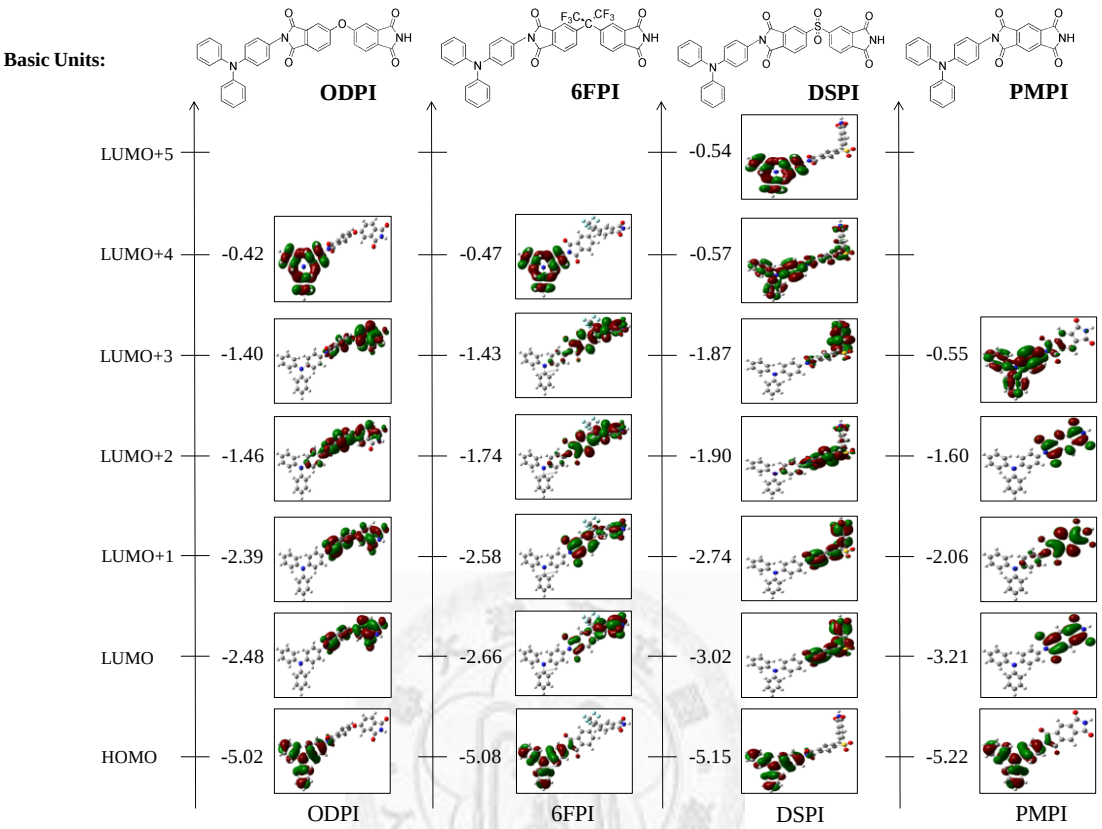

Figure 4.10. Calculated molecular orbitals and corresponding energy levels of the basic units (BU) for TPA-based **PIs**.

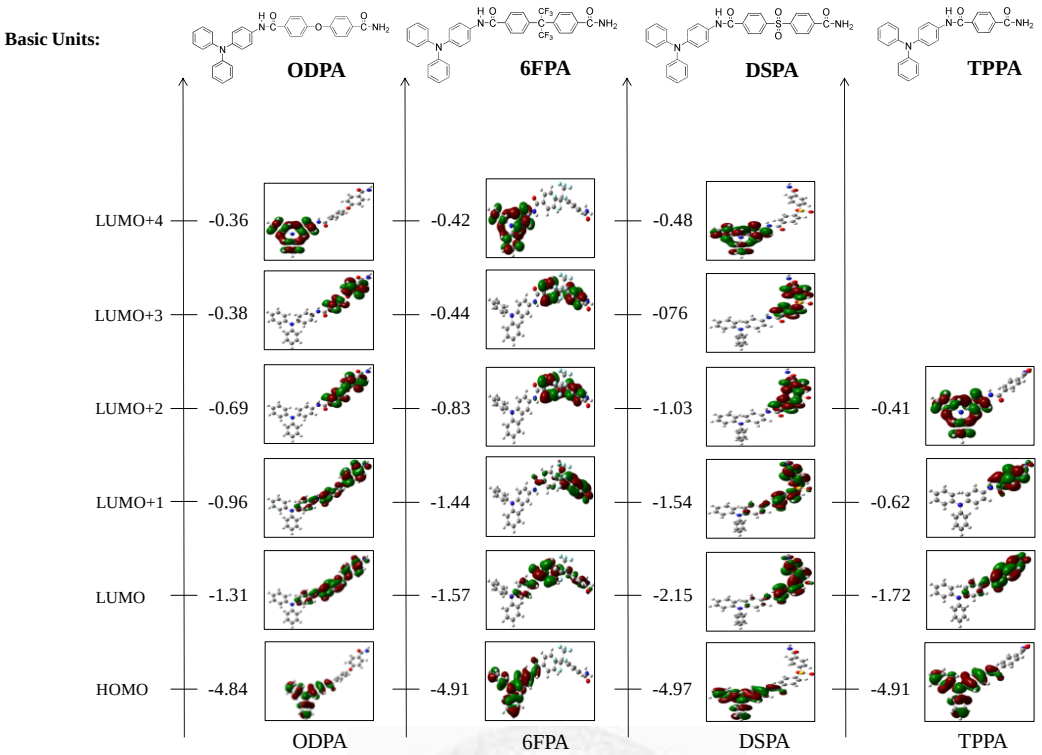

Figure 4.11. Calculated molecular orbitals and corresponding energy levels of the basic units (BU) for TPA-based **PAs**.

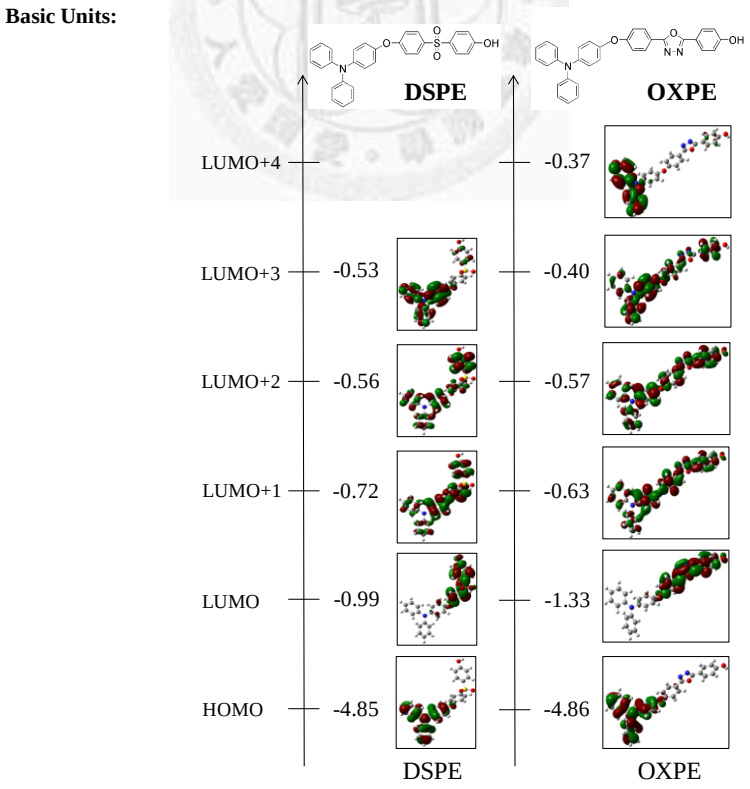

Figure 4.12. Calculated molecular orbitals and corresponding energy levels of the basic units (BU) for TPA-based **PEs**.

4.4 SUMMARY

In this chapter, memory device derived from the structural related TPA-based **PIs**, **PAs**, and **PEs** have been successfully fabricated for comparison and systematical research on both linkage and acceptor effect. The memory behaviors affected by different electron-withdrawing capability were discussed in each series by different acceptor moiety, and the linkage effect was also investigated by structural analogous **PI**, **PA** and **PE**. The memory devices with the configuration of ITO/polymer thin film/Al exhibited various memory characteristics. **ODPI, ODPA**, and **PEs** demonstrate no memory but insulator behaviors. Among the other **PIs**, **6FPI** exhibited DRAM characteristic, and the stronger electron-withdrawing moiety containing **DSPI** revealed SRAM behavior, and the strongest electron-withdrawing nature of PMDA moiety leads **PMPI** extending the retention time from 4 to 8 minutes. In the rest of **PAs**, SRAM characteristic could be measured by the memory device with the retention time from 2 to 8 minutes influenced upon the electron-withdrawing capability. When comparing to its structural related **PIs**, **PAs** exhibit a longer retention time although with weaker electron acceptor due to the linkage effect which reduced the co-planarity between donor and acceptor resulted from the amide linkage, providing a higher energy barrier for back charge transfer, and therefore extend the retention time. By this facile D-L-A design, choosing different kinds of electron accepter and linkage group, the memory devices with different characteristic could be fabricated easily.

REFERENCES AND NOTES

1. (*a*) R. H. Friend, R. W. Gymer, A. B. Holmes, J. H. Burroughes, R. N. Marks, C. Taliani, D. D. C. Bradley, D. A. Dos Santos, J. L. Bredas, M. Logdlund, W. R. Salaneck, *Nature*, 1999, **397**, 121; *(b)* Q. Peng, E. T. Kang, K. G. Neoh, D. Xiaob, D. Zou, *J. Mater. Chem.*, 2006, **16**, 376; (*c*) K. Lee, J. Y. Kim, S. H. Park, S. H. Kim, S. Cho, A. J. Heeger, *Adv. Mater.*, 2007, **19**, 2445; (*d*) Y. Shao, G. C. Bazan, A. J. Heeger, *Adv. Mater.*, 2008, **20**, 1191; (*e*) Y. Shao, X. Gong, A. J. Heeger, M. Liu, A. K. Y. Jen, *Adv. Mater.*, 2009, **21**, 1972.
2. (*a)* H. Sirringhaus, N. Tessler, R. H. Friend, *Science*, 1998, **280**, 1741; (*b*) L. L. Chua, J. Zaumseil, J. F. Chang, E. C. W. Ou, P. K. H. Ho, H. Sirringhaus, R. H. Friend, *Nature*, 2005, **434**, 194; (*c*) A. Babel, Y. Zhu, K. F. Cheng, W. C. Chen, S. A. Jenekhe, *Adv. Funct. Mater.*, 2007, **17**, 2542; (*d*) M. Morana, M. Wegscheider, A. Bonanni, N. Kopidakis, S. Shaheen, M. Scharber, Z. Zhu, D. Waller, R. Gaudiana, C. Brabec, *Adv. Funct. Mater.*, 2008, **18**, 1757; (*e*) H. Yan, Z. H. Chen, Y. Zheng, C. Newman, J. R. Quinn, F. Dotz, M. Kastler, A. Facchetti, *Nature*, 2009, **457**, 679-U1; (*f*) J. H. Tsai, W. Y. Lee, W. C. Chen, C. Y. Yu, G. W. Hwang, C. Ting, *Chem. Mater.*, 2010, **22**, 3290; (*g*) C. J. Lin, W. Y. Lee, C. Lu, H. W. Lin, W. C. Chen, *Macromolecules*, 2011, **44** , 9565.
3. (*a*) G. Yu, J. Gao, J. C. Hummelen, F. Wudl, A. J. Heeger, *Science*, 1995, **270**, 1789; (*b*) C. J. Brabec, N. S. Sariciftci, J. C. Hummelen, *Adv. Funct. Mater.*, 2001, **11**, 15; (*c*) M. H. Chen, J. Hou, Z. Hong, G. Yang, S. Sista, L. M. Chen, Y. Yang, *Adv. Mater.*, 2009, **21**, 4238; (*d*) J. H. Hou, T. L. Chen, S. Q. Zhang, L. J. Huo, S. Sista, Y. Yang, *Macromolecules*, 2009, **42**, 9217; (*e*) A. Kumar, H. H. Liao, Y. Yang, *Org. Electron.*, 2009**, 10**, 1615; (*f*) S. Sista, Z. R. Hong, M. H. Park, Z. Xu, Y. Yang, *Adv. Mater.*, 2010, **22**, E77.

4. *(a)* J. Ouyang, C. W. Chu, C. R. Szmanda, L. Ma, Y. Yang, *Nat. Mater.*, 2004, **3**, 918; *(b)* Q. Ling, Y. Song, S. J. Ding, C. Zhu, D. S. H. Chan, D. L. Kwong, E. T. Kang, K. G. Neoh, *Adv. Mater.*, 2005, **17**, 455; *(c)* C. W. Chu, J. Ouyang, J. H. Tseng, Y. Yang, *Adv. Mater.*, 2005, **17**, 1440; *(d)* Q. D. Ling, W. Wang, Y. Song, C. X. Zhu, D. S. H. Chan, E. T. Kang, K. G. Neoh, *J. Phys. Chem. B*, 2006, **110**, 23995; *(e)* G. Liu, Q. D. Ling, E. T. Kang, K. G. Neoh, D. J. Liaw, F. C. Chang, C. X. Zhu, D. S. H. Chan, *J. Appl. Phys.*, 2007, **102**, 024502; *(f)* A. Laiho, H. S. Majumdar, J. K. Baral, F. Jansson, R. Osterbacka, O. Ikkala, *Appl. Phys. Lett.*, 2008, **93**, 203309/1; *(g)* G. Liu, Q. D. Ling, E. Y. H. Teo, C. X. Zhu, D. S. H. Chan, K. G. Neoh, E. T. Kang, *ACS Nano*, 2009, **3**, 1929; *(h)* S. L. Lim, N. J. Li, J. M. Lu, Q. D. Ling, C. X. Zhu, E. T. Kang, K. G. Neoh, *ACS Appl. Mater. Interfaces*, 2009, **1**, 60; *(i)* J. Q. Liu, Z. Y. Yin, X. H. Cao, F. Zhao, A. P. Lin, L. H. Xie, Q. L. Fan, F. Boey, H. Zhang, W. Huang, *ACS Nano*, 2010, **4**, 3987; *(j)* S. Song, B. Cho, T. W. Kim, Y. Ji, M. Jo, G. Wang, M. Choe, Y. H. Kahng, H. Hwang, T. Lee, *Adv. Mater*. 2010, **22**, 5048; *(k)* J. C. Hsu, C. L. Liu, W. C. Chen, K. Sugiyama, A. Hirao, *Macromol. Rapid Commun*., 2011, **32**, 528; *(l)* Y. C. Lai, K. Ohshimizu, W. Y. Lee, J. C. Hsu, T. Higashihara, M. Ueda, W. C. Chen, *J. Mater. Chem.*, 2011, **21**, 14502; *(m)* Y. K. Fang, C. L. Liu, W. C. Chen, *J. Mater. Chem.*, 2011, **21**, 4778; *(n)* N. Li, J. Lu, H. Li, E. T. Kang, *Dyes Pigm.*, 2011, **88**, 18; *(o)* G. Liu, B. Zhang, Y. Chen, C. X. Zhu, L. Zeng, D. S. H. Chan, K. G. Neoh, J. Chen, E. T. Kang, *J. Mater. Chem.*, 2011, **21**, 6027; *(p)* G. Liu, B. Zhang, Y. Chen, C. X. Zhu, L. Zeng, D. S. H. Chan, K. G. Neoh, J. Chen, E. T. Kang, *J. Mater. Chem*., 2011, **21**, 6027; *(q)* Y. K. Fang, C. L. Liu, G. Y. Yang, P. C. Chen, W. C. Chen, *Macromolecules*, 2011, **44**, 2604; *(r)* J. E. Park, J. H. Eom, T. Lim, D. H. Hwang, S. Pyo, *J. Polym. Sci. Part A: Polym. Chem*. 2012, **50**, 2188; *(s)* T. W. Kim, D. F. Zeigler, O. Acton, H. L. Yip, H. Ma, A. K. Y. Jen, *Adv. Mater.*, 2012, **24**, 828; *(t)* B. Zhang, G. Liu, C.

Wang, K. G. Neoh, T. Bai, E. T. Kang, *ChemPlusChem*, 2012, **77**, 74; *(u)* Y. Chen, B. Zhang, G. Liu, X. Zhuang, E. T. Kang, *Chem. Soc. Rev.*, 2012, **41**, 4688.

5. *(a)* Q. D. Ling, F. C. Chang, Y. Song, C. X. Zhu, D. J. Liaw, D. S. H. Chan, E. T. Kang, K. G. Neoh, *J. Am. Chem. Soc.*, 2006, **128**, 8732; *(b)* N. H. You, C. C. Chueh, C. L. Liu, M. Ueda, W. C. Chen, *Macromolecules*, 2009, **42**, 4456; *(c)* S. G. Hahm, S. Choi, S. H. Hong, T. J. Lee, S. Park, D. M. Kim, W. S. Kwon, K. Kim, O. Kim, M. Ree, *Adv. Funct. Mater.*, 2008, **18**, 3276; *(d)* S. G. Hahm, S. Choi, S. H. Hong, T. J. Lee, S. Park, D. M. Kim, J. C. Kim, W. Kwon, K. Kim, M. J. Kim, O. Kim, M. Ree, *J. Mater. Chem.*, 2009, **19**, 2207. (*e*) D. M. Kim, S. Park, T. J. Lee, S. G. Hahm, K. Kim, J. C. Kim, W. Kwon, M. Ree, *Langmuir*, 2009, **25**, 11713; (*f*) Y. L. Liu, K. L. Wang, G. S. Huang, C. X. Zhu, E. S. Tok, K. G. Neoh, E. T. Kang, *Chem. Mater.*, 2009, **21**, 3391; (*g*) C. J. Chen, H. J. Yen, W. C. Chen, G. S. Liou, *J. Polym. Sci. Part A: Polym. Chem.*, 2011, **49**, 3709; (*h*) Y. Q. Li, R. C. Fang, A. M. Zheng, Y. Y. Chu, X. Tao, H. H. Xu, S. J. Ding, Y. Z. Shen, *J. Mater. Chem.*, 2011, **21**, 15643; (*i*) Y. Zhang, Y. W. Liu, Q. Lan, S. W. Liu, Z. X. Qin, L. H. Chen, C. Y. Zhao, Z. G. Chi, J. R. Xu and J. Economy, *Chem. Mater.*, 2012, **24**, 1212; (*j*) B. L. Hu, F. Zhuge, X. J. Zhu, S. S. Peng, X. X. Chen, L. Pan, Q. Yan, R. W. Li, *J. Mater. Chem.*, 2012, **22**, 520; (*k*) Y. Q. Li, Y. Y. Chu, R. C. Fang, S. J. Ding, Y. L. Wang, Y. Z. Shen, A. M. Zheng, *Polymer*, 2012, **53**, 229.

6. (*a*) S. H. Cheng, S. H. Hsiao, T. H. Su, G. S. Liou, *Macromolecules*, 2005, **38**, 307; (*b*) T. H. Su, S. H. Hsiao, G. S. Liou, *J. Polym. Sci. Part A:Polym. Chem*., 2005. **43**, 2085; (*c*) C. W. Chang, G. S. Liou, S. H. Hsiao, *J. Mater. Chem*., 2007, **17**, 1007; (*d*) G. S. Liou, C. W. Chang, *Macromolecules*, 2008, **41**, 1667; (*e*) S. H. Hsiao, G. S. Liou, Y. C. Kung, H. J. Yen, *Macromolecules*, 2008, **41**, 2800; (*f*) C. W. Chang, C. H. Chung, G. S. Liou, *Macromolecules*, 2008, **41**, 8441; (*g*) C. W.

Chang, G. S. Liou, *J. Mater. Chem*., 2008, **18**, 5638; (*h*) C. W. Chang, H. J. Yen, K. Y. Huang, J. M. Yeh, G. S. Liou, *J.Polym. Sci. Part A: Polym. Chem*., 2008, **46**, 7937; (*i*) H. J. Yen, G. S. Liou, *Chem. Mater*., 2009, **21**, 4062; (*j*) S. H. Hsiao, G. S. Liou, H. M. Wang, *J. Polym. Sci. Part A: Polym. Chem*., 2009, **47**, 2330; (*k*) G. S. Liou, H. Y. Lin, H. J. Yen, *J. Mater. Chem*., 2009, **19**, 7666; (*l*) G. S. Liou, H. Y. Lin, *Macromolecules*, 2009, **42**, 125; (*m*) L. T. Huang, H. J. Yen, C. W. Chang, G. S. Liou, *J. Polym. Sci. Part A:Polym. Chem*., 2010, **48**, 4747; (*n*) H. J. Yen, S. M. Guo, G. S. Liou, *J. Polym. Sci. Part A: Polym. Chem*., 2010, **48**, 5271; (*o*) H. J. Yen, G. S. Liou, *J. Mater. Chem*., 2010, **20**, 9886; (*p*) H. J. Yen, H. Y. Lin, G. S. Liou, *Chem. Mater*., 2011, **23**, 1874; (*q*) H. J. Yen, S. M. Guo, G. S. Liou, J. C. Chung, Y. C. Liu, Y. F. Lu, Y. Z. Zeng, *J. Polym. Sci. Part A: Polym. Chem*., 2011, **49**, 3805; (*r*) L. T. Huang, H. J. Yen, G. S. Liou, *Macromolecules*, 2011, **44**, 9595; (*s*) H. J. Yen, G. S. Liou, *Polym. Chem*., 2012, **3**, 255; (*t*) L. T. Huang, H. J. Yen, J. H. Wu, G. S. Liou, *Org. Electron.*, 2012, **13**, 840.

7. *(a)* Q. D. Ling, F. C. Chang, Y. Song, C. X. Zhu, D. J. Liaw, D. S. H. Chan, E. T. Kang, K. G. Neoh, *J. Am. Chem. Soc.*, 2006, **128**, 8732; (*b*) T. J. Lee, C. W. Chang, S. G. Hahm, K. Kim, S. Park, D. M. Kim, J. Kim, W. S. Kwon, G. S. Liou, M. Ree, *Nanotechnology*, 2009, **20**, 135204; (*c*) D. M. Kim, S. Park, T. J. Lee, S. G. Hahm, K. Kim, J. C. Kim, W. Kwon, M. Ree, *Langmuir*, 2009, **25**, 11713; (*d*) C. J. Chen, H. J. Yen, W. C. Chen, G. S. Liou, *J. Polym. Sci. Part A: Polym. Chem.*, 2011, **49**, 3709; *(e)* T. J. Lee, Y. G. Ko, H. J. Yen , K. Kim , D. M. Kim, W. Kwon , S. G. Hahm , G. S. Liou, M. Ree, *Polym. Chem.*, 2012, **3**, 1276; *(f)* Y. G. Ko, W. Kwon, H. J. Yen, C. W. Chang, D. M. Kim, K. Kim, S. G. Hahm, T. J. Lee, G. S. Liou, M. Ree, *Macromolecules*, 2012, **45**, 3749; *(g)* C. J. Chen, H. J. Yen, W. C. Chen, G. S. Liou , *J. Mater. Chem.*, 2012, **22**, 14085.

8. (*a*) Q. D. Ling, D. J. Liaw, E. Y. H. Teo, C. X. Zhu, D. S. H. Chan, E. T. Kang, K. G. Neoh, *Polymer*, 2007, **48**, 5182; (*b*) T. Kuorosawa, C. C. Chueh, C. L. Liu, T. Higashihara, M. Ueda, W. C. Chen, *Macromolecules*, 2010, **43**, 1236.
9. (*a*) K. L. Wang, Y. L. Liu, J. W. Lee, K. G. Neoh, E. T. Kang, *Macromolecules*, 2010, **43**, 7159; (*b*) K. L. Wang, Y. L. Liu, I. H. Shih, K. G. Neoh, E. T. Kang, *J. Polym. Sci. Part A Polym. Chem.*, 2010, **48**, 5790; *(c)* B. Zhang, G. Liu, C. Wang, K. G. Neoh, T. Bai, E. T. Kang, *ChemPlusChem*, 2012, **77**, 74.
10. *(a)* Y. Oishi, H, Takado, M. Yoneyama, M. Kakimoto, Y. Imai, *J. Polym. Sci. Part A Polym. Chem.*, 1990, **28**, 1763; *(b)* M. Faccini, M. Balakrishnan, M. B. J. Diemeer, R. Torosantucci, A.Driessen, D. W. Reinhoudt, W. Verboom. *Mater. Chem.*, 2008, **18**, 5293; *(c)* J. L. Hedrick, R. Twieg, *Macromolecules*, 1992, **25**, 2021.
11. *(a)* G. S. Liou, H. J. Yen, M. C. Chiang, *J. Polym. Sci. Part A: Polym. Chem.*, 2009, **47**, 5378; *(b)* H. J. Yen, G. S. Liou, *Org. Electron.*, 2010, **11**, 299.
12. D. W. van Krevelen, *Polymer*, 1975, **16**, 615.

CHAPTER 5

CONCLUSIONS

CONCLUSIONS

The major conclusions are summarized as following: In chapter 2, the memory devices with the configuration of ITO/**P-TPA:PCBM**/Al exhibited both DRAM and WORM controlled by the concentration of PCBM. The switching behavior could be attributed to the charge transfer effect between TPA and PCBM proved by the corresponding TEM images and photoluminescence of these hybrid thin films indicated the PCBM aggregation and the charge transfer formation. The devices with the sandwich structure of ITO/**P-TPAAQ** and **P-TPAOAQ**/Al exhibited the volatile bistable electrical switching characteristics due to the charge transfer effect between the TPA donor moiety and incorporated pendent AQ acceptor moiety. While the introduced isolated ether group stabilized the charge transfer complex then extend the retention time at the ON state leading the SRAM behavior of the device of ITO/ **P-TPAOAQ**/Al comparing to the DRAM characteristic of **P-TPAAQ**.

In chapter 3, TPA-based aromatic polyimides containing pendent anthraquinone both directly attached to and incorporated via ether linkage into backbone as electron acceptor have been successfully synthesized for memory device applications. The memory devices with the configuration of ITO/**AQ-6FPI**/Al exhibited distinct volatile memory characteristics of DRAM while the ITO/**OAQ-6FPI**/Al showed volatile SRAM memory property. Thus, these results indicated the isolated D-A system could effectively extend the retention time in the memory device application. Both of ITO/**AQ-DSPI/**Al and ITO/**OAQ-DSPI/**Al show volatile SRAM memory property, high ON/OFF current ratio, and exhibit the retention time for 10 and 8 minutes, respectively. The SRAM behavior could be attributed to the strong charge-transfer effect between donor and acceptor result from TPA donor and backbone sulfone-containing phthalimide units. The theoretical analysis results, electrochemical and spectroelectrochemical studies suggest that the CT mechanism

could be used to explain the memory characteristics of these competitive acceptor containing polyimides and confirmed the linkage effect between the donor and acceptor and the strong charge-transfer effect between donor and acceptor result from TPA donor and backbone sulfone-containing phthalimide units.

In chapter 4, the memory behaviors affected by different electron-withdrawing capability were discussed in each series by different acceptor moiety, and the linkage effects were investigated by structural analogous **PIs**, **PAs** and **PEs**. **ODPI, ODPA**, and **PEs** demonstrate no memory but insulator behaviors. Among the other **PIs**, **6FPI** exhibited DRAM characteristic, and the stronger electron-withdrawing moiety containing **DSPI** revealed SRAM behavior, and the strongest electron-withdrawing nature of PMDA moiety leads **PMPI** extending the retention time from 4 to 8 minutes. In the rest of **PAs**, SRAM characteristic could be measured by the memory device, and the retention time could be extended as increased electron-withdrawing capability. **PAs**, consist of weaker acceptor, exhibit a longer retention time comparing to **PIs** due to the linkage effect which reduced the coplainity between donor and acceptor resulted from the amide linkage, providing a higher energy barrier for back charge transfer, and therefore extend the retention time.

By the above approaches, morphological control over the embedded PCBM, or facile D-L-A design of the electrical functionality including various linkage groups and electron accepters, the memory devices with the tunable characteristic could be fabricated readily.

Appendix

Curriculum Vitae

Yi-Cheng Hu

Nationality	Republic of China, Taiwan
3rd of Nov. 1987	Born in Kaohsiung
Sep. 2006-June 2010	***Bachelor*** / Dept. of Chemical Engineering, National Cheng Kung University, Tainan, Taiwan, Republic of China
Sep. 2010-	***Master*** / Institute of Polymer Science and Engineering, National Taiwan University, Taipei, Taiwan, Republic of China.
	Thesis Preceptor: Professor Guey-Sheng Liou.
	Thesis Title: "Synthesis and Memory Device Applications of Novel Triphenylamine Moiety Based High-Performance Polymers"

List of Publication

Journal paper:

1. **Yi-Cheng Hu**, Chih-Jung Chen, Hung-Ju Yen, Kun-Ying Lin, Jui-Ming Yeh, Wen-Chang Chen, and Guey-Sheng Liou* "Novel Triphenylamine-Containing Ambipolar Polyimides with Pendant Anthraquinone Moiety for Polymeric Memory Device, Electrochromic and Gas Separation Applications" *J. Mater. Chem.*, **2012** (*accepted*)

Conference papers:

Oral Presentation

1. **Y. C. Hu**, K. Y. Lin, H. J. Yen, and G. S. Liou* "Triphenylamine-base Aramids Bearing Pendent Anthraquinone Electron Acceptor for Polymeric Memory Devices" Oral Presented at the 4th IEEE International NanoElectronics Conference Tao-Yuan, Taiwan. (**2011**).
2. **Y. C. Hu**, K. Y. Lin, and G. S. Liou* "High Performance Polyimides Containing Triphenylamine and Dual Competitive Electron Acceptors for Polymeric Memory Devices" Oral Presented at the Annual Meeting of R.O.C Polymer Symposium. Jan, 2012. Chung Li, Taiwan. (**2012**).